MECHANISMS AND MODELING OF WHITE LAYER FORMATION IN ORTHOGONAL MACHINING OF STEELS

A Thesis
Presented to
The Academic Faculty

by

Sangil Han

In Partial Fulfillment
of the Requirements for the Degree
Doctor of Philosophy in the
George W. Woodruff School of Mechanical Engineering

Georgia Institute of Technology
May 2006

MECHANISMS AND MODELING OF WHTIE LAYER FORMATION IN ORTHOGONAL MACHINING OF STEELS

Approved by:

Dr. Shreyes Melkote, Advisor
School of Mechanical Engineering
Georgia Institute of Technology

Dr. Hamid Garmestani
School of Materials Science & Engineering
Georgia Institute of Technology

Dr. Steven Liang
School of Mechanical Engineering
Georgia Institute of Technology

Dr. Paul Griffin
School of Industrial & Systems Engineering
Georgia Institute of Technology

Dr. Thomas Kurfess
School of Mechanical Engineering
Georgia Institute of Technology

Date Approved: March, 6, 2006

ACKNOWLEDGEMENTS

The author is grateful to the suggestions and advice of the committee of Sangil Han's dissertation, Dr. Melkote, Dr. Liang, Dr. Kurfess, Dr. Garmestani and Dr. Griffin to achieve the goal of this research. The author also appreciates Dr. Haluska and school of material science and engineering for the access and advice for the X-ray diffraction tests. The author would like to thank Dr. Watkins for the X-ray diffraction tests and Liester for the nano indentation test. The user program of the Oak Ridge National Laboratory is appreciated for the approval of my proposal and access to the facilities. NIST ATP Award and National Science Foundation are appreciated for the funding for this research. The author would like to thank Kennametal for providing PCBN inserts, Thirdwave AdvantEdge® for offering their software and technical support, and Torrington for giving hardened steel bars for the hard turning research. Special thanks to the staffs in Georgia Institute of Technology, Steven Sheffield and John Graham and a name a few in the Precision Machining Research Consortium and machine shop in the department of mechanical engineering and Tim Banks in the general lab in the department of material science and engineering. Special thanks to Sathyan Subbiah, Kai Liu, Ramesh Singh, Bongjae Lee, Jungchul Lee, Haiyan Deng, and Tommy Newton, just name a few. Finally, I would like to thank all people, my family, my friends, my former and present labmates, classmates to encourage and inspire my work.

TABLE OF CONTENTS

LIST OF TABLES

LISTS OF FIGURES

LIST OF SYMBOLS

F_c	Cutting force
F_t	Thrust force
w	Width of cut
q_{shear}	Heat intensity of the primary heat source
$q_{friction}$	Heat intensity of the secondary heat source
$q_{rubbing}$	Heat intensity of the rubbing heat source on the tool flank-workpiece interface
B_1	Fraction of secondary heat source transferred into the chip
B_2	Fraction of rubbing heat source transferred into the workpiece
F_{cw}	Cutting force increase between an unworn tool and tool with a flank wear land
F_{tw}	Thrust force increase increase between an unworn tool and tool with a flank wear land
ø	Shear angle
F_s	Shear force
V_s	Shear velocity
L	Length of the shear zone
t_u	Depth of cut
$T_{workpiece\text{-}shear}$	Temperature rise due to primary heat source
$k_{workpiece}$	Thermal conductivity of the workpiece
$a_{workpiece}$	Thermal diffusivity of the workpiece

$V_{cutting}$	Cutting speed
$T_{workpiece\text{-}rubbing}$	Temperature rise on the workpiece due to rubbing heat source
$T_{tool\text{-}rubbing}$	Temperature rise on the tool due to rubbing heat source
k_{tool}	Thermal conductivity of the tool
T_{max}	Calculated maximum temperature at the trailing edge of the flank wear Land
$T_{calculated}$	Calculated workpiece surface temperature
$T_{measured}$	Measured workpiece surface temperature at each bead located point behind from the trailing edge
d	Distance from flank wear trailing edge to upper edge of the bead
τ	Average shear stress on the flank wear land-workpiece interface
σ	Average normal stress on the flank wear land-workpiece interface
σ_{eff}	Effective stress on the flank wear land-workpiece interface
$\bar{\varepsilon}$	Effective strain below the flank wear land-workpiece interface
θ	Contact angle between the flank wear land and the workpiece
A_o	Entrapped area beneath the tool flank wear and the workpiece contact
A_f	Side extruded area beneath the tool flank wear and the workpie contact

SUMMARY

With the advent of new cutting tool materials such as polycrystalline cubic boron nitride (PCBN), turning of hardened materials (>45 HRC) is becoming increasingly feasible. However, undesirable microstructure change, specifically, the formation of white layer, has become a hurdle in its widespread acceptance by industry. Despite knowledge of the various characteristics of white layer, its formation mechanisms have not been fully understood. While it is commonly believed that white layer in hard turning is produced by thermally-induced phase transformation, there is limited understanding of the exact thermo-mechanical conditions present during its formation. Specifically, the workpiece surface temperatures, and the simultaneous contributions of thermal and mechanical effects on white layer formation in hard turning have not been adequately studied. Additionally, a systematic investigation of the effects of work material chemical composition and heat treatment on white layer formation is lacking.

Therefore, the research objectives of this thesis are as follows: (1) Investigate the effects of carbon content, alloying, and heat treatment of steels on white layer formation, (2) Prove/disprove that the temperature for phase transformation in machining is the same as the nominal phase transformation temperature (A_s) of the steel in the Fe-C phase diagram, (3) Quantify the contributions of thermal and mechanical effects to white layer generation in machining, (4) Develop a semi-empirical procedure for prediction of white layer formation that accounts for both thermal and mechanical effects. These research objectives are realized through a combination of experimental (turning, optical

microscopy, X-ray diffraction, nanoindentation) and modeling efforts on AISI 1045, 4340 and 52100 steels.

Depth and hardness measurements of the white layers formed in different types of steels show the importance of heat treatment and carbon content on white layer formation. Measurements of workpiece surface temperature and X-Ray Diffraction (XRD) characterization of the machined surfaces show that phase transformation occurs below the nominal A_s temperature suggesting that mechanical effects play an important role in white layer formation. The maximum workpiece surface temperature, the effective stress, and plastic strain on the workpiece surface are measured and/or calculated and shown to affect the white layer depth and amount of retained austenite. A semi-empirical procedure is developed by correlating the maximum workpiece temperature and the unit thrust force increase with white layer formation. The procedure is experimentally verified and shown to be capable of predicting the presence/absence of white layer and its approximate depth for a given range of machining conditions.

CHAPTER 1

INTRODUCTION

1.1 Background

Hard turning as a material removal process is being increasingly considered by industry. Hard turning with single-point cutting tools has received a great deal of attention in recent years as a potential substitute for the grinding process [1]. However, issues related to surface integrity in addition to economics have prevented widespread adoption of the hard turning process in industry. In particular, under certain conditions, hard turning is known to produce microstructure changes in the surface layers of the part such as the formation of a featureless, hard, and brittle white-etching layer ("white layer") on the machined surface. A typical example of white layer is shown in Figure 1.1.

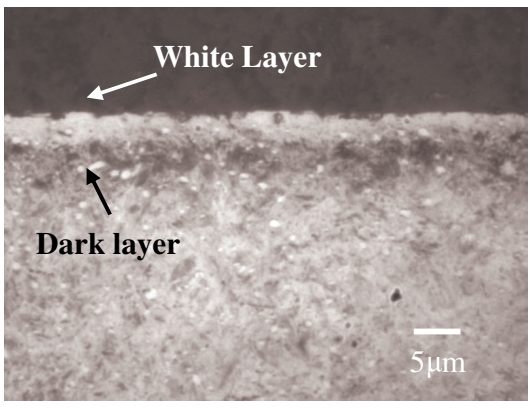

Figure 1.1. White layer formed in turning of AISI 52100 hardened steel (62 HRC) at 182.9 m/min and 0.15 mm/rev feed with 120 μm flank wear.

The white layer has drawn attention from researchers because it is observed in other processes, besides conventional hard turning, such as cryogenic hard turning [2],

grinding [3,4,5], rubbing and wear [6], reaming [7], built-up edge [8], EDM [9,10], impact [11], equi-channel angular extrusion [12], and nitriding [13]. It is also observed in service parts such as railroad track [14,15,16] and bearings [17]. Its properties are different from the bulk [18], and it can affect the residual stresses in the part and its tribological performance [19], wear resistance [20], temper resistance [21] and fatigue life [22, 23]. White layer formation in steels has been of great interest to industry due to the widespread use of steels for structural and machine components, although white layer is also known to occur in non-ferrous metals such as titanium [24] and brass [25]. Despite knowledge of its various characteristics and influence, the underlying conditions and mechanisms of white layer formation are not completely understood. It is commonly believed that there are three major mechanisms of white layer formation [26]: (1) Phase transformation as a result of rapid heating and quenching, (2) Severe plastic deformation that results in ultra fine grain size (10~300nm) due to grain refinement and/or recrystallization effects, and (3) Reaction of the surface with the environment.

Although the role of thermal and mechanical effects on the formation of white layer in machining has been acknowledged in the literature, little work to confirm and quantify those effects has been done. Researchers have focused their efforts mainly on modeling the thermally induced phase change mechanism. In other words, the austenitization temperature, A_s is suggested by many researchers as the only characteristic of the work material needed to determine the presence or absence of white layer. This is based on the assumption that only thermal effects play a role in the formation of the white layer. Also, no experimental evidence of the actual workpiece surface temperature generated during white layer formation in machining of steels has

been presented to date. Finally, little work to systematically examine the role of other characteristics of the workpiece material such as the carbon content, alloying elements and heat treatment in the formation of white layer in steels has been done.

1.2 Research Objectives

As discussed above, there is a need to study the combined effects of thermal and mechanical deformation phenomena on white layer formation in machining of steels. There is also a need to quantify the mechanical effects, while confirming the thermal effect reported in the literature by measuring the workpiece temperature. The effects of material characteristics on white layer formation also need to be studied. Therefore, the specific objectives of this thesis are as follows;

1. Prove/disprove that the workpiece surface temperature for phase transformation to occur in machining of steels is the same as the nominal A_s temperature obtained from the Fe-C phase diagram.
2. Investigate the roles of carbon content, alloying elements, and heat treatment on white layer formation in machining of steels.
3. Identify *and* quantify the contributions of thermal and mechanical effects to white layer generation in machining.
4. Develop a semi-empirical procedure for prediction of white layer formation while accounting for both thermal and mechanical effects.

1.3 Research Approach

Hence, in order to achieve the objectives of this research, the approach taken is as follows:

1. Measurement of workpiece surface temperature and X-Ray diffraction (XRD) characterization of the machined steel surface.
2. Orthogonal machining of various unhardened and hardened steels that vary in carbon content, alloying and heat treatment and measurement of white layer depth and hardness.
3. Calculation of workpiece surface temperature as a measure of the thermal effect, and stress and strain as a measure of the mechanical effect for a chosen material, under certain cutting conditions.
4. Development of a semi-empirical procedure for predicting white layer formation as a function of the workpiece surface temperature, stress and/or strain.

1.4 Dissertation Outline

The dissertation is laid out as follows. Chapter 2 reviews past work reported in the areas of mechanisms of white layer formation, effects of material characteristics on white layer formation in machining, modeling of thermal and mechanical effects on the workpiece and modeling of white layer formation in machining. The effect of alloying, heat treatment, and carbon content on white layer formation in machining of steels is examined in Chapter 3. Calculation of workpiece surface temperature, stress and strain is

described in Chapter 4. Experiments designed to confirm the occurrence of phase transformation during machining of an annealed steel and measurement of the corresponding workpiece surface temperature are described in Chapter 5. The semi-empirical procedure for predicting white layer formation is discussed in Chapter 6. Finally, conclusions and recommendations are outlined in Chapter 7. A flow chart summarizing this research is shown in Figure 1.2.

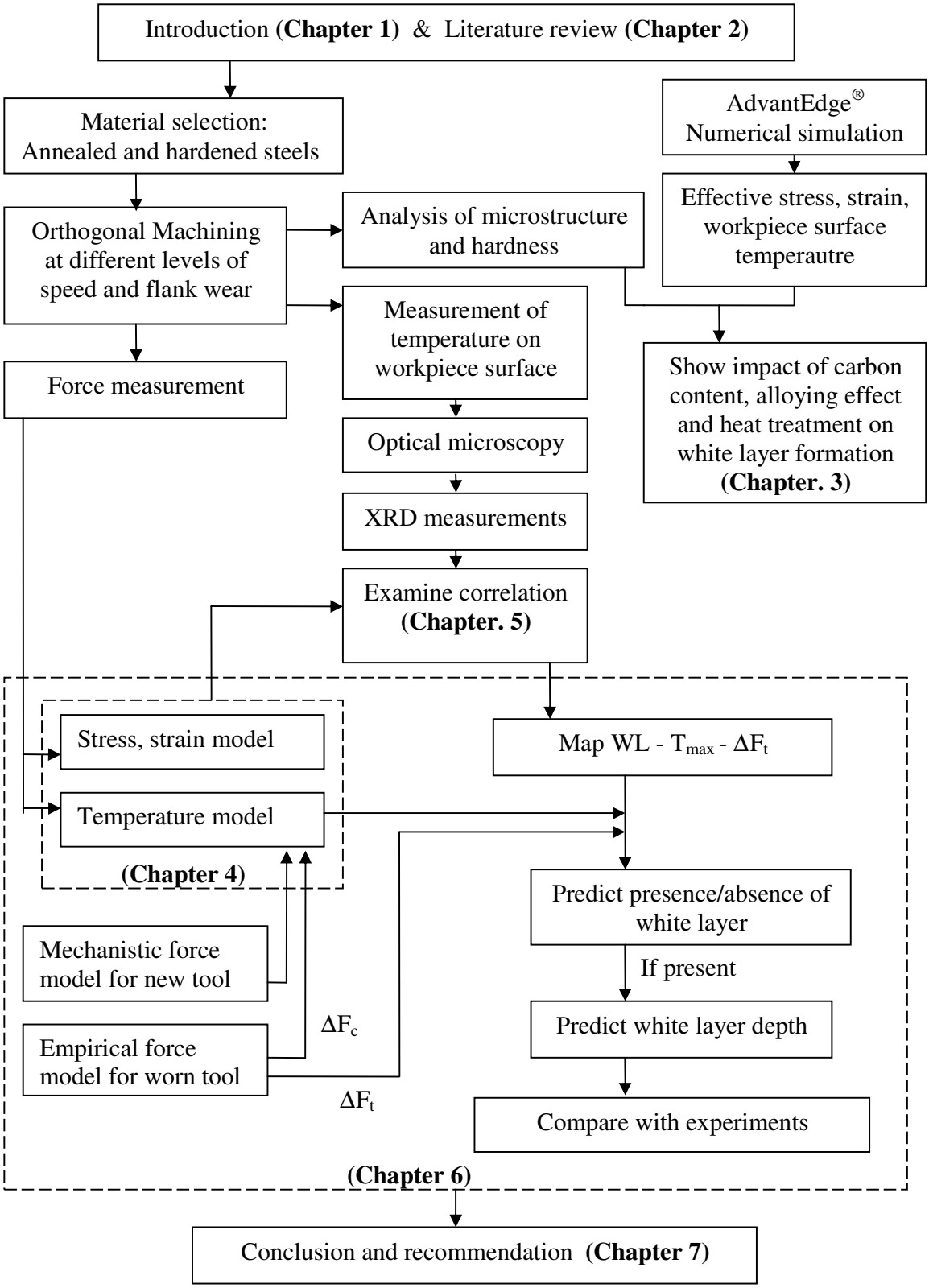

Figure 1.2 Flow chart summarizing this research.

CHAPTER 2

LITERATURE REVIEW

This section reviews past work in four areas relevant to the proposed work: (1) Mechanisms of white layer formation in machining, (2) Effect of material characteristics on white layer formation in machining, (3) Modeling of thermal and mechanical effects on the workpiece during machining, and (4) Modeling of white layer formation in machining.

2.1 Mechanisms of White Layer Formation in Machining

Mechanisms of white layer formation in machining have been investigated over the past thirty years. Griffith [26] categorized three major mechanisms that cause white layer in various processes; (1) *Thermal*: Phase transformation as a result of rapid heating and quenching, (2) *Mechanical*: Severe plastic deformation that results in ultra fine grain size (10~300nm) due to grain refinement and/or recrystallization effects, and (3) *Environmental*: Reaction of the surface with the environment. In particular, the mechanical and thermal effects are considered to be the major mechanisms for formation of white layer in machining.

2.1.1 Thermal Effect on White Layer Formation

While both thermal and mechanical effects in the formation of white layer have been acknowledged by researchers [26, 27], the primary focus of prior work has been limited to attributing only the thermal effect to mechanism of white layer formation and finding evidence of thermal effects only. Brinksmier and Brockhoff [28] state that a very fine grain structure in martensitic hardened steel can form due to the extreme heating and quenching rates encountered in machining. They note that under these conditions a white layer can form if the temperature exceeds the austenitization temperature of steel. Vyas and Shaw [4] investigated white layer formation due to reverse martensitic transformation in the chip while no white layer was found on the workpiece surface after machining with a sharp tool. Eyre and Baxter [6] found that white layer at a rubbing surface can be formed by frictional heating and quenching. Barbacki et al. [29] studied dark and white layers formed in machining of steels and concluded that a dark layer is not observed in machining high-speed steel due to its high tempering temperature.

Barry and Byrne [30] used Transmission Electron Microscopy (TEM) to analyze white layers generated in hard turning of BS 817M40 steel (equivalent to AISI 4340 steel) (52 HRC) with worn and unworn tools. They attributed white layer formation to a combination of thermal and dynamic recrystallization effects. Österle et al. [31] analyzed white layer generated in pearlitic steel used in railroad tracks using TEM and XRD techniques. They reported evidence of martensitic structure and some cementite in the white layer. Although no retained austenite was observed, quenching from 850°C was required for the martensitic structure to form. Consequently, white layer formation was attributed to both severe plastic deformation and rapid heating and quenching. Kim and

Kwon [32] machined AISI annealed 1045, 1070 and 4340 steels. In all cases, white layers with 1-2 μm thickness were observed after increasing the cutting speed to over 200m/min. XRD tests showed retained austenite and untempered martensite in AISI 1045 and 1070 but only untempered martensite in AISI 4340 steel. They confirmed that pearlite-austenite-martensite phase transformation was responsible for white layer formation in the steels investigated. Interestingly, a cutting speed of 225m/min for 1070 steel, which is lower than the speed used for 1045 steel (275m/min), was required to produce white layer. This was justified using the fact that austenitization temperature, A_3, of 1070 steel (738 ºC) is lower than that for 1045 steel (800 ºC).

Sauvage et al. [33] machined two different steels (0.38 and 0.8 wt. % C) at 200 m/min and obtained 1-2 μm thick white layer. XRD and Mössbauer spectrometry tests were performed to identify phase change. In both cases, retained austenite was observed indicating phase change. Consequently, the austenitization temperature of each steel in the Fe-C phase diagram was assumed to be the workpiece surface temperature during machining.

Akcan et al. [34] selected different types of hardened steels, which have different levels of A_3 temperature. They compared AISI 52100 hardened steel (60~62 HRC), 4340 hardened steel (56~57 HRC) and M2 steel (60~62 HRC) in terms of their different A_3 temperatures (AISI 52100 and 4340 have an A_3 temperature of 800 ºC while M2 has an A_3 temperature of 1200 ºC). They observed the presence of white layer in AISI 52100 and 4340 steels and its absence in M2 steel after machining with a worn tool (200 μm flank wear) at a cutting speed of 150 m/min. However, white layer was still observed after turning both AISI 52100 and 4340 hardened steels under less aggressive conditions of 50

m/min and 100μm flank wear, where the temperature should be far below the A_3 temperature [35]. Similarly, Ramesh et al. [36] conducted hard turning tests on AISI 4340 and 52100 steels (57 HRC) and observed white layer at a cutting speed of 122 m/min with a new chamfered tool. However, no dark layer (overtempered layer) below the white layer was observed in AISI 4340 hardened steel. The absence of the dark layer was attributed to the lack of overtempering in the sub surface layers due to insufficient maximum surface temperature of 4340 hardened steel.

2.1.2 Temperature Measurement Correlated with White Layer Formation

As discussed in section 2.1.1, it is often assumed in the literature that if the temperature at the tool flank-workpiece interface exceeds the nominal phase transformation temperature for the steel, white layer forms. Regarding measurement of temperatures in machining, several studies have been done to measure the tool-chip interface temperature using various methods [37,38] and some efforts to use the measured temperatures to account for microstructure alteration in chips have been reported [39]. However, few attempts have been made to measure the workpiece surface temperature [40,41,42,43,44], and none to use the measured temperatures to account for microstructural changes in the workpiece surface. Bosheh et al. [45] used the temperature of the just-machined surface measured using a pyrometer to point out one cause of white layer formation. However, no attempt was made to actually measure the temperatures produced at the tool flank-workpiece interface during cutting and correlate it with microstructural evidence of phase transformation.

2.1.3 Mechanical Effect on White Layer Formation

Few works have shown evidence of mechanical effects in the formation of white layer. Turley [7] compared white layers produced in reaming of high strength steel (49 HRC) with those produced by hand abrasion where temperature rise is relatively small. In both cases, the white layers did not show evidence of carbide and retained austenite phases. Since carbide annihilation can occur due to plastic deformation whereas retained austenite is typically a consequence of thermally induced martensitic phase transformation, he concluded that white layer produced in reaming was due to severe plastic deformation occurring far below the austenitization temperature.

Ramesh et al. [46,47] carried out TEM, XRD, Energy Dispersive Spectra (EDS), analyses and nano-indentation hardness tests of white layers formed in hard turning of AISI 52100 steel (62 HRC) and found cementite to be absent in the white layer formed at high cutting speeds (274 m/min) at which thermal effects are expected to be dominant. The absence of cementite phase was attributed to the dissolution of all carbon in the martensitic structure produced by reverse martensitic phase transformation of the material. In contrast, cementite was observed in the white layer formed at a lower cutting speed (91 m/min) at which mechanical effects tend to dominate and the temperatures may not exceed the austenitization temperature of the steel. Consequently, they concluded that white layer formed at the lower cutting speed (91 m/min) was primarily due to mechanical grain refinement arising from severe plastic deformation whereas the white layer at the higher cutting speed (274 m/min) was primarily due to thermally-induced martensitic phase transformation.

Xu et al. [11] observed nano crystallized ferrite and cementite in the white layer (see Figure 2.1) formed in annealed AISI 1045 steel during impact wear. TEM analysis of the white layer reveals that neither retained austenite nor martensite was present in the fine grain structure. Large angle sub grain formation of ferrite due to dislocations and cementite grain refinement due to shearing fracture were proposed as the underlying mechanisms responsible for the fine grain structure.

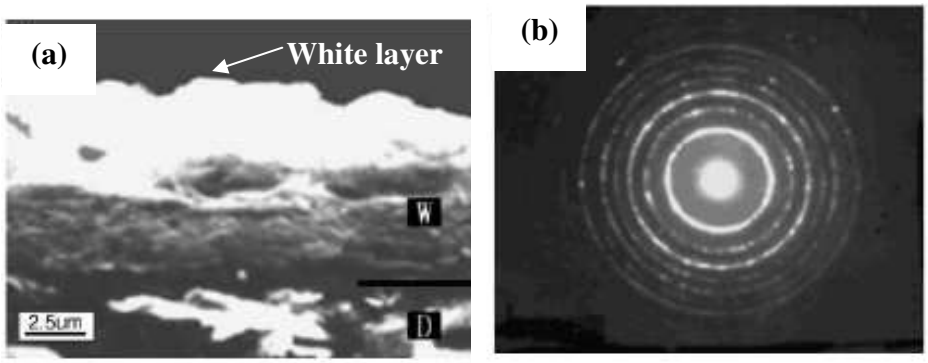

Figure 2.1. (a) White layer created in impact wear process of annealed AISI 1045 steel, and (b) Corresponding TEM diffraction pattern (Xu et al. [11]). Note that neither retained austenite nor martensite were observed in the diffraction pattern.

Properties of white layer such as its high hardness also imply the role of both thermal and mechanical effects on formation of white layer because such a high hardness cannot be achieved solely by pure heat treatment process. Surface hardening after machining of 4340 annealed steel was recently reported by Chou [48]. Thick (13 μm) white layer was observed combined with the surface hardness increases of up to 49 HRC compared to 28 HRC for the bulk material after machining with 1.2mm flank wear at 3 m/s machining speed. Thermal and mechanical loading during machining was considered as the major cause of the presence of white layer and surface hardening. Mahajan et al.

[49] measured the Knoop hardness variation at different depths in the white layer formed in hot-rolled 4340 steel (350 HK_{500}) as a result of machining with very large flank wear (>1mm) at different cutting speeds. The big increase in the Knoop hardness of up to 700 HK_{500} was hypothesized to be due to because martensitic phase transformation, high stresses and large strains. Attempts to induce different thermal and mechanical effects by turning and grinding of 52100 hardened steel (62~63 HRC) were made by Guo et al. [50]. Since the grinding process is characterized by greater wheel-work contact length than hard turning, it leads to higher surface temperatures, deeper penetration depth of heat into the workpiece, and less average stress over the entire contact length. As a result, 14 μm and 140 μm thick white layers were generated by turning and grinding, respectively. The higher microhardness of white layer of the ground surface was found to be 40 % higher than that of hard turning and was caused by the different thermal and mechanical effects in the processes. Guo et al. [51] examined nano hardness and the modulus of elasticity of the sub-surface in hard turned 52100 hardened steel (62 HRC), in 1070 hardened steel (62 HRC) generated by grinding and honing. Effects of strain hardening, size effect, residual stress and microstructure change were attributed to the observed change in surface hardness.

2.1.4 Environmental Effect on White Layer Formation

Environmental effect is one of the mechanisms that can cause white layer, which is usually observed in surface treatment processes such as nitriding [13,52] and carburizing [53]. A typical example of white layer formed as a result of the nitriding process is shown in Figure 2.2.

Figure 2.2. White layer formed as a result of nitriding BS 905M39, En 41 B for 5h period at 500ºC and 20% degree of dissociation (high gas flow rate) then for 25 h at 500ºC and 55% degree of dissociation [52].

Atomic nitrogen infiltrates into the surface of steels by applying gas nitriding. As a result, white layer occurs due to dislocation without phase transformation. High temper resistance, high fatigue strength, and improved corrosion resistance can be achieved by this process.

Although environmental effect on white layer formation in other processes has been reported, it is widely accepted that thermal and mechanical effects are the major mechanisms responsible for formation of white layer in machining process.

As discussed above, the majority of prior work is focused on the nominal A_s (austenitization) temperature of the steels as the primary material characteristic that affects white layer formation in machining.

2.2 Effect of Material Characteristics on White Layer Formation in Machining

It is widely believed that material characteristics of steels such as carbon content, alloying and heat treatment play a role in the formation of white layer in machining. Shaw and Vyas [4] pointed out that carbon diffused into the γ phase during rapid heating

leading to formation of untempered martensite during quenching in the grinding process. They inferred from the Fe-C phase diagram that 0.025 wt. % carbon content was the minimum amount needed to achieve the observed phase change to cause the microstructural change because austenite (γ) transformed to ferrite (α) without martensite phase (α') with less than 0.025 wt. % carbon. Okusa et al. [8] ran machining tests on different types of steels, which contained different levels of alloying to study their effect on the tendency for white layer formation. Their results show that white layer is observed in the built-up edge formed on the tool in machining carbon steel and a low alloy steel such as Cr-Mo steel, while no white layer is observed in the built-up edge formed during machining high alloy steels such as alloy tool steel and stainless steel. But, they did not look at the machined surface to study white layer formation in those steels.

Kim and Kwon [32] performed machining tests on AISI 1045, 1070 and 4340 annealed steels, which contained different levels of carbon or alloying. White layer occurred in 1070 steel at a machining speed as low as 225 m/min. However, in 1045 steel, white layer was observed only at the higher machining speed of 275 m/min. Lower A_3 temperature was attributed to the higher likelihood of formation of white layer in 1070 annealed steel. Thicker white layer was observed in machining of 4340 steel compared to that in 1045 steel at the same machining speed. A lower A_3 temperature for 4340 steel (compared to 1045 annealed steel) was suggested as the cause of the thicker white layer. However, this is contradictory to expectation since the Mo and Si alloyed in 4340 steel tend to increase the A_3 temperature [54].

Shaw and Vyas [4] ground 1045 annealed steel and compared the microstructure changes in the surface with that produced in grinding of 4340 hardened steel (51 HRC).

A very thick (130μm) heat affected zone, five times greater than in the 4340 ground steel surface and a more complex structure including an overtempered layer was observed in the ground 1045 annealed steel surface. Large pearlite patches in the 1045 annealed steel are thought to hinder carbon diffusion into the γ phase and are responsible for the complex structure such as the cementite band present in the heat affected zone. Coolant application during grinding of 1045 annealed steel is considered to be a factor responsible for the fine pearlite structure formed on the surface because coolant application provides another quenching source on the surface in addition to quenching by the bulk. However, it is hard to make a direct comparison of the structure in the ground 1045 annealed steel and the ground 4340 hardened steel surfaces to identify the effect of material characteristics on white layer formation because the grinding conditions such as work speed, wheel material, and wheel depth of cut used in the study for the two materials are different.

Little work has been done to investigate the effects of other material characteristics such as the carbon content, alloying and heat treatment on white layer formation in a systematic way.

2.3 Modeling of Thermal and Mechanical Effects on the Workpiece during Machining

Considerable research has have been done in the past five decades on modeling the temperatures, stresses and strains produced in machining. However, a majority of works are focused on the temperature at the tool-chip interface [55,56,57,58], stresses and strains [59,60,61] in the shear zone band. Several works have reported on the modeling of

temperatures, stresses and strains in the workpiece and/or the tool flank-workpiece interface during machining [62,67,68,69,70]. Since the objective of this research is to quantify thermal and mechanical effects on white layer formation on the workpiece in machining, the following literature review focuses on these efforts.

2.3.1 Modeling of Thermal Effects on the Workpiece during Machining

Chao and Trigger [62] modeled the temperature distribution at the interface between the tool flank wear land and workpiece using the moving heat source theory [63]. The diagram of moving heat source at the interface between the tool flank wear land and workpiece is shown in Figure 2.3.

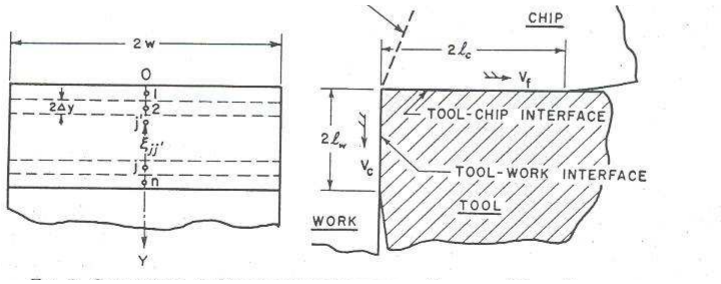

Figure 2.3. Moving heat source at the interface between the tool flank wear land and workpiece[62].

The temperature rise due to a uniform heat flux $q_{w,j}$ from the band source *j* is given by:

$$\Delta\theta_{w,j'j} = \frac{2q_{w,j}}{\pi C_w \rho v_c}\int_{E_{jj'}-\Delta Y}^{E_{jj'}+\Delta Y} e^{-u} K_o(|u|)du \qquad \textbf{(2.1)}$$

where, $E_{jj'} = \frac{v_c \xi_{jj'}}{2k_w}, \Delta Y = \frac{v_c \Delta y}{2k_w}$, v_c is cutting speed, $\xi_{jj'}$ is the distance from j to j′, k_w is the thermal diffusivity, ρ is the density, and C_w is the specific heat of the workpiece material.

Their calculated temperature distribution on the interface between the flank wear land and workpiece in machining of AISI 4142 annealed steel at varying speeds with 250 µm flank wear width and 0.16 mm/rev feed is shown in Figure 2.4.

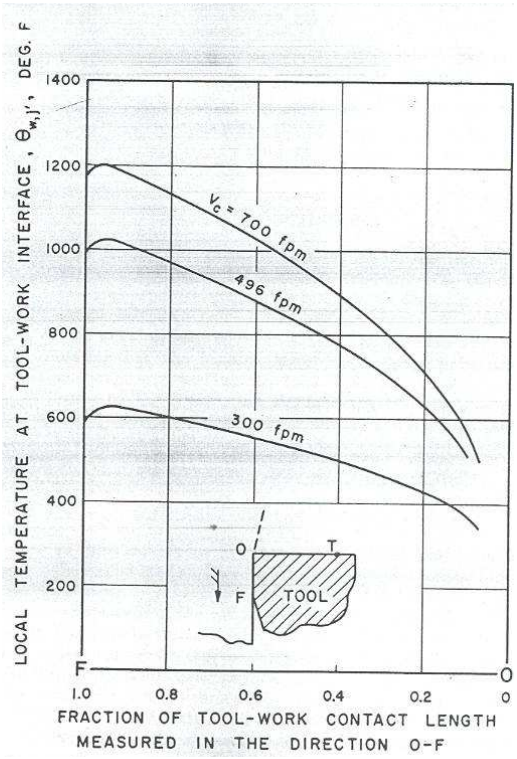

Figure 2.4. Temperature distribution on the interface between flank wear land and workpiece [62].

As can be seen in Figure 2.4, their temperature simulation shows that the temperature at the interface between the flank wear land and the workpiece increases with increase in the cutting speed. Also, the maximum temperature typically occurs at the trailing edge of the flank wear land. However, no comparison between the calculated temperatures and experimental data was made.

Usui et al. [44] calculated the temperature distribution at the tool flank wear-workpiece interface during machining of carbon steel and compared it with experimental

data obtained in machining with very large flank wear (>600μm) and found good agreement.

Komanduri and Hou [64] calculated the temperature rise in the workpiece sub surface due to the moving heat source in the shear zone when machining with a new tool. Since there is little experimental data on workpiece temperatures during machining with a new tool, comparison between the calculated average temperature at the tool-chip interface and experimental data from the literature for temperatures at the interface between tool and chip was made [65,66].

Haung [67] calculated the workpiece surface temperature at the contact between the workpiece and tool flank wear land due to the combined moving heat sources of shear zone and rubbing between tool flank wear land and workpiece during turning of 52100 hardened steel (62 HRC) with worn CBN tool. However, due to lack of workpiece surface temperature data in machining of 52100 hardened steel, calculation using Boothroyd's experimental condition [40], i.e. machining of pure iron with large flank wear (> 380 μm) was made.

2.3.2 Modeling of Mechanical Effects on the Workpiece during Machining

Thomsen et al. [68] calculated the normal and shear stresses acting on the workpiece surface during cutting with a tool with flank wear using the thrust and cutting force difference between a new tool and a tool with flank wear land. A diagram to describe the forces during machining with a tool with flank wear land and force data with increasing flank wear land are given in Figure 2.5.

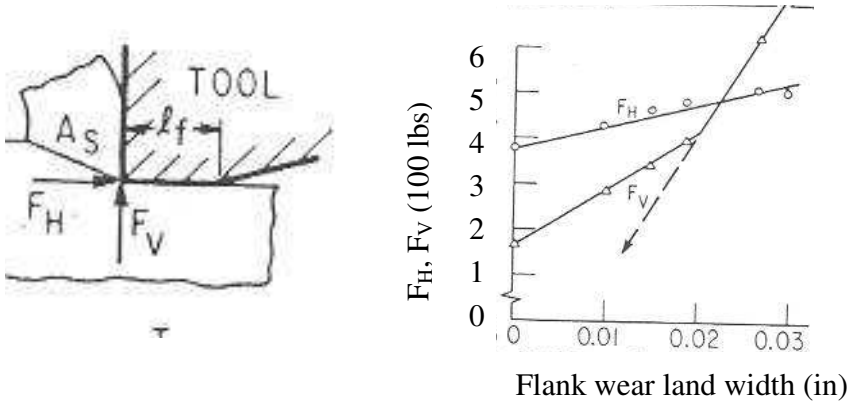

(a) (b)

Figure 2.5. (a) Forces during machining with a tool with flank wear land, (b) Force data with increasing flank wear land [68].

The average normal stress acting on the workpiece surface was calculated as [68]:

$$\sigma = \frac{\Delta F_V}{l_f w_o} \tag{2.2}$$

The average shear stress acting on the workpiece surface was calculated as [68]:

$$\tau = \frac{\Delta F_H}{l_f w_o} \tag{2.3}$$

Where, ΔF_v and ΔF_H are the cutting and thrust force increases due to flank wear, respectively; l_f is the flank wear land width and w_o is the wall thickness of the tube in orthogonal machining. As can be seen in Figure 2.5, a linear force increase with increase in flank wear land width was observed. Plastic flow observed in the workpiece under the flank wear land was attributed to the linear force increase and the plastic deformation was calculated using wedge analysis of entrapped metal under flank wear land region. Chen et al. [69] also reported a consistent linear force increase with flank wear and calculated the stress acting on the workpiece surface contacting the tool flank wear. Waldorf [70]

calculated the elastic and plastic stress distributions under flank wear using slip line theory and predicted a linear force increase with flank wear increase. The stress distribution on the flank wear land computed by Waldorf is shown in Figure 2.6.

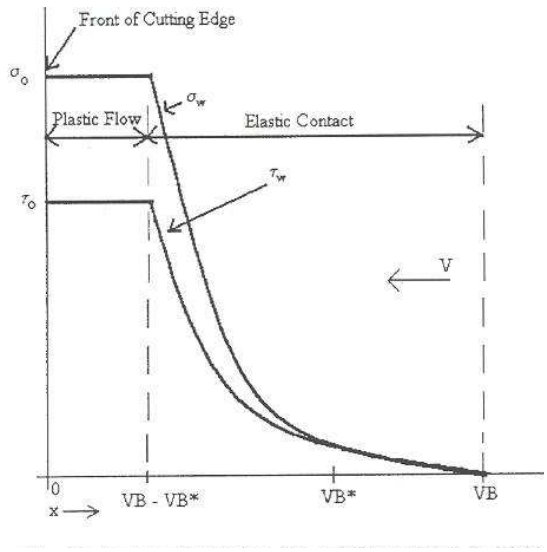

Figure 2.6. Stress distribution on the flank wear land [70].

As seen in Figure 2.6, the model assumes that plastic flow occurs in the front region of the critical flank wear width, VB*, and elastic stresses occur behind the critical flank wear width. However, in order to calculate the elastic and plastic stress distributions, several assumptions for the many parameters such as critical flank wear width, friction coefficient, and slip-line field angle were required.

As can be seen, most of the modeling work is concentrated on quantifying the thermal and mechanical work and accounting for other phenomena such as tool wear. Little modeling and analysis effort to account for microstructural change on the workpiece surface during machining due to both thermal and mechanical effects has been reported.

2.4 Modeling of White Layer Formation in Machining

Very few attempts to model white layer formation in machining have been reported. Barbacki et al. [71] established a purely empirical (regression) model of white and dark layer thickness as a function of the cutting conditions produced by turning AISI 52100 hardened steel (60 HRC). However, the empirical model does not provide any physical reasoning of white layer formation. Ali and Zhang [72] employed fuzzy modeling methods to predict the level of grinding burn in steels in terms of the process parameters as shown in Figure 2.3. Their model is based on a number of physical rules and assumptions. One major assumption is that grinding burn as a microstructure alteration occurs when surface temperature exceeds nominal phase transformation temperature of the steel given by the Fe-C diagram.

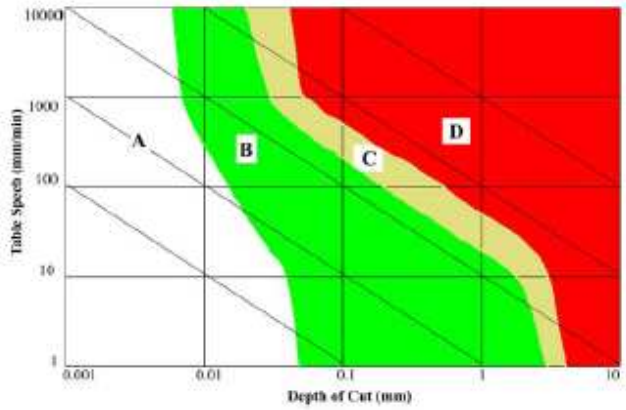

Figure 2.7. Fuzzy set modeling to delineate different levels of grinding burn in terms of the grinding parameters (Ali and Zhang [72]). Region A denotes the region where no burn occurs. Regions B and C denote the region where burns can be prevented with coolant. Region D denotes where surface occurs happen irrespective of the amount of coolant used.

Akcan [35] proposed that white layer forms when the workpiece temperature exceeds the austenitization temperature, A_3, in the Fe-C phase diagram. White layer

depth was predicted by identifying the depth below the workpiece surface where the austenitization temperature, A_3, is reached. Predicted white layer depth in machining of 52100 hardened steel (60~62 HRC) and 4340 hardened steel (56~57 HRC) at high speed (200 m/min) and with large flank wear width (300 μm) matched fairly well with experimental data. On the other hand, at cutting speeds less than 150 m/min and with flank wear less than 200 μm, the subsurface temperature prediction was far below the A_3 value. Consequently, no white layer was predicted even though a 3-6 μm thick white layer was observed in the experiment. Although Akcan acknowledged the role of mechanical effects in machining, no attempt to incorporate those mechanical effects in modeling of white layer formation was made.

Song [73] used the austenitization temperature, A_1, to predict the white layer depth in machining of 52100 hardened steel (60~62 HRC). White layer depth was predicted at the depth where the A_1 temperature was reached. However, the prediction of white layer depth and comparison with experimental data was made only for machining at very high feeds (> 0.3 mm/rev) or at high machining speeds (> 3 m/s), where the workpiece temperature was above the A_1 temperature for the steel.

Chou and Evans [27] hypothesized that the austenitization temperature would be lowered to 560 ºC (80% of A_1) due to mechanical working. White layer depth in machining of 52100 hardened steel (63 HRC) was determined at the depth where the reduced austenitization temperature occurred. However, the lowered A_1 was suggested only for a specific machining machining speed of 3 m/s and flank wear width of 110 μm. The value of A_1 for other machining conditions was not provided. Little explanation of the relation between A_1 and the mechanical effects was given.

Ramesh [46] estimated the change in A_s (austenitization temperature) due to mechanical effects using the Clausius-Clayperon equation, which accounts for the effect of pressure on phase equilibrium. Temperature, effective stress and plastic strain in the workpiece sub surface in machining of 52100 hardened steel (62 HRC) were calculated using a numerical model of the orthogonal hard machining developed in ABAQUS®, a finite element software. In his model, the fractional increase of martensite and strain due to volume change and phase transformation plasticity were incorporated. White layer depth was determined at the depth where the estimated A_s temperature occurred. However, machining condition was in the range of high speeds in excess of 213 m/min and flank wear width of 100 µm, where thermal effects are expected to be dominant. Formation of white layer over a wider range of machining speeds and flank wear width, where different levels of thermal and mechanical effects are anticipated, was not investigated.

As can be seen, a majority of the previous modeling efforts are based on the hypothesis that the thermal effect is the major effect responsible for the formation of white layer. In contrast, very little effort has been made to develop a white layer formation model that accounts for both mechanical and thermal effects.

2.5 Summary

After reviewing the relevant literature on white layer formation in machining, the following conclusions can be drawn:

1. There is no experimental evidence of the actual workpiece surface temperature generated during white layer formation in machining.
2. Little work has been reported to systematically examine the role of other characteristics of the workpiece material such as the carbon content, alloying elements and heat treatment in the formation of white layer.
3. Despite acknowledgement of the roles of thermal and mechanical effects on the formation of white layer, little work to confirm and quantify those effects has been reported.
4. Very little effort has been made to develop a white layer formation model/procedure that accounts for both mechanical and thermal effects.

The research objectives of this were established to answer these questions raised from the limitations of prior work. Therefore, the following chapters are devoted to the research tasks designed to fulfill these objectives.

CHAPTER 3

EFFECT OF ALLOYING, HEAT TREATMENT, AND CARBON CONTENT ON WHITE LAYER FORMATION

This chapter describes an experimental investigation of the effects of alloying, carbon content, and heat treatment on white layer formation in machining of steels. The investigation is carried out by machining steels that differ in alloying, heat treatment and carbon content, via orthogonal cutting tests performed with low cBN content tools. The depth of white layer and its hardness are measured for every case. Specifically, the thickness and hardness of white layer produced in cutting AISI 1045 and AISI 4340 annealed steels are compared to determine the effect of alloying on white layer formation. The effect of heat treatment on white layer formation and its hardness are investigated by machining annealed and hardened (53 HRC) AISI 4340 steels. The effect of carbon content on white layer formation is investigated by cutting hardened AISI 52100 and AISI 4340 steels of the same hardness (53 HRC). Since 52100 steel has almost twice the amount of carbon and less number of alloying elements than AISI 4340 steel, an approximate understanding of the effect of carbon content on white layer formation and its hardness can be inferred. The results of the study show that alloying, heat treatment, and carbon content influence white layer formation and its hardness. The possible roles of the maximum workpiece surface temperature, effective plastic strain and stress on white layer formation in the different steels are also analyzed via finite element simulations performed in a commercially available code.

3.1 Experimental Work

Orthogonal tube cutting experiments were performed. Sections of the tube were then cut using a precision saw, molded, polished and etched using 2% Nital solution and observed under an optical microscope (Nikon Microphot-FXL). Measurement of the hardness of white layer and transition layer (between the bulk and white layer regions) was performed using the nano-indentation method (MTS-80^{TM}). The following sections describe the workpiece materials and the procedures adopted in this work.

3.1.1 Material Selection and Preparation

Four different steels, AISI 1045 annealed steel, AISI 4340 steel - annealed and hardened (53 HRC), and AISI 52100 hardened steel (53 HRC), were chosen to investigate the effects of alloying, heat treatment and carbon content on white layer formation. Nominal contents [32,84] and austenitization temperatures [84,86] for the four steels are listed in Table 3.1.

Table 3.1. Nominal contents [32,84,85] and austenitization temperatures [84,86] of the four steels.

Steel (AISI)	Composition (Weight %)								Ac_1 (ºC)	Ac_3 (ºC)
	C	Mn	P	S	Cr	Mo	Ni	Si		
Annealed 1045	0.42-0.5	0.6-0.9	Max 0.04	Max 0.05					738	800
Annealed 4340	0.37–0.43	0.7	Max 0.035	Max 0.04	0.7-0.9	0.2-0.3	1.83	0.23	738	815-845
Hardened 4340	0.38-0.44	0.73	Max 0.025	Max 0.02	0.8	0.2-0.3	1.78	0.23	738	815-845
Hardened 52100	0.98-1.1	0.35	Max 0.025	Max 0.025	1.45			0.23	738	775-800

The Fe-C phase diagram illustrating the nominal A_{c1} and A_{c3} temperatures for steels that have different carbon content is shown in Figure 3.1. The change in A_{c1} due to alloying (4340 steel) can be calculated using the experimentally developed formula [54] (see Eq. 3.1) and is found to be less than 17 ºC and therefore considered insignificant.

$$A_{c1} = 723 - 10.7Mn - 16.9Ni + 29.1Si + 16.9Cr + 290As + 6.38W \quad \textbf{(3.1)}$$

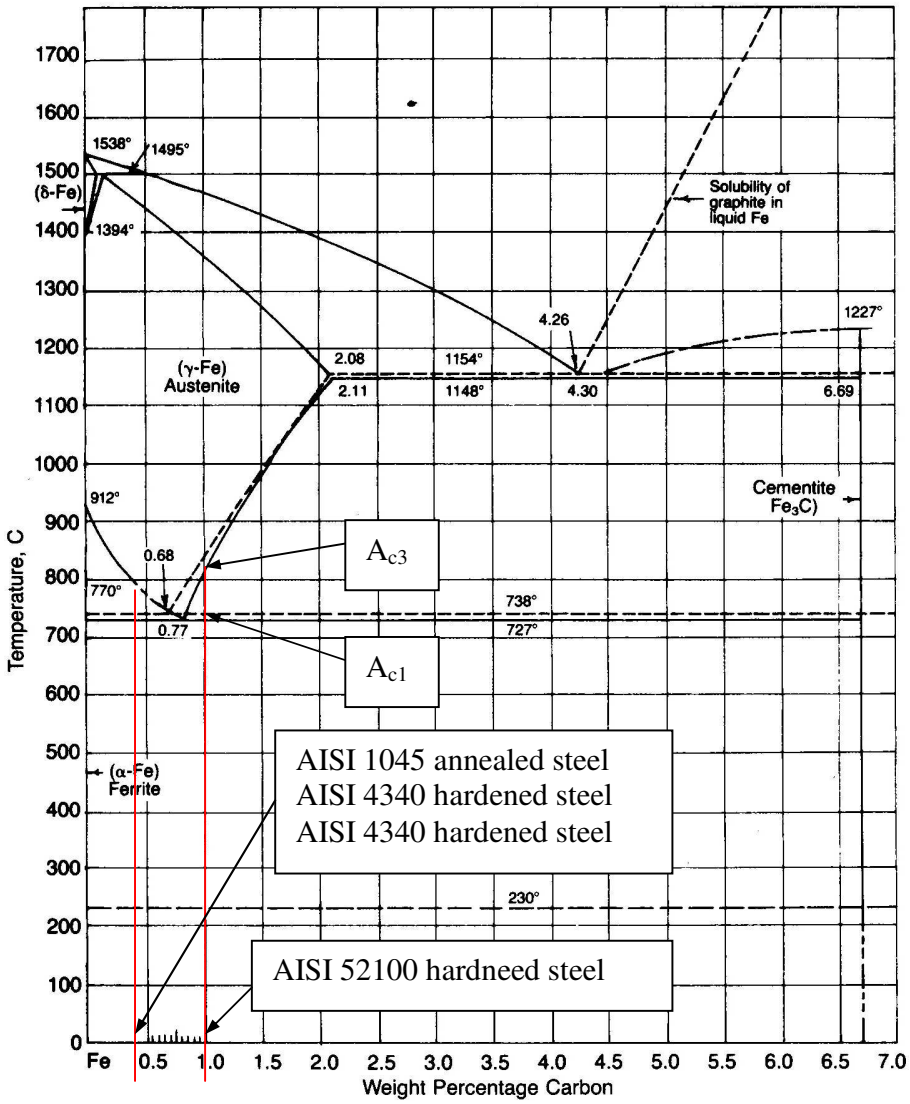

Figure 3.1. The Fe-C equilibrium phase diagram [54].

The thickness of white layer produced in orthogonal cutting of AISI 1045 and AISI 4340 annealed steels were compared to determine the effect of alloying on white layer formation. The effect of heat treatment on white layer formation was analyzed by comparing the annealed and hardened AISI 4340 steels. The effect of carbon content on white layer formation was studied by cutting through hardened AISI 52100 and AISI 4340 steels having the same hardness (53 HRC). Note that 52100 steel has almost twice the amount of carbon and fewer alloying elements than AISI 4340 steel. Consequently, an approximate understanding of the effect of carbon content on white layer formation can be obtained by comparing the results for the two hardened steels.

The average surface hardness of AISI 1045 and 4340 annealed steels was measured to be 99.1±1.4 and 98.0±0.8 HRB, respectively. Both AISI 52100 and 4340 annealed steel tubes (41 mm diameter, 2 mm thickness) were heat treated by holding them at 843 ºC and 830 ºC, respectively, for 2 hours, quenching in oil, and tempering at 316 ºC and 204 ºC, respectively, for 2 hours to obtain the same hardness. The average surface hardness of AISI 52100 and 4340 hardened steels was measured to be 53.5±0.8 and 53.1±0.5 HRC, respectively.

3.1.2 Cutting Conditions

The workpieces were prepared in the form of a tube with an average wall-thickness of 1.5 mm using a cleaning cut performed at 100 m/min, 0.05 mm depth of cut and 0.1 mm/rev feed. During the cleaning cut, coolant was applied to minimize the thermal and mechanical effects on the tube material. However, no coolant was used in the actual tests. Kennametal NG 3125L PCBN (KD081 grade) with a 0º rake angle tool

holder (NER-163D) was used for the machining tests listed in Table 3.2. The machining tests were done on a Hardinge T-42 SP CNC lathe. The experimental set-up used is shown in Figure 3.2. At the end of cut (5 mm axial length of cut), the tool was retracted quickly using the drill pecking cycle command.

Table 3.2. Orthogonal machining test matrix.

Workpiece material	Tool material	Speed	Flank wear	Feed
		(m/min)	(µm)	(mm/rev)
1045 annealed steel	PCBN KD081	100	100-120	0.1
4340 annealed steel	PCBN KD081	100	100-120	0.1
1045 annealed steel	PCBN KD081	300	100-120	0.1
4340 annealed steel	PCBN KD081	300	100-120	0.1
4340 hardened steel	PCBN KD081	100	100-120	0.1
52100 hardened steel	PCBN KD081	100	100-120	0.1
4340 hardened steel	PCBN KD081	300	100-120	0.1
52100 hardened steel	PCBN KD081	300	100-120	0.1

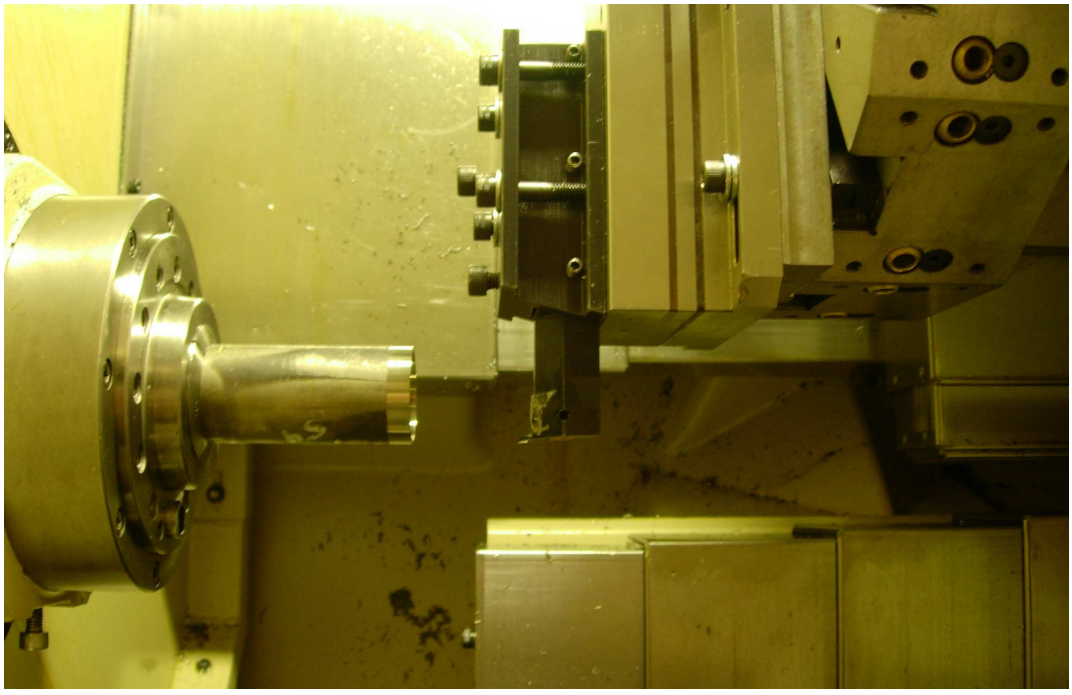

Figure 3.2. Experimental set-up for the orthogonal machining tests.

Each test was performed twice. Cutting forces were measured with a piezoelectric force dynamometer (Kistler Model 9257B). In order to ensure that crater wear generated during machining tests does not affect the rake angle of the tool, the tool flank and rake faces were inspected after each test. The total change in flank wear width and crater wear depth after all cutting tests was less than 10 μm.

3.1.3 Tool Wear Generation

Low content PcBN tools (Kennametal grade KD081) with upsharp edge preparation were used in all the tests. A known amount of flank wear was generated in the cutting tool by dry machining AISI 52100 hardened steel tube at 200 m/min and at a low depth of cut of 0.004 mm to minimize crater wear. After machining a total length of cut of 15 mm, flank wear in the range of 100-120 μm was generated. Very little crater wear was observed. The typical crater and flank wear of the PcBN tool before performing the cutting tests listed in Table 3.2 are shown in Figure 3.3. It can be seen that the flank wear generated is fairly uniform.

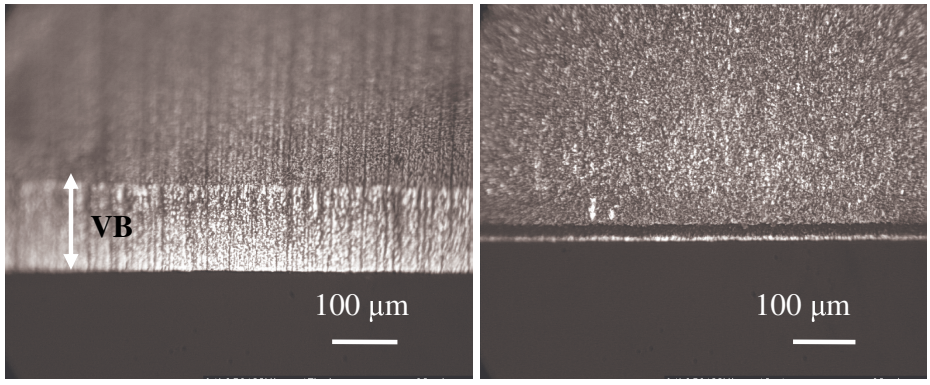

(a) (b)

Figure 3.3. (a) Flank and (b) Crater wear of the PCBN tool before cutting tests.

3.1.4 Procedure for Nano Indentation

In general, the white and transition layers in the machined sub-surface are very thin (less than 5 μm). Therefore, the nano indentation method was needed to measure the hardness of these layers. However, the region for nano indentation measurements should be at least 10 μm thick. Hence, the samples for nano indentation were taper-cut using a precision saw at 11° to the machined surface, which resulted in the exposure of a 20-25 μm thick white layer. The procedure for the taper-cut is shown schematically in Figure 3.4.

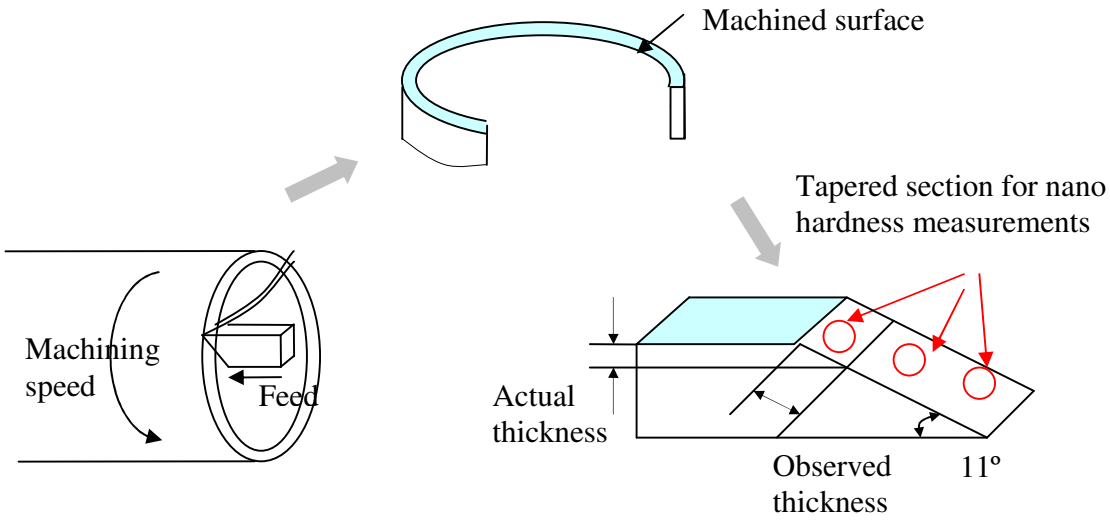

Figure 3.4. Procedure for taper sectioning the machined surface.

The samples were then mounted in a thermosetting compound and polished with 240 and 320 grit papers and Beuhler UltraPad™, Texmet 1000™, and Texmet 2000™ polishing cloths. Etching was performed using 2% Nital solution for 3-5 seconds to distinguish the white layer from the transition layer and the bulk. Nanoindentation tests using the MTS-80™ were then conducted on the etched specimens in the High Temperature Materials Laboratory at Oak Ridge National Laboratories. Hardness

measurements were made at 9-15 points each in the white layer, transition layer, and the bulk. Indentations using a Berkovich indenter [87] were made by loading until the given penetration depth was reached, the load held for 15 seconds, and then unloaded up to 20 % of the maximum loading. Each measurement was performed at three penetration depths of 100nm, 200nm, and 400nm. This was done to check the abrupt change in elastic modulus, which indicates an effect of the surface roughness and taper section. The elastic moduli change between the penetration depths of 100 nm and 200 nm were noted. For changes within 10 %, then the hardness data at 200nm penetration depth is reported, but when the change in elastic moduli is greater than 10 %, the hardness data at a penetration depth of 400 nm is reported.

3.2 Results and Discussion

3.2.1 Forces

A sample cutting force signal measured by the dynamometer is shown in Figure 3.5. It can be seen from this that the tool retraction is fairly fast and any effect on the cutting force signal is minimal.

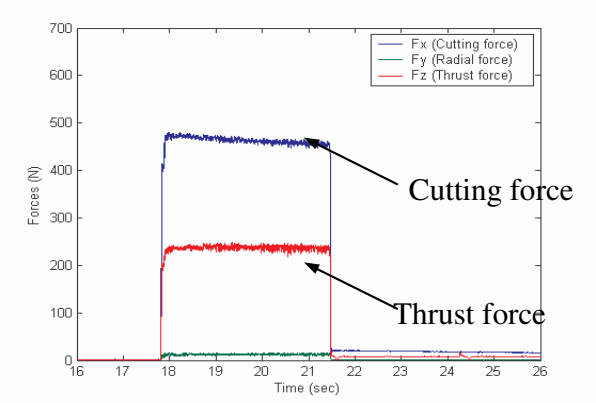

Figure 3.5. Cutting forces in machining of AISI 1045 annealed steel at 100 m/min with 110 µm flank wear.

The measured average cutting and thrust forces for all cutting conditions are shown in Figure 3.6. It can be seen from the figure that a higher thrust force compared to the cutting force is observed when machining hardened steel. The reverse is true for the annealed steels. This is attributed to the increased material hardness in the former case that is thought to lead to an increase in the frictional force on the tool rake face, which causes the higher thrust force.

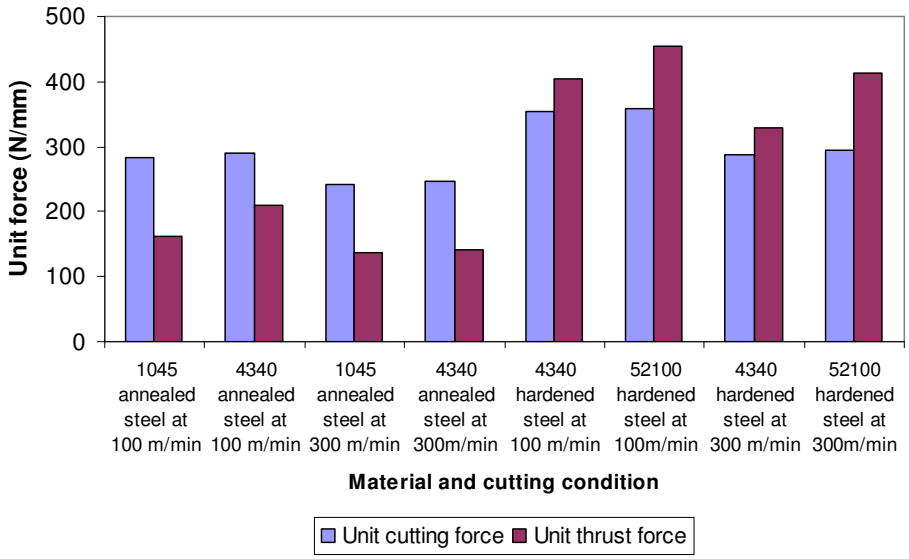

Figure 3.6. Average forces in machining of annealed and hardened steels.

3.2.2 White Layer Depth

The optical micrographs of the machined sub-surface and the average depth of white layer for each test condition are shown in Figure 3.7 and Figure 3.8 (for 100 m/min cutting speed) and Figure 3.9 and Figure 3.10 (for 300 m/min cutting speed), respectively. The average depth of white layer was estimated from the micrographs using 10 measurements per test condition. The variation of white layer depth around the tube was also examined and found to be less than 0.3 μm.

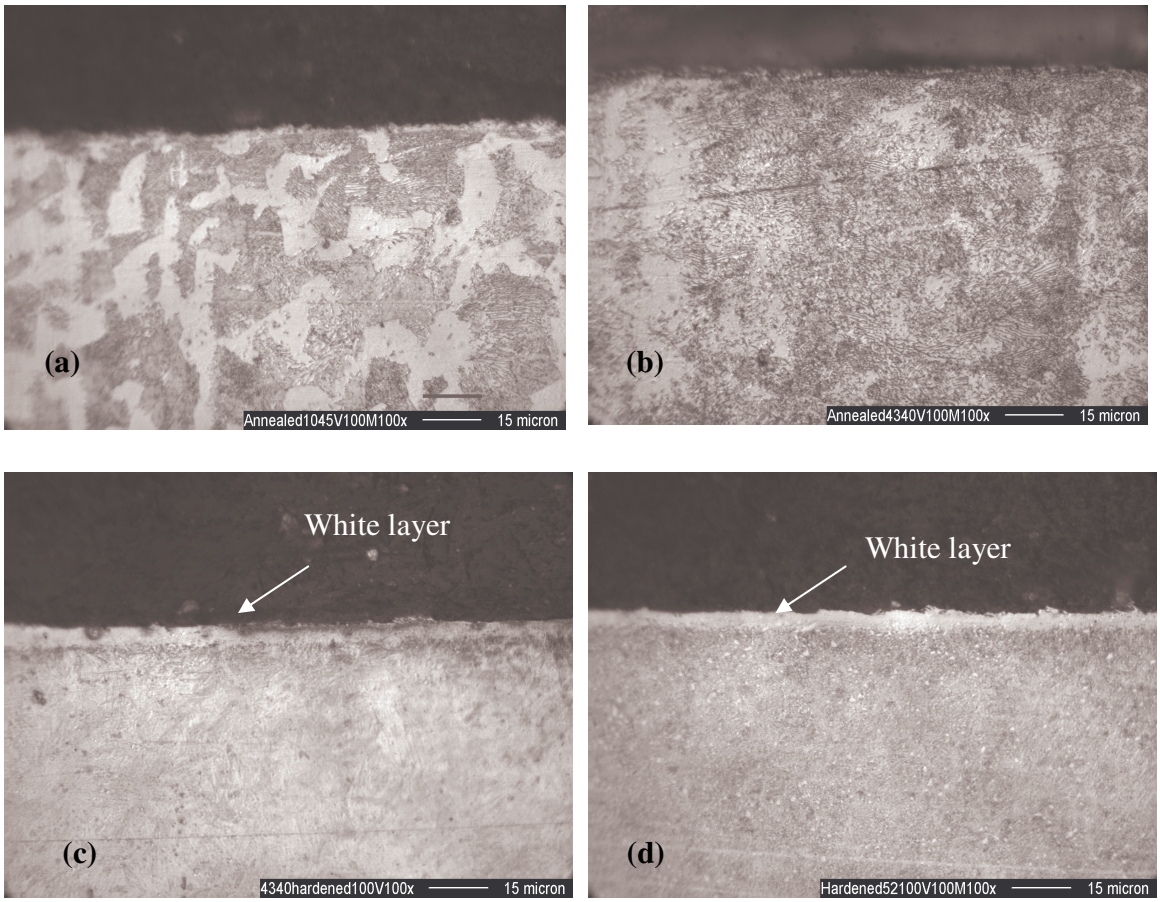

.

Figure 3.7. Micrographs of the four steels at 100 m/min with moderate flank wear land (100-120 µm): (a) AISI 1045 annealed steel, (b) AISI 4340 annealed steel, (c) AISI 4340 hardened steel, (d) AISI 52100 hardened steel.

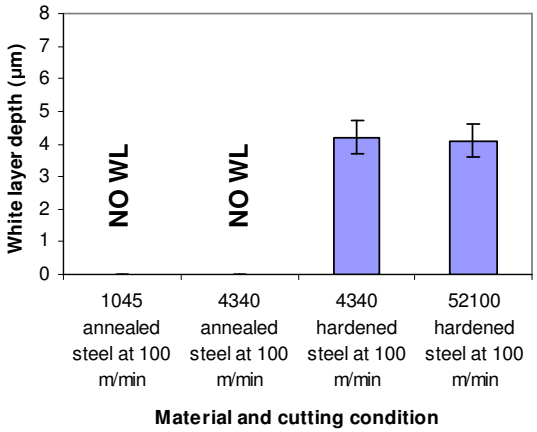

Figure 3.8. Depth of white layer at 100 m/min.

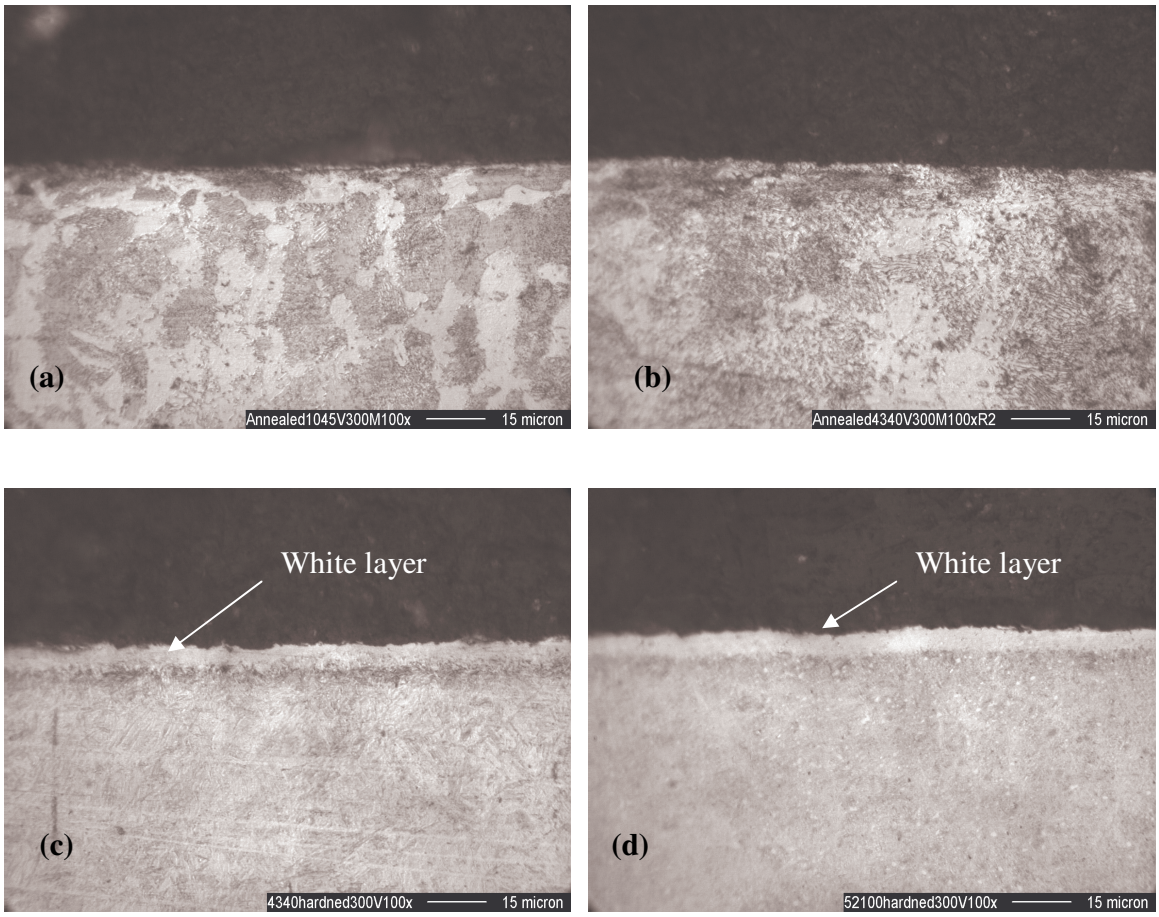

Figure 3.9. Micrographs of the four steels at 300 m/min with moderate flank wear land (100-120 µm): (a) AISI 1045 annealed steel, (b) AISI 4340 annealed steel, (c) AISI 4340 hardened steel, (d) AISI 52100 hardened steel.

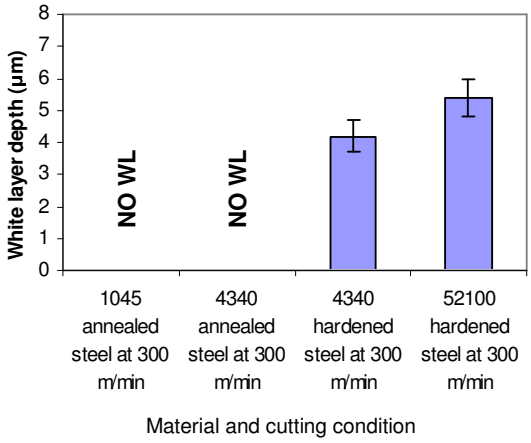

Figure 3.10. Depth of white layer at 300 m/min.

It can be seen from Figure 3.7 and Figure 3.8 that at 100 m/min no white layer is observed in both 1045 and 4340 annealed steels, while white layer is observed in the 4340 and 52100 hardened steels. Thus, at the lower cutting speed, it appears that alloy composition (1045 vs. 4340 annealed steel) does not affect white layer formation. At this speed, the carbon content (hardened 4340 vs. hardened 52100) does not appear to influence white layer depth significantly. However, heat treatment (annealed 4340 vs. hardened 4340) does have a significant effect on white layer formation at the lower cutting speed.

At 300 m/min (see Figure 3.9 and Figure 3.10), where cutting temperatures are generally higher, no white layer is observed in the 1045 and 4340 annealed steels, while white layer is observed in the hardened 4340 and 52100 steels. In addition, for cases exhibiting white layer, the variation in white layer depth with heat treatment and carbon content is noticeably large. Specifically, at the higher cutting speed, heat treatment and carbon content have a noitceable effect on white layer formation and its depth.

Possible explanations for the above observations of the effects of alloying, heat treatment and carbon content on white layer formation are given in the following paragraphs and sections. The explanations given below are derived from considerations of the influence of these variables on metallurgical transformation phenomena in steels. Possible correlations between the cutting temperature, plastic strains and stresses and white layer formation are analyzed later in section 4.3.

It is well known that the martensite start temperature (M_s) and TTT diagrams for steels are functions of the alloy composition of the steels [88]. The TTT diagrams are affected by any factor that affects the rate of nucleation and rate of growth of pearlite,

bainite, primary ferrite and primary iron carbide. One of these factors is chemical composition. Between 1045 and 4340 annealed steels, substantial differences in alloying elements such as Cr, Mo, Ni and Si can be noted (see Table 3.1). In pure heat treatment, these differences are known to lower the M_s temperature for 4340 annealed steel, thus lowering the extent of martensitic phase transformation [88]. The formula to calculate M_s as a function of alloying element concentration is given in Eq. 3.2. The M_s values for the 1045 and 4340 annealed steels were estimated from Eq. (3.2) [54] to be 334 ºC and 282 ºC, respectively, which differ by about 50 ºC.

$$M_s(^{\circ}C) = 561 - 474C - 33Mn - 17Cr - 17Ni - 21Mo \quad \textbf{(3.2)}$$

However, no difference in white layer thickness due to alloying (1045 vs. 4340 annealed steel) was observed in the current study suggesting that the temperatures produced in machining of the two annealed steels were most likely not high enough to cause α-γ transformation.

Heat treated 4340 and 52100 steels usually have some amount of retained austenite in the bulk [36, 46]. Annealed 1045 and 4340 steels typically do not have any austenite in the bulk. The formation of martensite depends on the start and the completion of α-γ transformation in the TTT diagram [89]. It is well-known that more martensite forms when more austenite is present prior to quenching. The martensite formation from austenite is shown schematically in Figure 3.11.

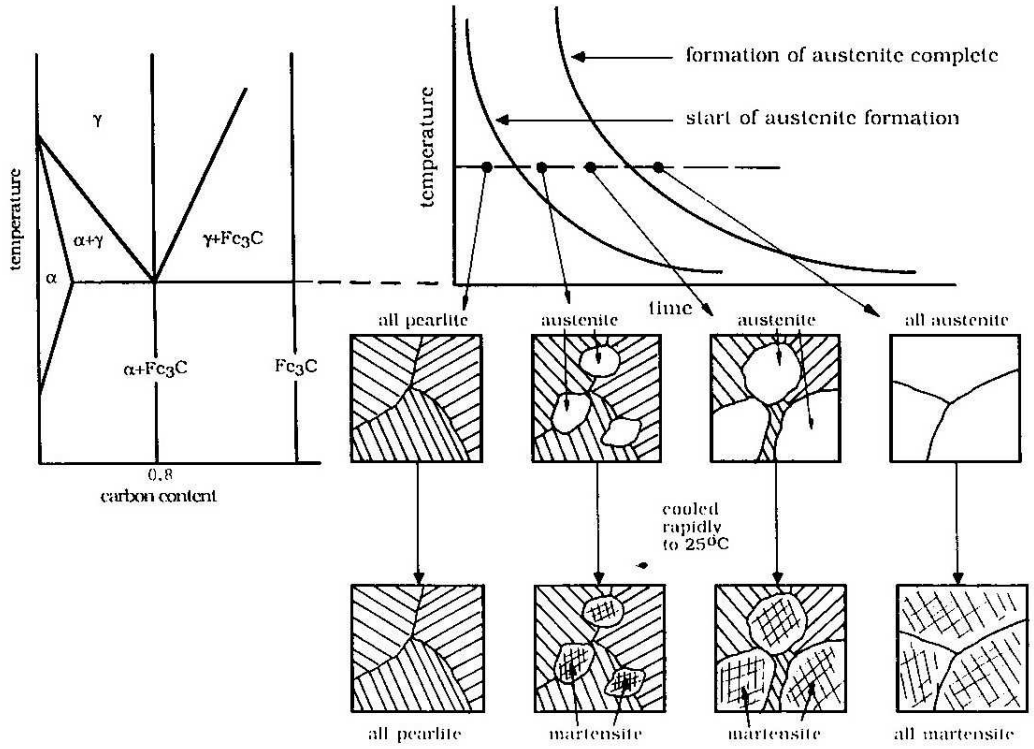

Figure 3.11. Schematic illustration of the formation of martensite from austenite [89].

The retained austenite present in the hardened 4340 steel prior to machining contributes to more martensitic phase transformation than the annealed 4340 steel. Thus, this factor enhances the formation of white layer in the hardened 4340 steel at both cutting speeds. The same reasoning can be extended to the general case of annealed versus hardened steels.

Thermally-induced phase transformation leading to martensitic hardening of steels is highly dependent on the presence of carbon. It is known that the amount of carbon and its distribution along with the thermal process that the steel undergoes, determines the final state. Also, it has been suggested that in machining/grinding of 4340 hardened steel [4] the time available at high temperature (800 ºC) for diffusion of atomic carbon in the austenite phase is sufficient. In addition, the associated plastic deformation is thought to assist in the decomposition of the carbide phase and the carbon diffusion process. Consequently, more martensitic phase transformation is likely to occur with increased carbon content. Therefore, a higher carbon content of steel (e.g. 52100 vs. 4340 hardened steel) combined with high temperature and plastic deformation tend to induce more martensitic phase transformation and hence white layer formation. Notice that this effect is more pronounced at the higher cutting speed used in the current study (see Figure 3.10) because higher cutting temperatures are expected at the higher speed. In contrast, no noticeable difference in white layer thickness (4340 vs. 52100 hardened steel) is observed at the low machining speed where the temperatures should be lower. Analysis of workpiece surface temperatures presented in section 3.3.1 also suggest that the maximum temperature for hardened 52100 steel is lower than for hardened 4340 steel at the lower cutting speed.

3.2.3 Hardness of White Layer

Typical micrographs showing the nano indents are given in Figure 3.12. Additional micrographs are given in APPENDIX A. Since the surface is taper cut at an 11 ° angle, a white layer of 20-25 µm thickness, five times thicker than cut by normal sectioning, is observed. In the machined annealed steel surface, where white layer is not

observed, indentations are performed in different phases such as ferrite and pearlite as shown in Figure 3.12. Hardness of the ferrite and pearlite grains is averaged over each region labeled as surface, transition, and bulk in Figure 3.12.

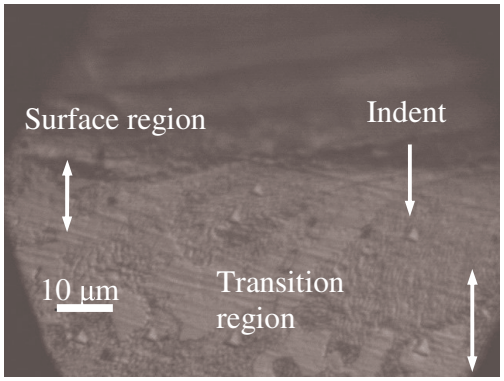

(a)

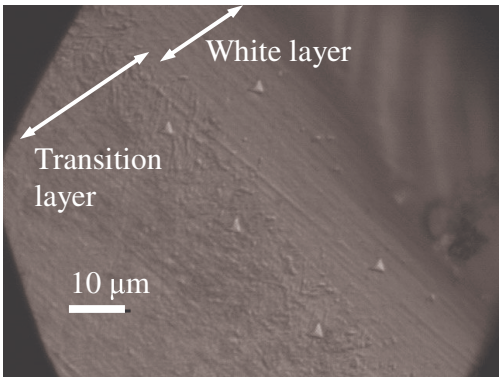

(b)

Figure 3.12. Micrographs showing nano indents in: (a) Surface and transition region in 1045 annealed steel machined at 300 m/min with 110 µm flank wear, (b) White layer and transition layer in 4340 hardened steel machined at 100 m/min with 110 µm flank wear.

The nano hardness was measured in the surface layer, transition layer, and in the bulk region of all the machined steel samples. Hardness data obtained at the cutting speed of 100 m/min are shown in Figure 3.13.

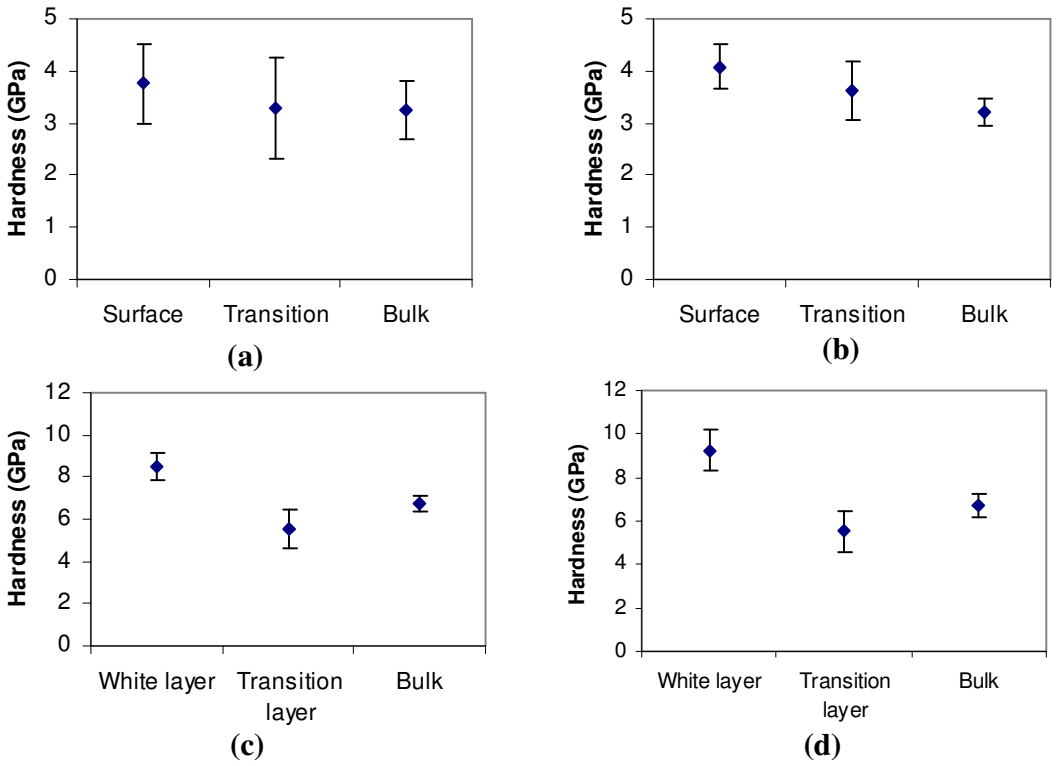

Figure 3.13. Nano hardness of the sub surface machined at 100 m/min with 110 µm flank wear land: (a) AISI 1045 annealed steel, (b) AISI 4340 annealed steel, (c) AISI 4340 hardened steel, (d) AISI 52100 hardened steel.

It can be seen from Figure 3.13 (a) and (b) that a higher mean hardness is observed in the 4340 annealed steel than in the 1045 annealed steel. This is attributed to alloying elements such as Mo and Cr present in the 4340 steel that tend to retard softening due to heat produced during cutting. It is not meaningful to compare the surface hardness measurements made in 4340 annealed and hardened steels, since the latter has been heat treated. However, substantial increase in the mean hardness of the white layer, about 2 GPa over the mean bulk hardness, is observed in the 4340 hardened steel after machining. This is in contrast to the small increase in hardness, about 0.5 GPa over the

bulk hardness, in 4340 annealed steel. Higher hardness is observed in the 52100 hardened steel white layer than in the 4340 hardened steel white layer. The former has about twice the carbon content, and have a chance to go through more martensitic phase transformation. It is well known that higher hardness is achieved in a more martensitic microstructure [88]. Therefore, higher hardness in the 52100 hardened steel white layer can be attributed to the higher carbon content. This result is consistent with other observations reported in the literature [46, 88].

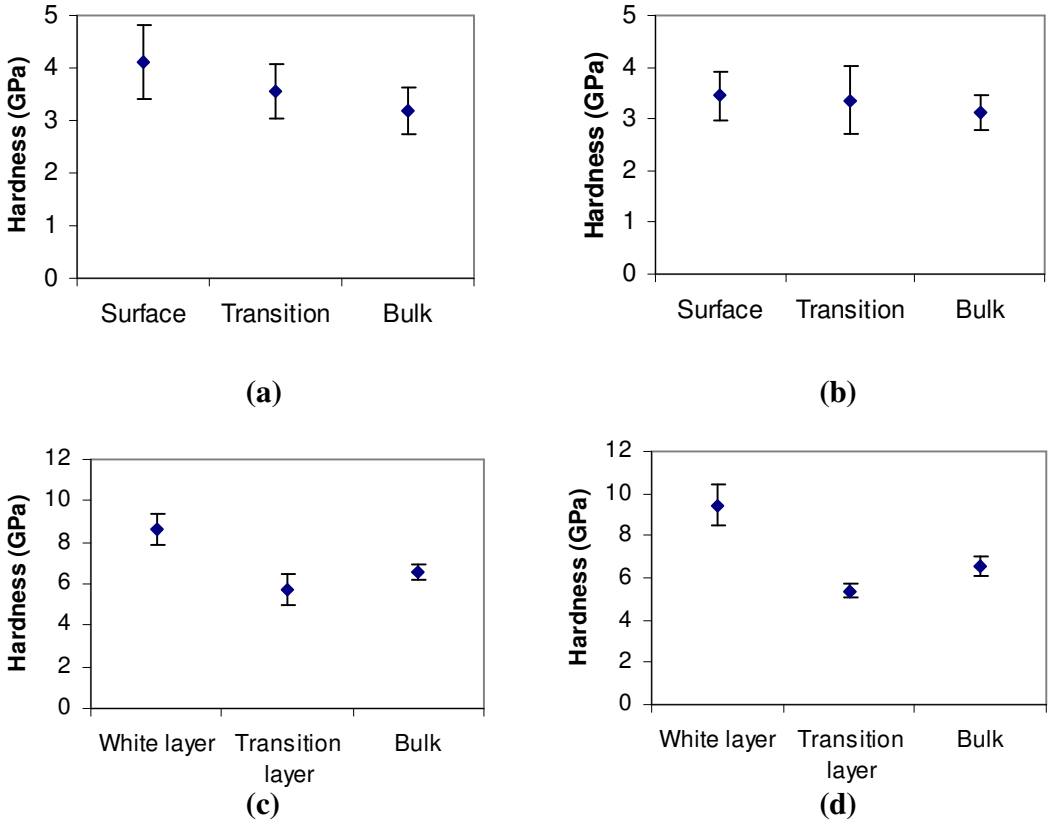

Figure 3.14. Nano hardness of the sub surface machined at 300 m/min with 110 µm flank wear land : (a) AISI 1045 annealed steel, (b) AISI 4340 annealed steel, (c) AISI 4340 hardened steel, (d) AISI 52100 hardened steel.

Hardness data obtained at the cutting speed of 300 m/min are shown in Figure 3.14. Cutting temperatures are higher at the higher cutting speed of 300 m/min. At this cutting speed, the mean hardness of the white layer in 4340 annealed steel is seen to be lower than in 1045 annealed steel (Figure 3.14). The difference in the hardness values for the two steels is found to be statistically significant at 5% level of significance. This can be attributed to the higher tempering temperature for 4340 annealed steel. It is also seen from Figure 3.14(b) and (c) that heat treatment affects the mean hardness at the higher machining speed. A substantial increase in the mean hardness, about 2 GPa over the mean bulk hardness, is observed in 4340 hardened steel due to white layer formation. A higher hardness is observed in the 52100 white layer at the high cutting speed. This is again attributed to the higher carbon content of 52100 steel, which promotes martensitic phase transformation. In all hardened steels, a higher mean hardness was seen in the surface and white layer regions compared to the bulk. In hardened steel, the transition layer had a noticeably lower mean hardness than the bulk due to a tempering effect.

3.3 Analysis of Temperatures, Plastic Strain and Stress

In order to further understand the effect of alloying, heat treatment and carbon content on the thermo-mechanical response of the four steels and how this response may be correlated with white layer formation and its hardness, finite element simulations were performed using a commercially available machining simulation software AdvantEdge® from Third Wave Systems. Of particular interest in these simulations was the maximum

workpiece surface temperature, and the maximum effective plastic strain and stress produced in the workpiece surface for each test condition examined earlier.

AdvantEdge® uses six node triangular elements as default. By implementing an adaptive remeshing technique [90], explicit use of a chip separation criterion is avoided in the analysis. The tool geometry was created and tool flank wear land incorporated using a custom tool editor. The top and right sides of the tool were fully constrained using a displacement boundary condition and a thermal boundary condition of 25°C. A velocity boundary condition, equal to the cutting speed, was applied to the workpiece. A constant friction coefficient was assumed to apply at the tool and workpiece interface. Flow stress models for the four kinds of steels available in the material database of the software were used in the analysis. For annealed and hardened steels, the hardness was modified in the software to reflect the measured hardness values given earlier. The model was verified by comparing the predicted and measured cutting forces as shown in Figure 3.16, which yielded average prediction errors less than 26%. Consequently, the simulation model is considered to be reasonable for the following analysis.

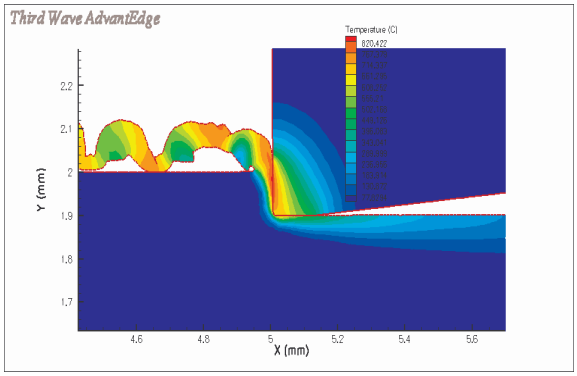

Figure 3.15. Temperature distribution at the tool flank-machined surface interface during machining of AISI 52100 hardened steel at 300 m/min and 0.1 mm/rev feed.

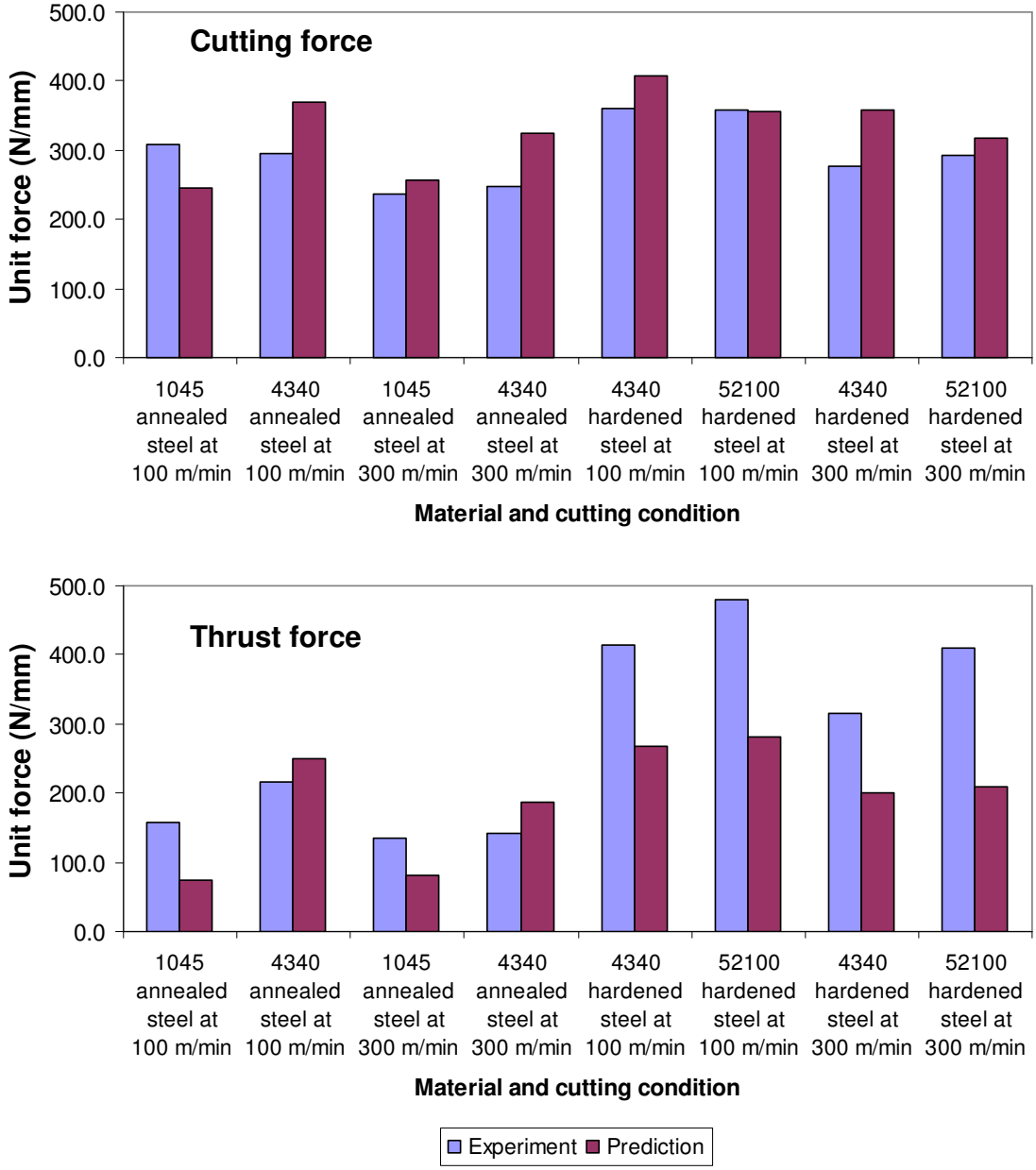

Figure 3.16. Comparison between the measured and predicted forces: (a) Cutting force, (b) Thrust force; 0.1 mm/rev feed, 100μm VB, dry cutting.

3.3.1 Workpiece Surface Temperatures

Figure 3.15 shows a typical simulated temperature distribution obtained from the software for one of the test conditions. The maximum workpiece surface temperature at

the tool flank-workpiece interface was obtained as follows: after the cutting force values reached steady state, the maximum workpiece surface temperature underneath the tool flank was extracted and averaged over ten time-steps in the simulation. The temperature values thus obtained were superimposed on the plot of white layer depth as shown in Figure 3.17 and Figure 3.18.

It can be seen from Figure 3.17 and Figure 3.18 that in almost all cases (except for 52100 hardened steel at 300 m/min), the simulated maximum workpiece surface temperature is less than the corresponding nominal austenitization temperature listed in Table 3.1. Also, the workpiece surface temperature generally tends to increase with alloying, heat treatment and carbon content, especially at the higher cutting speed. However, a clear-cut correlation between the computed maximum workpiece temperature and white layer formation/depth cannot be established.

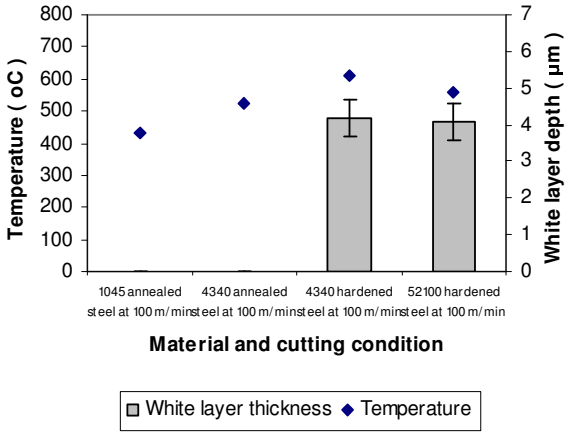

Figure 3.17. Maximum workpiece surface temperature and depth of white layer for each test condition at 100 m/min.

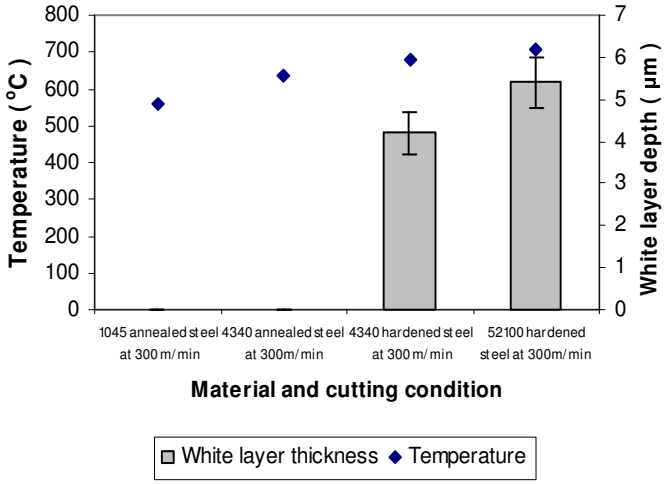

Figure 3.18. Maximum workpiece surface temperature and depth of white layer for each test condition at 300 m/min.

Workpiece surface temperatures in 1045 and 4340 annealed steels at both low and high machining speeds are below the nominal phase transformation temperature. They are not high enough to cause austenite formation, thus, martensitic phase transformation does not occur. Consequently, no white layer is observed in annealed steels at both high and low machining speeds.

On the other hand, at 100 and 300 m/min cutting speeds, as the predicted maximum workpiece surface temperature increases with heat treatment (4340 annealed steel vs. 4340 hardened steel), there is a significant increase in the white layer thickness. At 300 m/min cutting speed, a slight increase in the maximum surface temperature with increased carbon content (4340 vs. 52100 hardened steels) is accompanied by an increase in white layer thickness. Also, as noted before, all four steels have very similar values of the nominal austenitization temperatures – A_{C1} and A_{C3}. Thus, temperatures produced in the workpiece surface during cutting alone cannot explain the differences in white layer formation in the four materials.

In order to correlate the thermal effect with nano hardness measurements of the machined surface in annealed steel and white layer in hardened steel, the temperature values obtained in the simulation were superimposed on the nano hardness data as shown in Figure 3.19 and Figure 3.20.

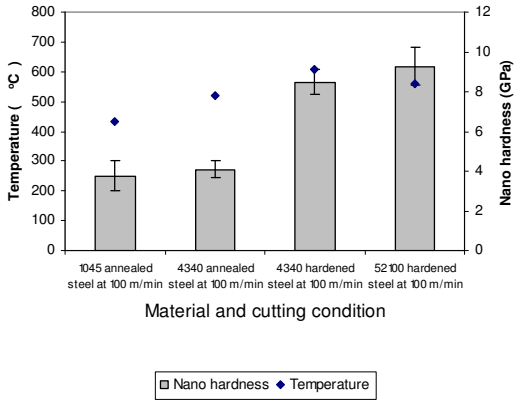

Figure 3.19. Maximum workpiece surface temperature and nano hardness of annealed steel surface and white layer in hardened steel for each test condition at 100 m/min.

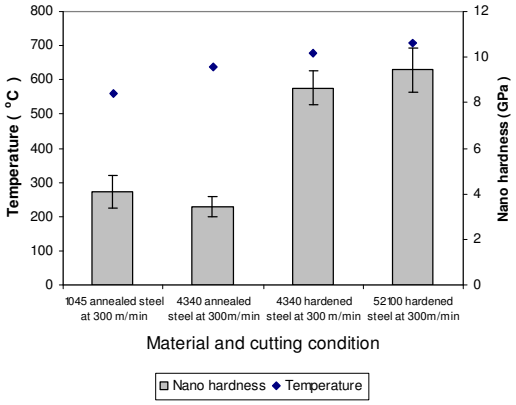

Figure 3.20. Maximum workpiece surface temperature and nano hardness of surface of annealed steel surface and white layer in hardened steel for each test condition at 300 m/min.

It is clear from the figures that there is no strong correlation between the increase in temperature and the white layer hardness at either cutting speed when considering the effects of alloying, heat treatment and carbon content. This suggests the role of factors

other than temperature on white layer formation. The following sections discuss the possible correlations with mechanical effects and white layer depth and hardness.

3.3.2 Effective Plastic Strain

The maximum effective plastic strain in the workpiece surface, an indicator of the severity of plastic deformation, was obtained by the same procedure used to find the maximum workpiece surface temperature. The strain values were then superimposed on the measured white layer depths as shown in Figure 3.21 and Figure 3.22.

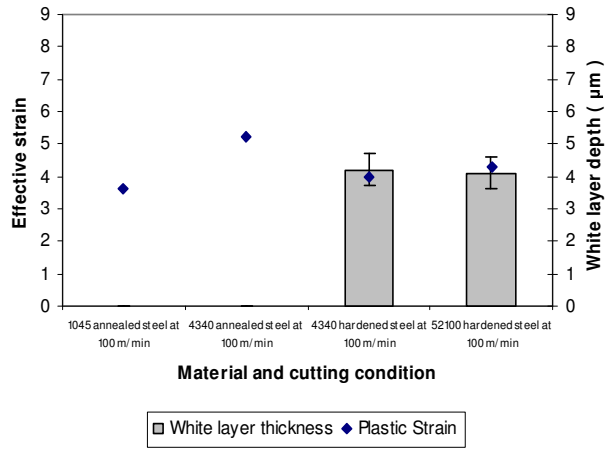

Figure 3.21. Maximum effective plastic strain and depth of white layer for each test condition at 100 m/min.

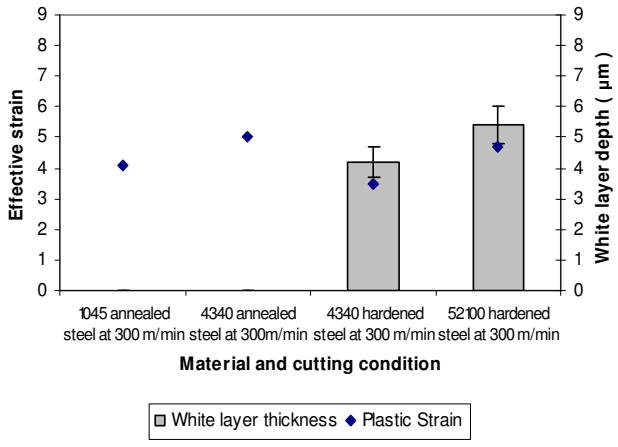

Figure 3.22. Maximum effective plastic strain and depth of white layer for each test condition at 300 m/min.

It can be seen from the figures that with alloying (1045 vs. 4340 annealed steel) the plastic strain increases at both cutting speeds. Since no white layer is observed in annealed steel, it is hard to conclude any correlation between white layer formation and plastic strain. However, the surface hardness data can provide some insight into the effect of mechanical working on white layer formation.

Increase in carbon content (4340 vs. 52100 hardened steels) produces a noticeable increase in the average plastic strain at the higher cutting speed. This, in combination with the higher workpiece surface temperature (see Figure 3.18), appears to be correlated with the observed increase in white layer depth. It can also be seen from Figure 3.22 that the increase in plastic strain with carbon content is accompanied by an increase in white layer depth.

In order to discuss possible correlation between the thermo-mechanical effect with nano hardness of the machined surfaces, the effective strain values obtained from the simulations were superimposed on the nano hardness data as shown in Figure 3.23 and Figure 3.24.

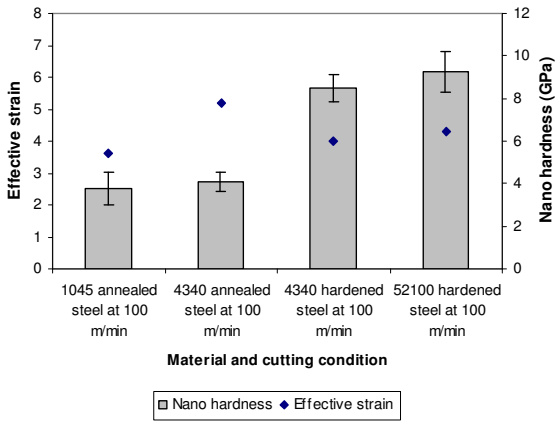

Figure 3.23. Maximum effective plastic strain and nano hardness for each test condition at 100 m/min.

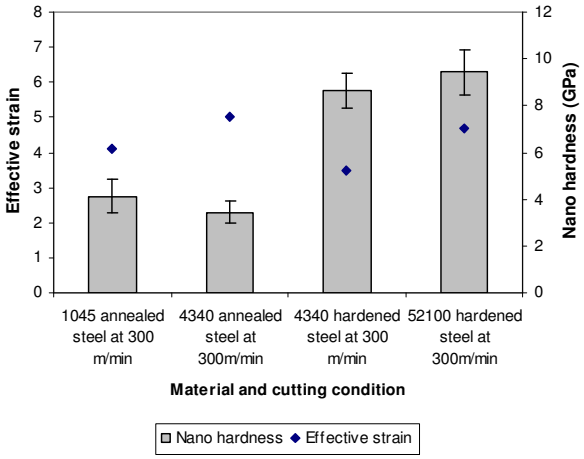

Figure 3.24. Maximum effective plastic strain and nano hardness for each test condition at 300m/min.

It is well-known that plastic deformation contributes to higher hardness in the sub surface [26]. Thus, higher strain in the surface layer of 4340 annealed steel compared to 1045 annealed steel is responsible for the higher hardness at 100 m/min as seen in Figure 3.23. The severe plastic deformation associated with cutting is known to yield a fine grain structure [36], which contributes to the higher hardness of the white layer. In contrast, a lower hardness for 4340 annealed steel compared to 1045 annealed steel at 300 m/min is seen. This is thought to be due to the higher workpiece surface temperature for 4340 annealed steel at 300 m/min, which causes a tempering effect. The increase in hardness of white layer with plastic strain is also evident for heat treated steels (4340 vs. 52100) at both cutting speeds.

3.3.3 Effective Stress

The maximum effective stress in the workpiece surface was determined by the same procedure used to find the maximum work surface temperature. The effective stress

values were then superimposed on the white layer depths as shown in Figure 3.25 and Figure 3.26.

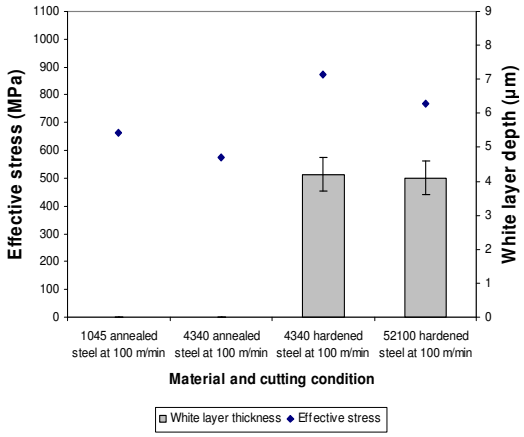

Figure 3.25. Maximum workpiece effective stress and depth of white layer for each test condition at 100 m/min.

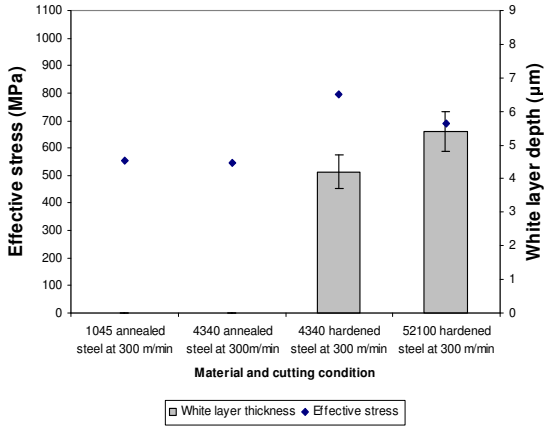

Figure 3.26. Maximum workpiece effective stress and depth of white layer for each test condition at 300 m/min.

As can be seen from Figure 3.25 and Figure 3.26, it is difficult to conclude any influence of the effective stress on white layer formation in annealed steels since no white layer was observed in this case.

The two hardened steels exhibit high effective stresses (700-900 MPa) at both cutting speeds. High effective stresses are believed to affect white layer formation by

promoting α - γ phase change through lowering of the phase transformation temperature [26,47]. Note that the maximum surface temperature in machining of hardened steels was below the nominal phase transformation temperature. The high effective stress is thought to lower the phase transformation temperature and therefore promote white layer formation. A higher effective stress would be expected to cause thicker white layer due to lowering of the phase transformation temperature. However, in Figure 3.25 and Figure 3.26, the same or thicker white layer is produced at a lower effective stress in 52100 hardened steel than in 4340 hardened steel. This suggests that other factors such as temperature and plastic strain associated with higher carbon content may affect white layer formation significantly.

In order to correlate the thermo-mechanical effect with nano hardness of the surface in the annealed steel and white layer in the hardened steel, the effective stress values obtained in the simulations were superimposed on the nano hardness (bar graphs) as shown in Figure 3.27 and Figure 3.28.

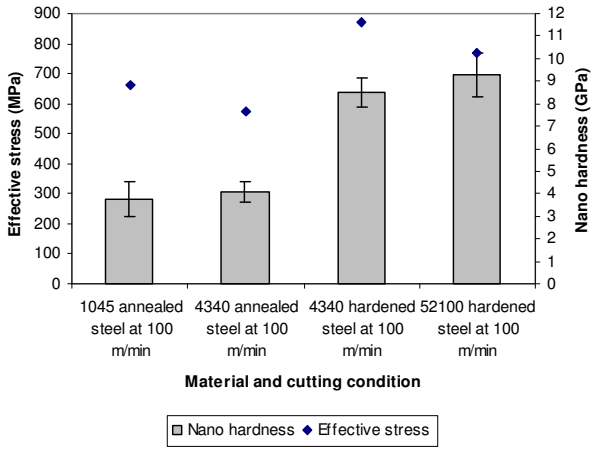

Figure 3.27. Maximum workpiece effective stress and nano hardness for each test condition at 100 m/min.

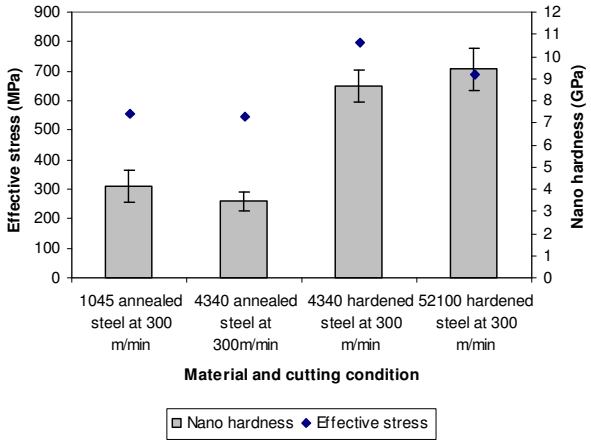

Figure 3.28. Maximum workpiece effective stress and nano hardness for each test condition at 300m/min.

As can be seen in Figure 3.27 and Figure 3.28, the higher stresses in hardened steel are thought to contribute to martensitic phase transformation by lowering the phase transformation temperature. Thus, the high hardness observed in hardened steel can be attributed to the martensitic structure in white layer.

3.4 Summary

The following conclusions can be drawn from this Chapter:

- No noticeable effect of alloying (1045 vs. 4340 annealed steel) on white layer formation and hardness is seen. This is possibly because the temperature was not high enough to cause α-γ transformation.

- Effect of heat treatment (4340 annealed vs. 4340 hardened steel) is to produce white layer at both cutting speeds. The retained austenite present in the bulk hardened steel enhances martensitic phase transformation, and thus promotes formation of white layer. Heat treatment leads to a substantial increase in white layer hardness (up to 2 GPa more than bulk hardness) at both cutting speeds.

- Increased carbon content of the steel (4340 vs. 52100 hardened steels) tends to increase white layer depth at the higher cutting speed while no difference is observed at the lower cutting speed. The former is attributed to the enhancement of martensitic phase transformation with more carbon diffusing into the austenite phase. Increased carbon content tends to increase white layer hardness at both cutting speeds.

- No correlation is evident between the workpiece surface temperatures, effective stresses and strains and white layer formation or hardness when considering the effect of alloying.

- The increase in white layer depth and hardness with heat treatment appears to be associated with an increase in workpiece surface temperature and effective stress.

- When considering the effect of carbon content, higher workpiece surface temperatures and higher effective plastic strains appear to increase the white layer depth at higher cutting speeds.

CHAPTER 4

CALCULATION OF THERMAL AND MECHANICAL EFFECTS ON THE WORKPIECE SURFACE

In order to quantify the influence of thermal (temperature) and mechanical phenomena (plastic deformation) that may be responsible for white layer formation, it is necessary to calculate the temperatures, stresses and strains acting on the workpiece surface during machining. It is well known that the maximum workpiece surface temperature (T_{max}) occurs at the trailing edge of the flank wear land [62, 68]. Since, in Chapter 5, the temperature is measured at the workpiece surface slightly behind the trailing edge of the flank wear land, it is necessary to calculate the maximum temperature at the trailing edge with the help of an analytical model. Also, the stresses and strains induced in the workpiece surface due to machining cannot be measured easily. Hence, an analytical model is used to calculate these quantities as well. The following sections describe the models used.

4.1 Maximum Workpiece Surface Temperature

4.1.1 Introduction

Temperature models for an unworn tool proposed by Komanduri [64,65,66] and for a worn tool proposed by Huang [67], and Chou [91] are employed to calculate the maximum temperature produced at the workpiece surface. The three major heat sources

in orthogonal cutting are: (1) Primary heat source due to plastic deformation in the shear zone, (2) Secondary heat source due to rubbing between the chip and the rake face of the tool, and (3) Heat source due to rubbing between the workpiece surface and the tool flank wear land. These heat sources are shown systematically in Figure 4.1.

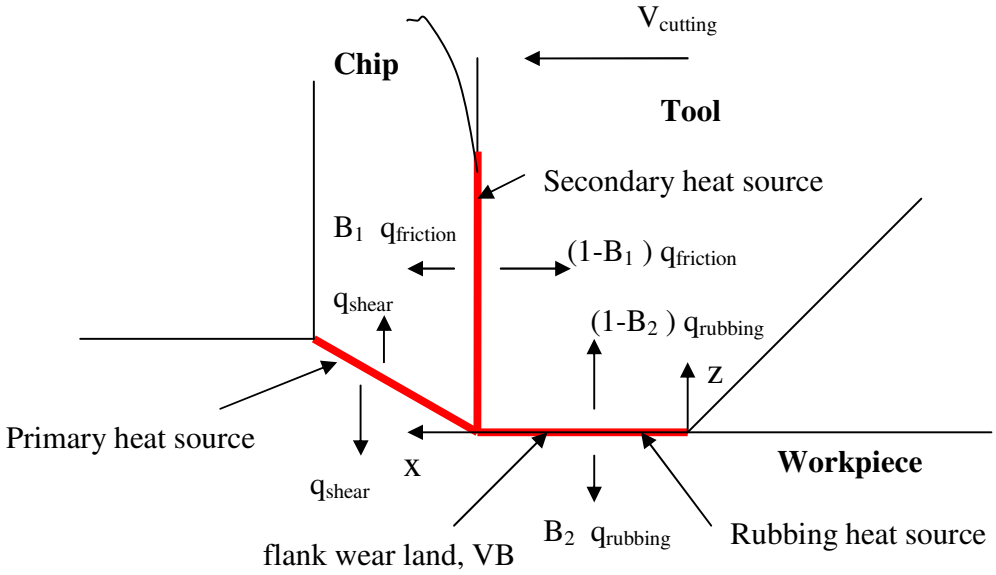

Figure 4.1. Major heat sources in orthogonal cutting [67].

As seen in Figure 4.1, q_{shear} , $q_{friction}$, and $q_{rubbing}$ denote the heat intensities generated by the primary, secondary, and rubbing heat sources. B_1 and B_2 are the fractions of the heat intensities transferred into the chip and the workpiece, respectively. The main modeling assumptions are as follows: (1) All deformation energy is converted into heat, and (2) The effect of the flank wear land heat source on the chip and the effect of the secondary deformation zone heat source on the workpiece are not significant. The latter assumption is thought to be reasonable based on prior experimental data [92],

which shows that the nominal increase in temperature of the rake face of a tool when cutting with a 150 µm flank wear land tool and 200 m/min cutting speed is only 75 °C. Thus, the secondary heat source is not considered in calculation of the temperature on the workpiece surface.

The model uses cutting and thrust forces with and without tool wear as inputs (defined and used below), which are measured from actual cutting tests. The forces are used to estimate the heat intensities generated on the shear plane and the flank wear land. The force increases due to flank wear are defined as follows:

$$\begin{aligned} F_{cw} &= cutting\ \ force\ with\ \ flank\ \ wear - cutting\ \ force\ without\ \ flank\ \ wear \\ F_{tw} &= thrust\ \ force\ with\ \ flank\ \ wear - thrust\ \ force\ without\ \ flank\ \ wear \end{aligned} \quad \textbf{(4.1)}$$

The heat intensities are calculated as shown in Eqs. (4.2), and are used to estimate the temperature rise on the workpiece surface.

$$\begin{aligned} q_{shear} &= \frac{F_s V_s}{Lw} \\ q_{rubbing} &= \frac{F_{cw} V_c}{VB\, w} \end{aligned} \quad \textbf{(4.2)}$$

Cutting ratio (r), shear angle (ϕ), shear force (F_s), shear velocity (V_s), length of the shear zone (L) are calculated using the standard theory of orthogonal cutting mechanics [93] and are by given by:

$$
\begin{aligned}
r &= \frac{t_u}{t_c} \\
\phi &= \tan^{-1}\left(\frac{r\cos\alpha}{1-r\sin\alpha}\right) \\
F_s &= F_c\cos\phi - F_t\sin\phi \\
V_s &= \frac{\cos\alpha}{\cos(\phi-\alpha)}V_c \\
L &= \frac{t_u}{\sin\phi}
\end{aligned}
\qquad \textbf{(4.3)}
$$

where, t_u is the depth of cut, t_c is the chip thickness and α is the rake angle.

Under the assumption that the temperatures in the workpiece and the tool are equal at the interface, the following equation can be written:

$$T_{workpiece-shear} + T_{workpiece-rubbing} = T_{tool-rubbing} \qquad \textbf{(4.4)}$$

where $T_{workpiece\text{-}shear}$ is the temperature rise due to primary heat source, $T_{workpiece\text{-}rubbing}$ is the temperature rise on the workpiece due to rubbing heat source, and $T_{tool\text{-}rubbing}$ is the temperature rise on the tool due to rubbing heat source.

The heat partition coefficient B_2 between the flank face and the workpiece is determined by matching the temperatures on each of the two contacting surfaces.

The next section describes the calculation of the temperatures on the workpiece surface and the tool at the flank wear land-workpiece interface.

4.1.2 Temperature Rise at the Workpiece Surface

The temperature model for the workpiece side of the flank wear land-workpiece interface is shown in Figure 4.2.

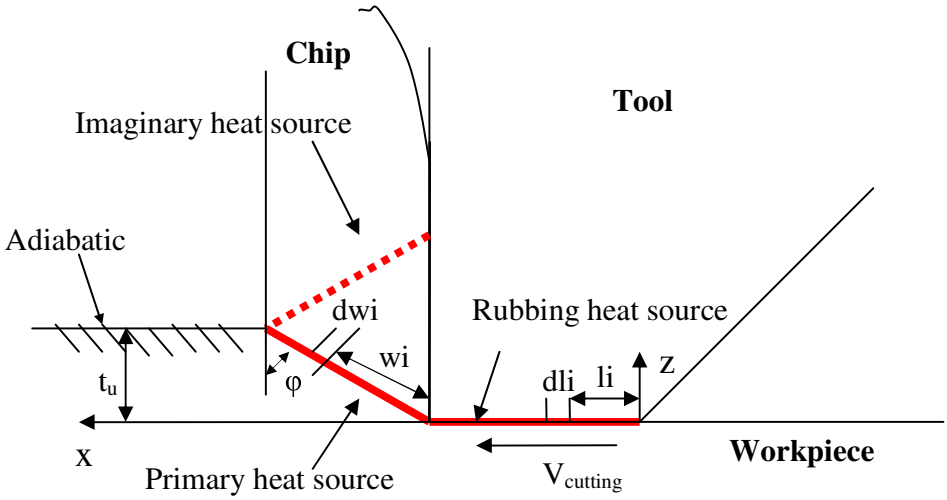

Figure 4.2. Temperature model for the workpiece side.

Komanduri and Hou [64] proposed that the primary heat source due to shear zone deformation moves obliquely at the cutting speed, $V_{cutting}$. The surface before machining is considered to be insulated. Thus, an imaginary heat source with the same heat intensity as the primary heat source is added as shown in Figure 4.2. Making use of Jeager's moving heat source theory [63], it can be shown that the temperature rise in the workpiece due to the shear plane heat source is given by:

$$T_{workpiece-shear}(x,z) =$$

$$\frac{1}{2\pi k_{workpiece}}\int_0^L q_{shear}\, e^{-\frac{(x-(VB-w_i\sin\varphi))V_{cutting}}{2a_{workpiece}}} \left\{ \begin{array}{l} K_0\left[\frac{V_{cutting}}{2a_{workpiece}}\sqrt{(x-(VB-w_i\sin\varphi))^2+(z-w_i\cos\varphi)^2}\right] \\ +K_0\left[\frac{V_{cutting}}{2a_{workpiece}}\sqrt{(x-(VB-w_i\sin\varphi))^2+(2t_u-z-w_i\cos\varphi)^2}\right] \end{array} \right\} dw_i \quad \textbf{(4.5)}$$

Huang [63] extended Komanduri and Hou's model by including the rubbing heat source at the flank-workpiece interface. He considered the rubbing heat source to

translate at a speed equal to $V_{cutting}$. He showed that the temperature rise at the workpiece surface due to rubbing by the flank wear land is given by:

$$T_{workpiece-rubbing}(x,z) = \frac{B_2 q_{rubbing}}{\pi k_{workpiece}} \int_0^{VB} e^{-\frac{(x-l_i)V_{cutting}}{2a_{workpiece}}} \left\{ K_0 \left[\frac{V_{cutting}}{2a_{workpiece}} \sqrt{(x-l_i)^2 + (z)^2} \right] \right\} dl_i \quad \textbf{(4.6)}$$

The temperature model for the tool side at the flank wear land-workpiece interface as proposed by Huang [67] is shown in Figure 4.3.

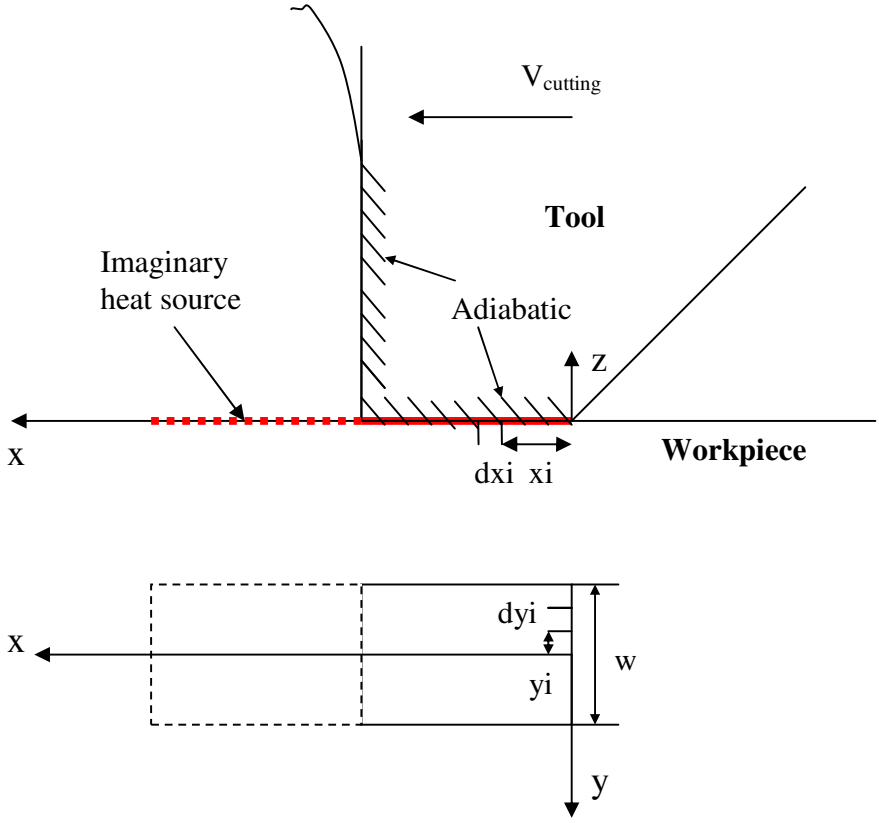

Figure 4.3. Temperature model for the tool side.

As can be seen in Figure 4.3, Huang [67] suggested a static rectangular heat source due to rubbing by the flank wear land. The tool-chip and tool-flank wear land

interfaces are assumed to be insulated. Thus, an imaginary heat source with the same heat intensity is added. Hence, the temperature rise at the tool due to rubbing by the flank wear land is given by [67]:

$$T_{tool-rubbing}(x, y, z) = \frac{[1-B_2]q_{rubbing}}{2\pi k_{tool}} \int_0^{VB} \int_{-\frac{w}{2}}^{\frac{w}{2}} \left(\frac{1}{R_i} + \frac{1}{R_i^{'}}\right) dx_i dy_i \qquad \textbf{(4.7)}$$

$$R_i = \sqrt{(x-x_i)^2 + (y-y_i)^2 + (z)^2}$$

$$R_i^{'} = \sqrt{(x-2VB+x_i)^2 + (y-y_i)^2 + (z)^2}$$

In each equation, the thermal properties such as thermal conductivity and diffusivity of the tool and the workpiece are involved. The thermal properties are known to vary with temperature. Hence, the next section discusses how the varying thermal properties are handled in the temperature calculations.

4.1.3 Thermal Property and Iterative Method of Calculation

The thermal conductivity of the carbide tool Kennametal grade (KC 730) is considered to be independent of the cutting temperature as suggested by Chao [62], Huang [63] and its value is taken to be taken to be 69 K/m-ºK. The variation of thermal diffusivity and thermal conductivity of the workpiece material (AISI 1045 annealed steel) with temperature is captured using a regression fit in the range between 100 and 800 ºC of thermal data obtained from literature [94]. Regression fits of the thermal diffusivity (denoted as *a*) and thermal conductivity (denoted as *k*) are shown in Figure 4.4.

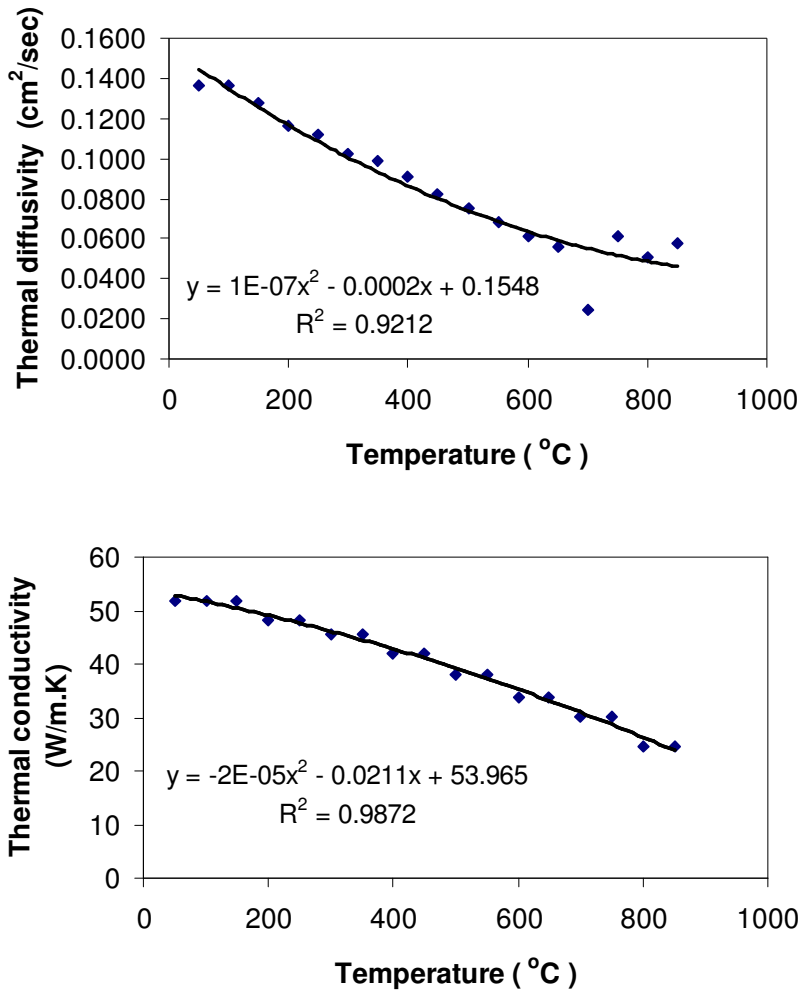

Figure 4.4. A regression fit of thermal diffusivity and thermal conductivity data for AISI 1045 annealed steel [94].

Iterative temperature calculations are performed to account for the temperature dependence of '*a*' and '*k*' as follows. Thermal diffusivity and conductivity at 300 ºC are used in the first step of the iteration. If the resulting maximum temperature obtained from the model is within 300±10 ºC, the iteration is terminated. Otherwise, thermal conductivity and diffusivity at the maximum temperature in the first iteration are input as the new diffusivity and conductivity values. The iterations are repeated until the

calculated temperature is within ±10ºC. In the case of VB=260 µm and VB=310 µm and for 200 m/min cutting speed, convergence was not obtained and for these cases the thermal conductivity and diffusivity values at 300 °C were used in the workpiece surface temperature calculations given in the next section and in Chapter 5. A flow chart summarizing the iterative temperature calculation procedure is shown in Figure 4.5.

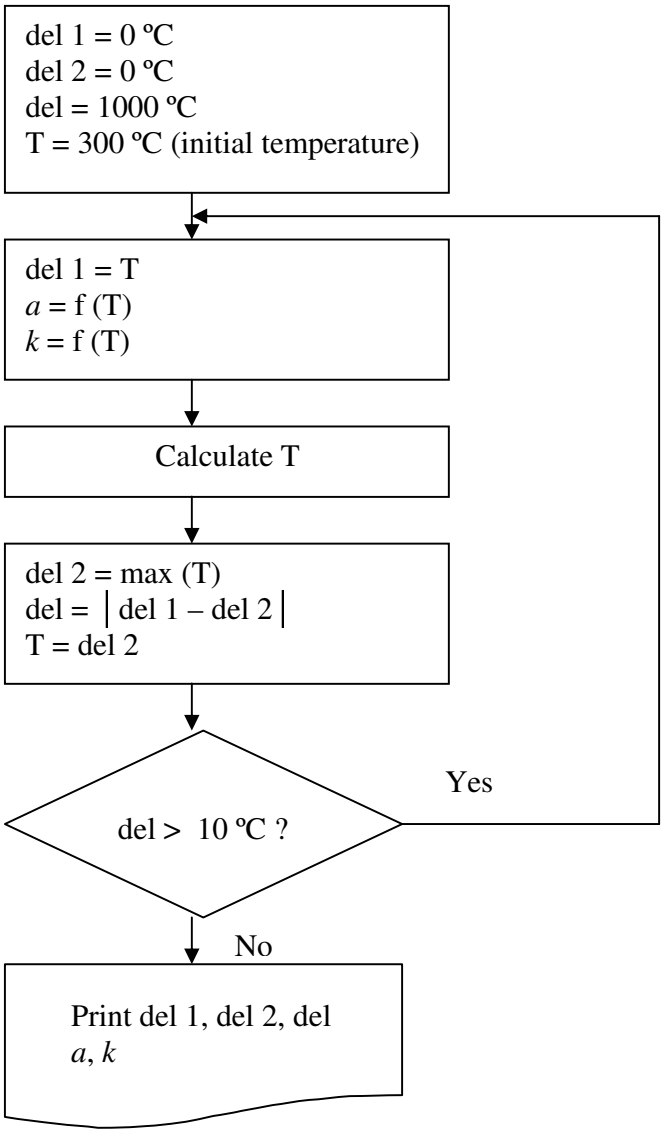

Figure 4.5. Flow chart of temperature calculation to account for temperature dependence of thermal conductivity and diffusivity.

4.1.4 Results and Discussion

The workpiece surface temperature distribution during orthogonal dry machining of AISI 1045 annealed steel as a function of the distance from the tool tip for different flank wear lands widths (100-600 µm VB), and for different machining speeds (100-200 m/min) with a fixed feed (0.1 mm/rev) are shown in Figure 4.6 and Figure 4.7. Thermocouple-based measurements of the workpiece surface temperatures right behind the trailing edge of the flank wear (presented in Chapter 5) are superimposed on the plot. The predicted temperatures are indicated by the curves while the marks represent experimental data. Note that in the two figures, the experimental data was obtained from thermocouples located a short distance behind the trailing edge of the tool flank wear land (see Chapter 5 for details). Consequently, the measured data points do not represent the maximum temperature, which is typically seen at the tool flank-workpiece interface.

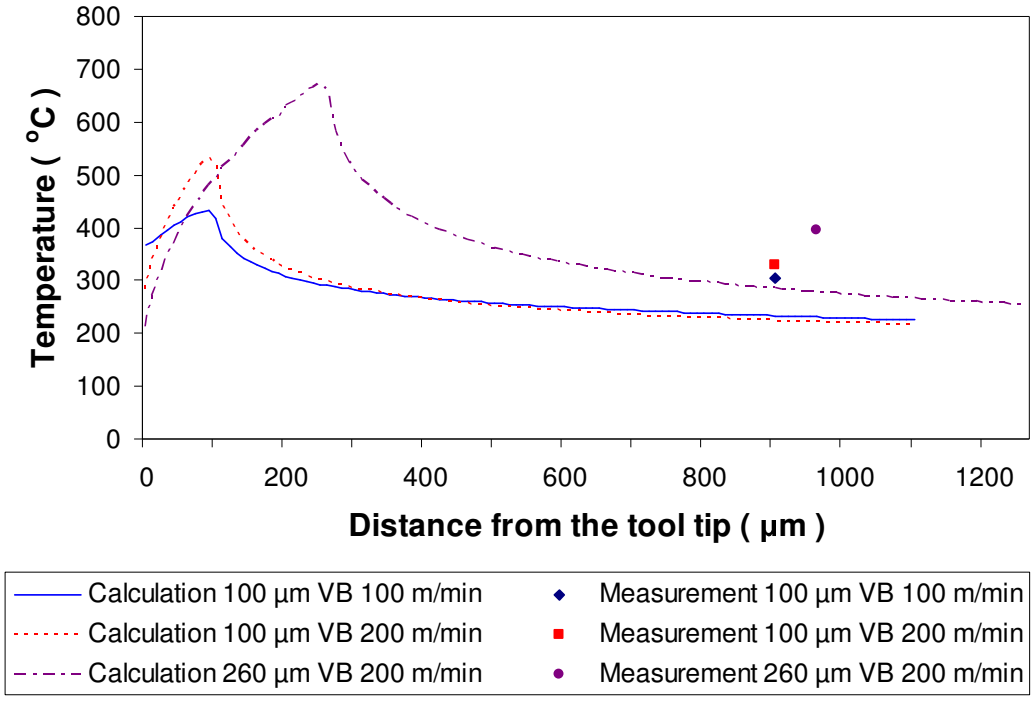

Figure 4.6.Temperature distribution on workpiece surface during machining of AISI 1045 annealed steel at different machining speeds and flank wear.

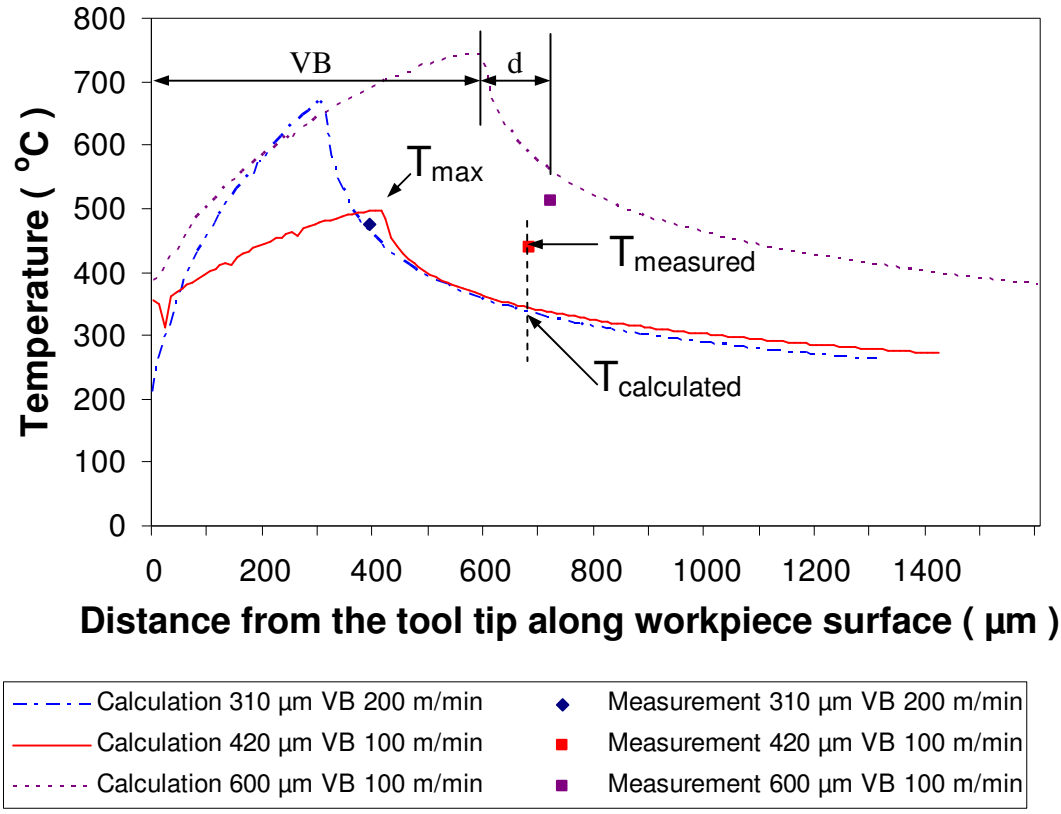

Figure 4.7.Temperature distribution on workpiece surface during machining of AISI 1045 annealed steel at different machining speeds and flank wear.

As can be seen in Figure 4.6 and Figure 4.7, the temperature model seems to provide a reasonable prediction of the workpiece surface temperatures during machining. Comparisons of the measured and calculated temperatures are given in Figure 4.8 and Table 4.1. Note that $T_{calculated}$ and $T_{measured}$ denote the calculated and measured temperatures, respectively, at each thermocouple bead located just behind the trailing edge of the flank wear land; *d* (in Table 4.1 and Figure 4.7) denotes the distance from the flank wear trailing edge to the upper edge of the thermocouple bead. T_{max} represents the

calculated maximum temperature at the trailing edge of the flank wear land. This temperature was calculated using the thermal model just described.

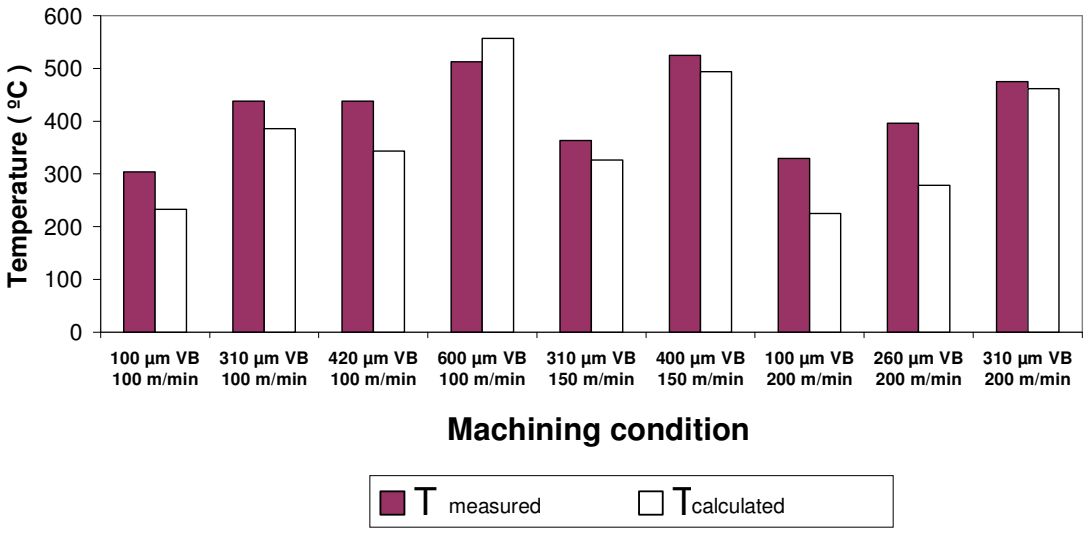

Figure 4.8. Measured vs. calculated workpiece surface temperatures for orthogonal dry machining of AISI 1045 annealed steel.

As can be seen in Figure 4.8, the measured temperature is slightly higher than the calculated temperature at the location of the measurement. In order to estimate the difference between the measured and calculated temperature, the % error is given in Table 4.1.

Table 4.1. Measured vs. calculated workpiece surface temperatures for orthogonal dry machining of AISI 1045 annealed steel.

Machining condition	T_{max} (ºC)	d (µm)	$T_{measured}$ (ºC)	$T_{calculated}$ (ºC)	Error between $T_{measured}$ and $T_{calculated}$ (%)
100 µm VB 100 m/min	433	800	304	233	23
310 µm VB 100 m/min	495	80	438	386	12
420 µm VB 100 m/min	497	260	438	343	22
600 µm VB 100 m/min	744	120	513	557	9
310 µm VB 150 m/min	612	580	363	326	10
400 µm VB 150 m/min	642	80	525	494	6
100 µm VB 200 m/min	532	800	329	225	32
260 µm VB 200 m/min	675	720	396	278	30
310 µm VB 200 m/min	668	80	475	462	3
Average					16

As can be seen from Table 4.1, the average percentage error between the calculated and measured temperature is less than 16%. Consequently, the maximum workpiece temperature, T_{max}, obtained from the temperature model in this chapter is considered to be a reasonable measure of the actual maximum workpiece surface temperature. This quantity is used in later chapters (5 and 6) to determine possible correlation with white layer formation.

The possible reason for the 16% or less prediction error is as follow. The flank wear land width and the distance between the thermocouple bead and the trailing edge of

the flank wear land are obtained by estimating the distance using a scale bar in the optical micrograph of the clearance face of the tool. This procedure can cause some error in the estimation of the bead location. Underestimation of the flank wear land width and overestimation of the bead location result in underestimation of the calculated temperatures. This can contribute to the observed differences between the measured and calculated temperatures.

It is noted that the measured workpiece surface temperature data obtained for AISI 1045 annealed steel in this study is comparable to the data reported in the literature. Hirao [41], Müller and Renz [43], and Usui et al. [44] have reported workpiece surface temperatures in cutting of 1045 annealed steel. Hirao measured the temperature by cutting the thermocouple wire embedded in the 1045 annealed workpiece while Müller obtained the temperature at a point 1 mm behind the major cutting edge using an optical pyrometer. In [41], the maximum workpiece temperature obtained was 400 ºC when cutting with 100 µm flank wear, 0.2 mm feed and 100 m/min cutting speed, which is comparable to the estimated maximum temperature of 433 ºC obtained in study when cutting with 100 µm flank wear, 0.1 mm feed and 100 m/min cutting speed. Usui et al. [44] used a very large flank wear land size of 600 µm because they had to cut the carbide insert in order to embed the thermocouple bead such that it was exposed on the flank wear land. Usui et al. report a maximum workpiece temperature of 737 ºC when cutting at 2 mm, 0.2 mm/rev feed and 100 m/min cutting speed cutting speed in bar turning. Even though the cutting process geometry is different between the current study and Usui et al's, it is interesting to note that their temperature is comparable to the estimated maximum temperature of 744 ºC in the current study for orthogonal cutting with 600 µm

flank wear land, 0.1 mm feed and 100 m/min cutting speed. The maximum temperature obtained from this temperature model is used as a measure of the thermal effect on white layer depth and the amount of retained austenite in Chapter 5.

4.2 Calculation of Stresses

4.2.1 Stresses on the Workpiece Surface

The mechanical stresses imposed on the workpiece surface due to tool flank-workpiece interaction are calculated in this section. Specifically, the normal and shear stresses (and the resulting effective stress) acting on the flank wear land are obtained using actual force measurements made during cutting. Cutting force (F_{cw}) and thrust force increase (F_{tw}) due to flank wear are obtained as discussed in the previous section.

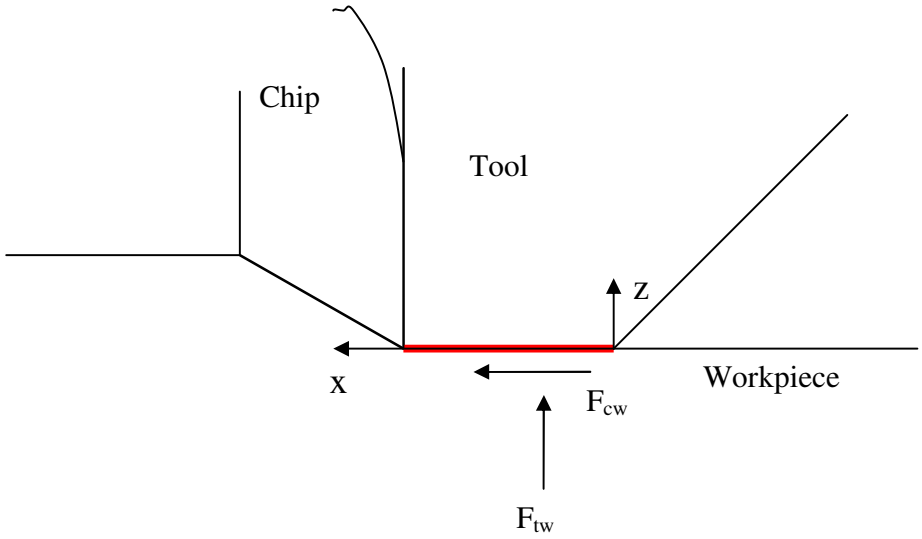

Figure 4.9. Average shear stress and normal stress on the flank wear.

The average shear and normal stresses acting on the flank wear land are then estimated as follows:

$$\tau = \frac{F_{cw}}{wVB} \tag{4.8}$$

$$\sigma = \frac{F_{tw}}{wVB} \tag{4.9}$$

Plane stress conditions are assumed because the ratio between uncut chip thickness and width of cut is less than 20 [95]. Thus, with the stress state, $\sigma_z = -\sigma$, $\tau_{xz} = \tau$ on the workpiece surface, the effective stress acting on the flank wear land is given by:

$$\begin{aligned} \sigma_{eff} &= \frac{1}{\sqrt{2}}\sqrt{(\sigma_x - \sigma_y)^2 + (\sigma_y - \sigma_z)^2 + (\sigma_z - \sigma_x)^2 + 6(\tau_{xy}^2 + \tau_{yz}^2 + \tau_{zx}^2)} \\ &= \sqrt{\sigma^2 + 3\tau^2} \end{aligned} \tag{4.10}$$

In case plane strain conditions are assumed, the stress state on the workpiece surface becomes [68] $\sigma_x = \sigma_y = \sigma_z = -\sigma$, $\tau_{xz} = \tau$. Thus, the effective stress acting on the flank wear land is given by:

$$\begin{aligned} \sigma'_{eff} &= \frac{1}{\sqrt{2}}\sqrt{(\sigma_x - \sigma_y)^2 + (\sigma_y - \sigma_z)^2 + (\sigma_z - \sigma_x)^2 + 6(\tau_{xy}^2 + \tau_{yz}^2 + \tau_{zx}^2)} \\ &= \sqrt{3\tau^2} \end{aligned} \tag{4.11}$$

4.2.2 Results and Discussion

The average shear/normal stress and the effective stress under plane stress and plane strain conditions at each machining condition are calculated and given in Table 4.2.

Table 4.2. Stresses on the workpiece surface at each machining condition.

Machining condition	σ (MPa)	τ (MPa)	σ_{eff} (plane stress) (MPa)	σ'_{eff} (plane strain) (MPa)
100 µm VB 100 m/min	329	271	573	469
420 µm VB 100 m/min	181	176	355	305
600 µm VB 100 m/min	222	222	444	385
100 µm VB 200 m/min	287	300	594	520
260 µm VB 200 m/min	316	336	662	582
310 µm VB 200 m/min	397	302	657	523

The plane strain condition leads to lower effective stress than under plane stress conditions. In what follows, plane stress condition is assumed because the ratio between the uncut chip thickness and width of cut is less than 20 [95] in the experimental work performed in this study. In some cases, the effective stress imposed on the workpiece surface under plane stress condition exceeds the tensile yield stress, 505 MPa of AISI 1045 annealed steel. This suggests that plastic deformation occurs in the workpiece surface layers. The level of stress is high enough to affect the A_{c1} temperature. The effect

of effective stress on A_{c1} temperature is discussed in Chapter 5. The effective stress obtained in this section is also used as a measure of the mechanical effect on white layer depth and the amount of retained austenite in Chapter 5.

4.3 Calculation of Strain

4.3.1 Plastic Strain on the Workpiece Surface

The calculation of plastic strain induced in the workpiece surface due to tool flank-workpiece interaction is discussed in this section. In the orthogonal cutting experiments performed in this study (See Chapters 5 and 6), the cutting force, thrust force, and the temperature increase as flank wear increases. Also, some material side flow is observed at both both edges of the workpiece surface. In addition, plastic flow in the workpiece surface in the machining of medium carbon steel is observed similar to other reports in literature [32,80] and is shown in Figure 4.10.

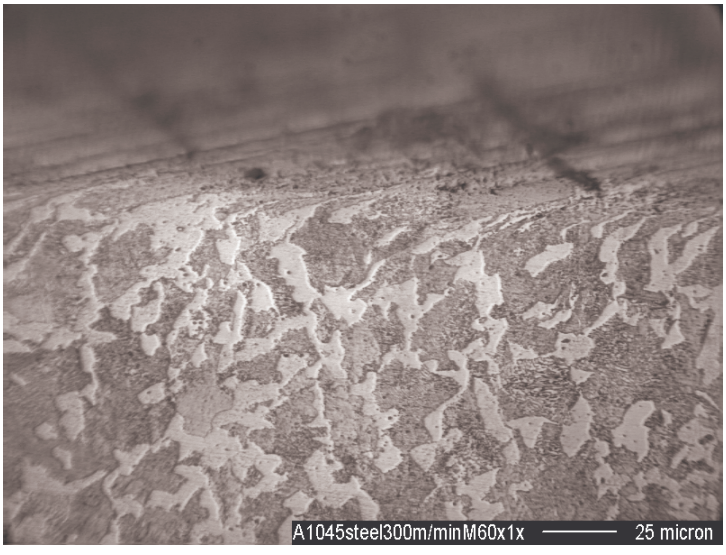

Figure 4.10. Microstructure revealing sub-surface plastic flow. (AISI annealed steel surface machined at 300 m/min cutting speed, 100 µm VB, 0.1 mm/rev feed with cBN tool).

The wedge analysis proposed by Thomsen et al. [68] is used to quantify the plastic deformation occurring beneath the flank wear land. Thomsen et al. [68] showed that the force and temperature increased when the workpiece made contact with a negative 1° clearance angle on the tool flank. Flash (material side flow) was observed at the tube edges as a result of plastic deformation. However, when the flank wear contact with the workpiece surface is flat, i.e. 0° clearance angle, the workpiece surface temperature and forces are constant. Hence, it is assumed here that the tool flank surface is not parallel to the cutting direction and that plastic deformation occurs in the workpiece surface layers under the flank wear land. A schematic diagram of the tool flank is shown in Figure 4.11.

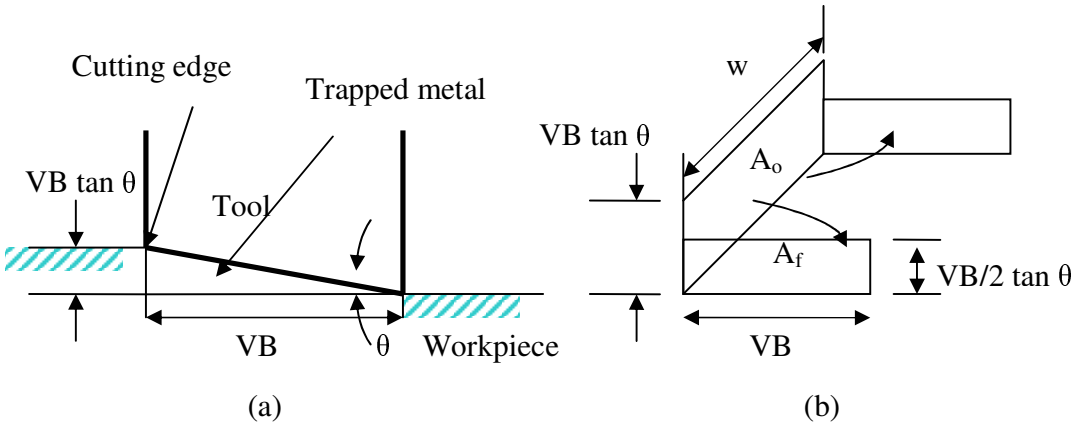

Figure 4.11. Schematic diagram: (a) side view, (b) 3D view to approximate entrapped work material area, A_o, and side extruded area, A_f, beneath the tool flank wear contact [68].

As illustrated in Figure 4.11, the metal trapped between the tool tip and the inclined flank is extruded to the workpiece sides. The plastic strain can then be calculated from the extrusion ratio as follows [68]:

$$\bar{\varepsilon} = \ln(\frac{A_o}{A_f}) = \ln(\frac{(VB\tan\theta)\times w}{2\times(\frac{VB\tan\theta}{2})\times VB}) = \ln(\frac{w}{VB}) \quad \textbf{(4.12)}$$

4.3.2 Results and Discussion

The effective strain on the workpiece surface for each machining condition is calculated and given in Table 4.2.

Table 4.3. Workpiece surface plastic strain.

Machining condition	$\bar{\varepsilon}$
100 µm VB 100 m/min	2.7
100 µm VB 200 m/min	2.7
260 µm VB 200 m/min	1.8
310 µm VB 200 m/min	1.6
420 µm VB 100 m/min	1.3
600 µm VB 100 m/min	0.9

The level of effective strain is fairly high and comparable to range of the shear strains in the shear zone (1.1-2.9) calculated using the parallel-sided shear zone model [61] for the cutting conditions used in the experiments (see Chapter 5). It is well known that the shear zone is characterized by a fine grain structure due to the shear deformation process. Thus, the plastic strains at the above machining conditions can contribute to the formation of fine grain structure in the machined surface as well. $\bar{\varepsilon}$ is used as a measure

of the mechanical effect on the presence/absence of white layer and retained austenite in Chapter 5.

4.4 Summary

The workpiece surface temperature was modeled analytically using the primary heat source due to plastic deformation in the shear zone and the heat source due to rubbing on the tool flank-workpiece interface. The calculated workpiece surface temperature shows good agreement with the measured temperature data with an average error of 16%. Thus, the maximum workpiece surface temperature obtained from the temperature model is considered to be reasonable for use in the analysis of the role of temperature on white layer formation. The maximum workpiece temperature obtained from the temperature model is used in Chapter 5 to analyze the thermal effect on white layer depth and amount of retained austenite.

The average normal and shear stress and the effective stress acting on the flank wear land are computed using actual force measurements made during cutting. The effective strain is obtained from an approximate wedge analysis of plastic flow below the interface between the tool flank wear land and the workpiece. Effective stress and plastic strain on the workpiece are used to analyze the role of mechanical effects on white layer depth and amount of retained austenite in Chapter 5. After examination of correlation between thermal/mechanical effects and formation of white layer in Chapter 5, an attempt is made in Chapter 6 to build a semi-empirical procedure that is a function of the thermal and mechanical effects to predict the presence or absence of white layer.

CHAPTER 5

WHITE LAYER FORMATION DUE TO PHASE TRANSFORMATION IN AISI 1045 ANNEALED STEEL

As discussed in Chapter 1 and 2, it is commonly believed that white layer formed during machining of steels is caused primarily by thermally-induced metallurgical phase transformation resulting from rapid heating and quenching. As a result, it is often assumed in the literature that if the temperature at the tool flank-workpiece interface exceeds the nominal phase transformation temperature for the steel, white layer forms. However, no attempt has been made to actually measure the temperatures produced at the tool flank-workpiece interface and correlate it with microstructural evidence of phase transformation. Consequently, this chapter aims to address these limitations through suitably designed experiments and analysis. AISI 1045 annealed steel is chosen as the workpiece material for the experiments because it does not contain any martensite or austenite prior to machining. Thus, the presence or absence of martensite or retained austenite after machining serves as evidence of phase change associated with white layer formation. Orthogonal machining tests are performed at different cutting speeds and tool flank wear. During machining, temperature measurements at the tool flank-workpiece interface are made using an exposed thermocouple technique. Metallography and optical microscopy of the machined sub-surface are conducted to detect the presence and depth of white layer. X-ray diffraction (XRD) measurements are performed to determine the

presence or absence of retained austenite phase in the machined surface layer. The measured workpiece surface temperatures and the underlying mechanisms that cause white layer on the machined surface of 1045 annealed steel are discussed.

5. 1 Experimental Work

Orthogonal machining of AISI 1045 annealed steel is performed at different cutting speeds and flank wear land widths to induce different thermal and mechanical effects on the workpiece surface. During machining, cutting forces and temperature at the tool flank-workpiece interface are measured to quantify the mechanical and thermal effects on the workpiece. After machining, optical micrographs generated using standard metallography techniques are used to confirm the presence/absence of white layer and XRD measurements are performed to check the presence/absence of retained austenite. The following section presents the details of the experimental work.

5.1.1 Workpiece Material

AISI 1045 annealed steel was chosen as the workpiece material for this study because it does not contain any martensite or austenite prior to machining. The presence/absence of retained austenite after machining then serves as evidence of metallurgical phase transformation. The workpiece hardness was measured to be 99.1±1.4 HRB using a Rockwell hardness tester. The nominal chemical content [32] and phase transformation temperature [54] for the steel are given in Table 3.1.

Table 5.1. Chemical content and nominal phase transformation temperatures (A_{c1} and A_{c3}) of AISI 1045 annealed steel.

Steel (AISI)	Composition (Weight %)								Ac_1 (ºC)	Ac_3 (ºC)
	C	Mn	P	S	Cr	Mo	Ni	Si		
Annealed 1045	0.42-0.5	0.6-0.9	Max 0.04	Max 0.05					727	800

5.1.2 Experimental Design

Several cutting speeds and flank wear land widths are used to induce different levels of thermal and mechanical effects on the workpiece surface. The experimental design used is given in Table 5.2. Note that the flank wear widths used in this study range from 100 – 600 µm. The unusually large flank wear land sizes are necessitated by the limitations of size and fragility of the thermocouple used in the temperature measurement technique discussed in section 5.1.3.

Table 5.2. Experimental design.

Worpiece material	Tool material	Machining speed	Flank wear width	Feed
		(m/min)	(µm)	(mm/rev)
1045 annealed steel	Carbide KC 730	100	100	0.1
		100	420	0.1
		100	600	0.1
		200	100	0.1
		200	260	0.1
		200	310	0.1

The workpiece was in the form of a 1.5 mm wall-thick tube with outer diameter of 41 mm. Kennametal NG3125L carbide (KC 730 grade) inserts with 0° rake angle tool holder (NER-163D) were used. A uniform flank wear land was generated by artificially

grinding the clearance face of the tool. Cutting forces were measured with a piezoelectric force dynamometer (Kistler Model 9257B). The tool flank-workpiece surface interface temperature was measured using an exposed thermocouple technique described below in detail.

5.1.3 Measurement of Workpiece Surface Temperature

The exposed thermocouple method [75] was employed to measure the workpiece surface temperature at the tool flank-workpiece interface during machining. A K-type thermocouple with a diameter of 75 μm insulated with Teflon® was used. A slot, perpendicular to the cutting edge and just intersecting the trailing edge of the flank wear land was made on the tool clearance face using the wire-EDM process (see Figure 5.1). Note that the 75 μm bead size necessitates the large flank wear land sizes used in the tests. Although smaller diameter thermocouples are available, they are very fragile and are typically uninsulated. These aspects made it difficult to use them in the current study.

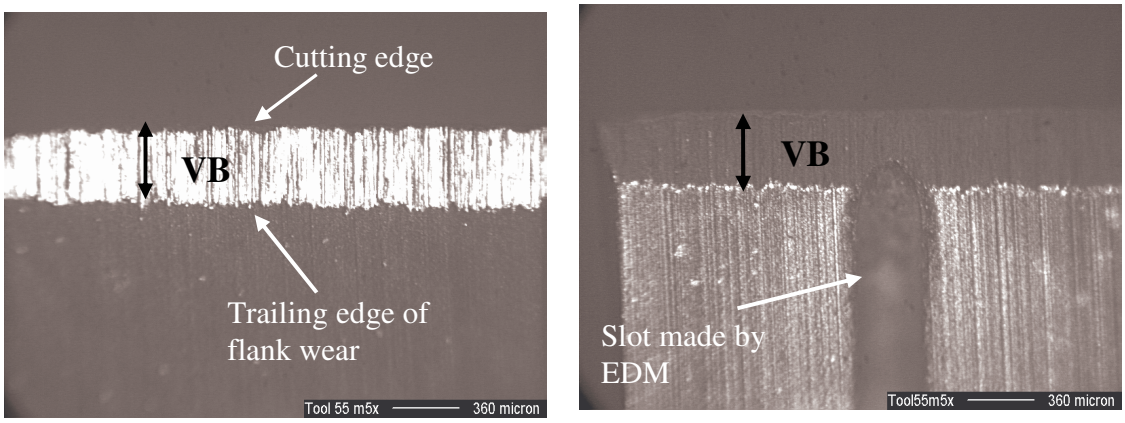

(a) (b)

Figure 5.1. (a) Tool flank wear generated by grinding, VB denotes mean flank wear land width, (b) Slot generated in clearance surface of the tool using wire-EDM.

The thermocouple bead was held in place in the slot by an epoxy glue (TRA-BOND 2151). The exposed part of the thermocouple bead was covered completely with epoxy. The epoxy was cured for 2 hours at a temperature of 65 ºC in a temperature-controlled furnace. The low thermal conductivity (0.95 W/m °K) and high dielectric strength (16 MV/m) of the epoxy provide the necessary thermal and electrical insulation for the thermocouple. During machining, the frictional interaction between the tool flank and machined surface exposes the thermocouple bead, which makes contact with the heated workpiece surface generating a small voltage signal. This signal is then amplified by a signal conditioner. The voltage signal was collected using ad data acquisition from system at a sampling frequency of 1 kHz. The exact location of the exposed bead was measured using an optical microscope after the test (see Figure 5.2 b).

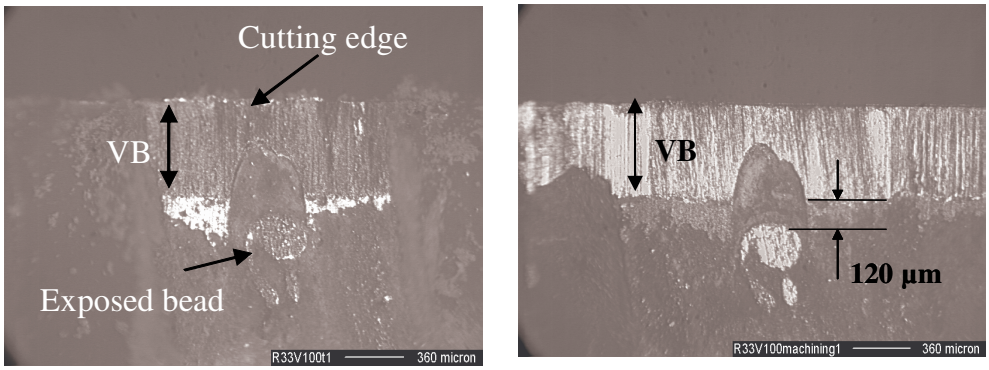

(a) (b)

Figure 5.2. Bead location after cleaning cut and after machining test.

Note that in the actual tests, a short cleaning cut of 0.1 mm axial length was used to expose the bead by removing the epoxy that covers it. Figure 5.2 (a) shows a picture of the exposed 200 µm diameter bead after the cleaning cut. It can be seen that the bead is close to the trailing edge of the flank wear land. Figure 5.2 (b) shows the bead after performing a 3 mm axial length of cut. The bead has moved about 120 µm away

from the trailing edge of the flank wear land after the machining test. As can be seen from Figure 5.2, the flank wear width is relatively unchanged after the machining test. Since the thermocouple slot overlapping the flank wear land is small compared to the entire contact area of the flank with the workpiece, the effect of the slot on the measured temperature is considered to be negligible.

Literature [41] reports that measurements made with thermocouples of diameters 25 µm, 200 µm and 1 mm, give almost the same temperature of the workpiece surface during machining of 1045 steel. Hence, in this study, the distance from the trailing edge of the flank wear to the upper boundary of the bead is the considered to be the location of measured temperature on the workpiece surface. A typical EMF (Electro Motive Force) signal obtained from the 75 µm diameter thermocouple and the corresponding cutting forces measured by the dynamometer during orthogonal machining with the 600 µm flank wear width tool at 100 m/min cutting speed is shown in Figure 5.3.

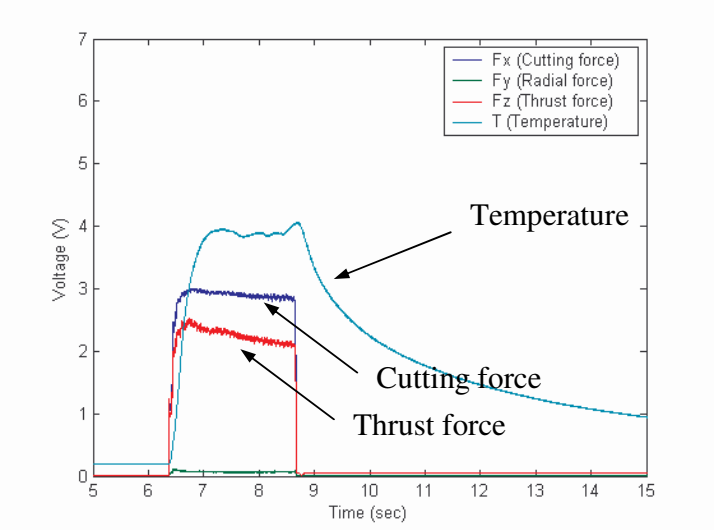

Figure 5.3. Sample temperature and force signals for 600 µm VB tool at 100 m/min and 0.1 mm/rev feed.

As can be seen in Figure 5.3, the workpiece surface temperature has reached steady state, which is consistent with the relatively steady force signal. Thus, the response time [76] of less than 0.05 sec of the 75 µm diameter thermocouple does not affect the temperature obtained in this measurement significantly. Similar trends in reaching steady state workpiece temperatures have been reported by Müller [42]. Using the thermocouple calibration data presented in Figure 5.4, the actual temperature data at each machining condition were obtained.

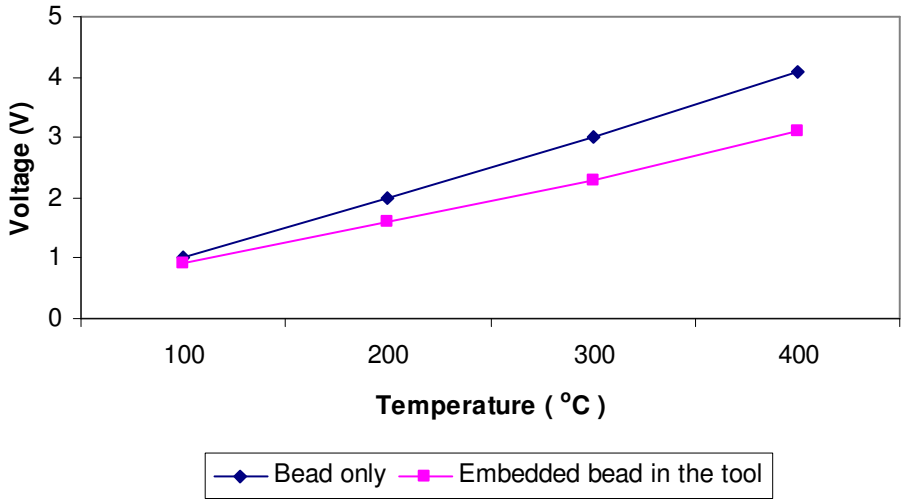

Figure 5.4. Voltage vs temperature of the thermocouple only and thermocouple embedded in the tool.

Calibration of the thermocouple is achieved by touching the exposed bead which is still embedded in the tool after machining to the hot plate in 100 °C intervals. It is known that the thermoelectric voltage can be affected by the environment [97]. To verify this, a thermocouple that is not embedded in the tool and that has not been used in any machining test is also used to the measure the hot plate surface in each 100 °C intervals. This is done to confirm the temperature and study the effect of the embedment. The voltage vs temperature of these two thermocouples, embedded and non-embedded is

shown in Figure 5.4. It can be noted that the effect of embedment is to reduce the voltage signal. The voltage signal of the embedded thermocouple is used for calibration purposes.

5.1.4 Test Procedure

Orthogonal dry machining tests of 3 mm axial length of cut were carried out on a Hardinge T-42 SP CNC lathe at the conditions listed in Table 5.2. In orthogonal tube cutting, the tool is fed axially into the tubular workpiece (See Figure 5.5).

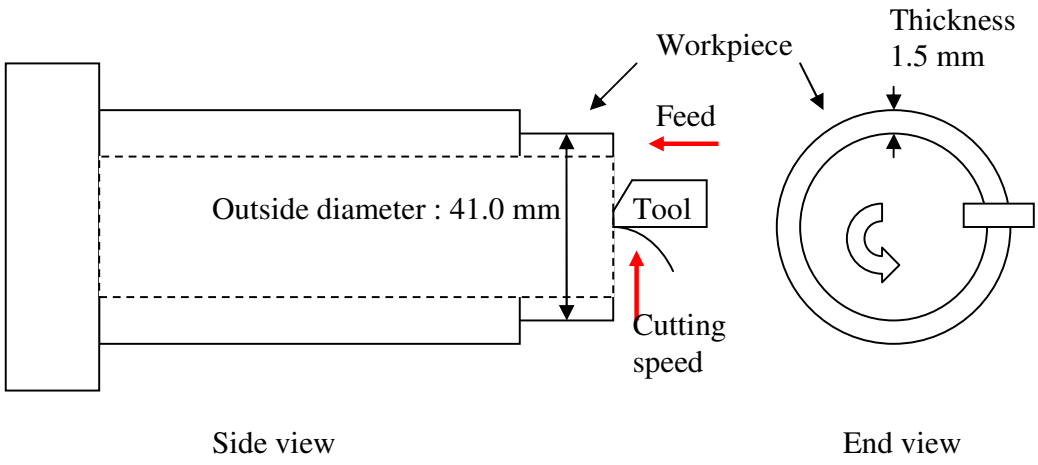

Figure 5.5. . Schematic diagram of the orthogonal machining performed on a lathe.

Upon stopping the feed movement of the tool or upon stopping the spindle, the tool continues to the rub against the workpiece surface for a short distance. In order to avoid the effect of rubbing on the white layer formed during actual chip formation, the following procedure was adopted. As the tool reached the final length of cut of 3 mm, it was retracted quickly (using the drill pecking cycle command G74), while maintaining the spindle speed for the test. Since the tool retraction occurs in a finite time interval,

parts of the machined tube face are subjected to a varying depth of cut as the tool disengages from the workpiece. In order to determine what portion of the tube is affected by this, the following test was conducted. The tube face was painted with a permanent marker and the tool fed into it at 0.1 mm/rev for a distance equal to half the feed i.e. 0.05 mm. Ideally, under instantaneous retraction, exactly one half of the tube face (180^o) should be cut by the tool. Since the retraction is not instantaneous, the cut extends past 180^o. The tube face was inspected and it was found that the cut extended beyond the expected amount by about 10 degrees at 100 m/min cutting speed and 30 degrees at 300 m/min cutting speed. This can be seen in Figure 5.6, where the bright, shiny surface is the actual cut surface while the dark portion is the painted surface. The dwell zone indicates the region of rubbing. Thus, in the actual machining tests, a 10^o portion of the tube at 100 m/min cutting speed and a 30^o portion at 300 m/min cutting speed contain a surface that is not representative of the intended machining conditions. After each test, the tube face was inspected and the tool retraction mark visually checked. Samples for photo micrographs were then taken from areas of the tube not subject to this artifact i.e. from a region of the surface that lies before the dwell zone.

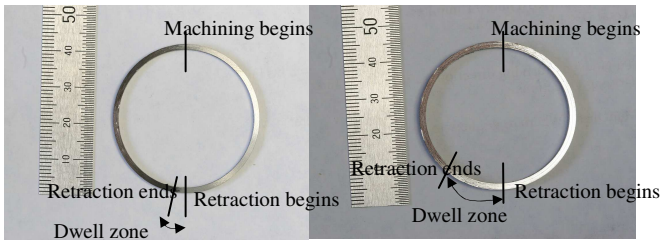

(a) **(b)**

Figure 5.6. Machined surface showing portion subject to rubbing during tool retraction: (a) 100 m/min cutting speed, (b) 300 m/min cutting speed.

A sample of the measured cutting force signal is also shown in Figure 5.3. It can be seen from the figure that tool retraction is fairly fast and its effect on the cutting force signal is minimal.

5.1.5 Metallography

After each test, workpiece sections measuring 1.5 mm x 5 mm were cut out from the machined surface using a precision diamond saw (Figure 5.7). The samples were then mounted in a thermosetting compound and polished with 240 and 320 grit papers and Beuhler UltraPad™, Texmet 1000™, and Texmet 2000™ polishing cloths. The samples were subsequently etched using a 2 % Nital solution to check for the presence/absence of white layer and its depth. A schematic diagram of the sectioning procedure used to prepare the samples for optical micrographs and XRD measurement is shown in Figure 5.7.

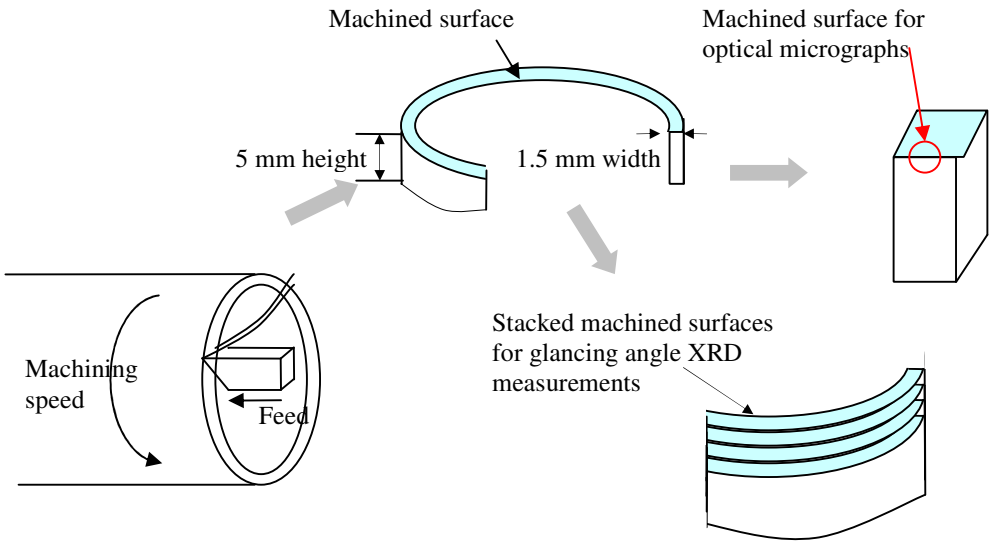

Figure 5.7. Schematic diagram of orthogonal machining and sectioning of samples for optical micrographs and XRD.

5.1.6 XRD Measurement

XRD measurements were made on the sectioned samples of the machined surfaces for selected cutting conditions to determine the presence/absence of retained austenite in the white layer. PANanalytical X'Pert Pro MPD Θ–Θ goniometer with PANanalytical 3 kW generator with X'Celerator detector (See Figure 5.8) was used. Table 5.3 lists the details of the equipment specifications for the XRD measurements.

Table 5.3. Equipment specifications for XRD measurement.

Equipment	PANanalytical X'Pert Pro MPD Θ–Θ goniometer PANanalytical 3 kW generator X'Celerator detector
Power	1.8 kW; 45 kV, 40 mA
Radiation	Cu, λ = 1.54059 Å
Incident optics	Parabolic mirror
Receiving optics	Graphite Monochromator
Incident and Receiving Axial Soller slits	±2.3°
Source to specimen distance	240 mm
Specimen to back slit distance	240 mm

Since the area of the machined surface of the tube is small, the machined surface was cut into four pieces and stacked along the arcs to increase the measurement area as shown in Figure 5.8. Specimen alignment was accomplished using a dial gauge probe, which was accurate to ±5 μm. Here, the relative distance to the center of rotation is

known, and the diffracting surface is positioned accordingly. With a 2.5° incidence beam fixed, the detector rotates with 0.0167° 2θ/step in the range 35° ≤ 2θ ≤ 90°. Scanning was performed for 23 hours. With 2.5° degree incidence beam angle, the penetration depth is about 200 nm [77].

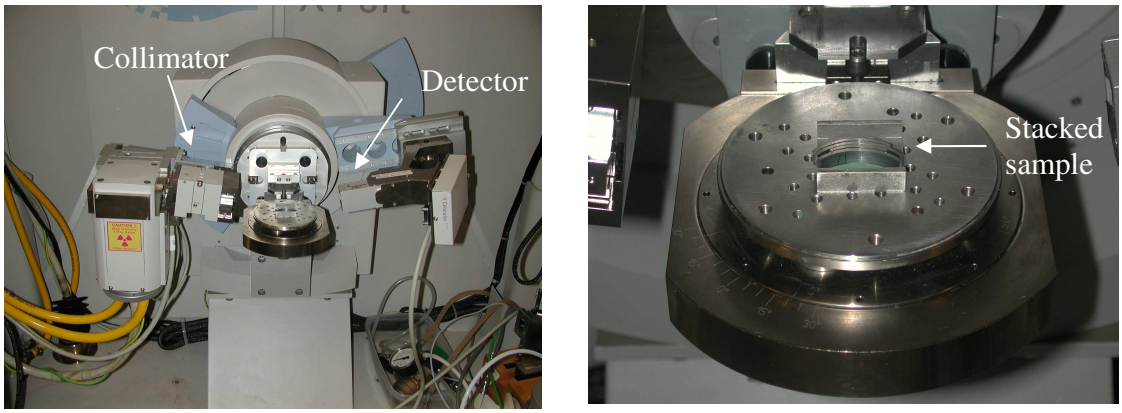

(a) **(b)**

Figure 5.8. (a) PANanalytical X'Pert Pro MPD Θ–Θ goniometer with PANanalytical 3 kW generator with X'Celerator detector, (b) Stacked sample placed on the stage of XRD equipment. (Courtesy, HTML, ORNL)

5. 2 Results

5.2.1 Forces

The average measured cutting and thrust force data are shown in Figure 5.9. Lower machining force at the higher machining speed of 200 m/min is observed because of the high temperatures that are typically generated at the higher machining speed. It can be seen that the cutting and thrust forces increase linearly as the flank wear land width increases. This observation is consistent with those reported by others [68,69,70]. Thomsen et al. [68] proposed that the increase in forces was because of plastic

deformation under the flank wear land since the change in chip ratio was not significant. This in turn may contribute to the mechanical effect (in addition to thermal) that causes white layer formation.

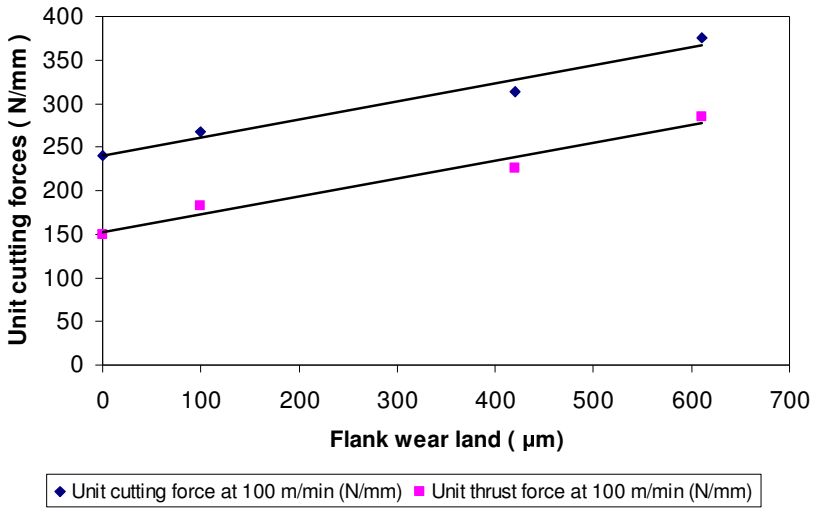

(a)

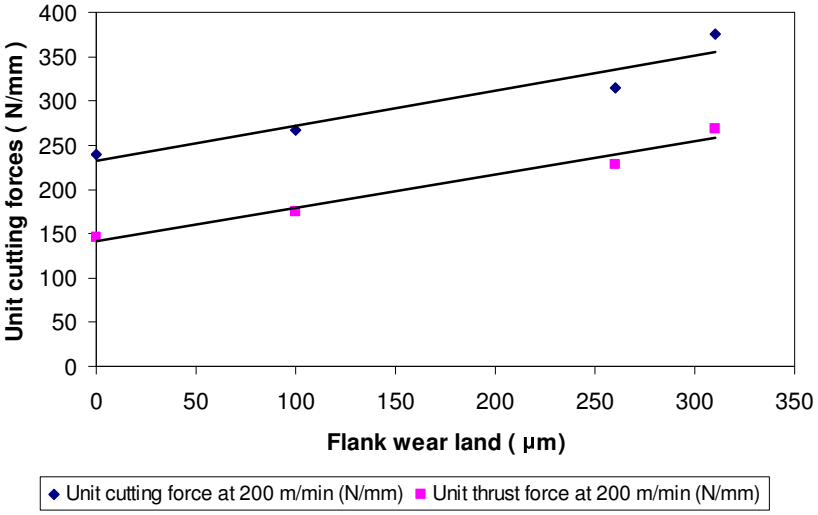

(b)

Figure 5.9. Cutting and thrust forces in machining with different flank wear land widths at (a) 100 m/min and (b) 200 m/min.

5.2.2 Optical Micrographs

Optical micrographs to check for the presence or absence of white layer in the machined samples are shown in Figure 5.10 and Figure 5.11. As can be seen that, white layer is present at all cutting conditions. The average white layer depth was estimated from the micrographs by measuring the depth at 10 different points for each test condition. The average white layer depth and the error bar to represent one standard deviation variation are plotted in Figure 5.12. Different depths of white layer are observed at different machining speeds and flank wear land widths. Thin (1-2 µm thick) white layer is observed for 100µm flank wear at 100 and 200 m/min cutting speeds. Thick white layer (~5 µm thick) is observed for large flank wear land (260µm) at a cutting speed of 200 m/min cutting speed. Very thick white layers (>8µm thick) are observed for very large flank wear land widths (more than 300µm) at both the 100 and 200 m/min cutting speeds.

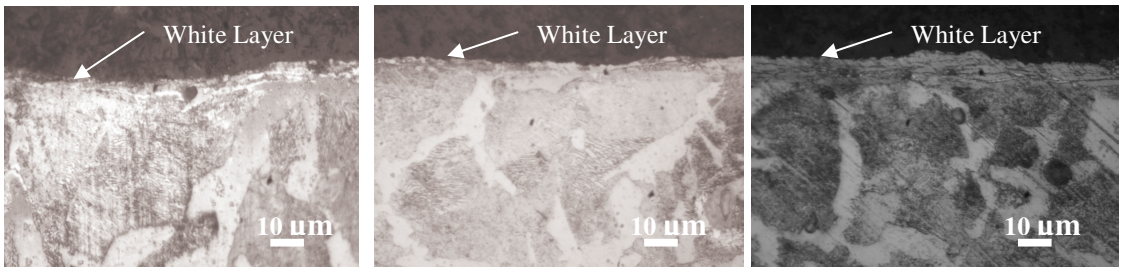

(a) (b) (c)

Figure 5.10. Surface of AISI 1045 annealed steel machined at: (a) 100m/min cutting speed with 100 µm VB, (b) 200 m/min cutting speed, 100 µmVB, (c) 200 m/min cutting speed, 260 µm VB.

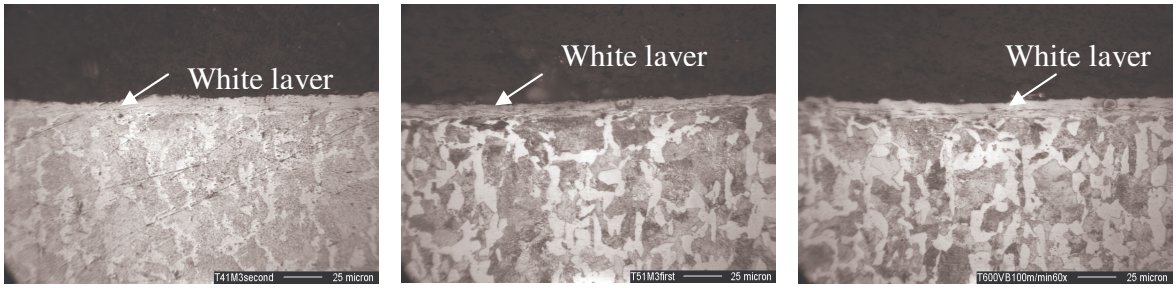

(a) (b) (c)

Figure 5.11. Surface of AISI 1045 annealed steel machined at: (a) 200 m/min cutting speed, with 310 µm VB, (b) 100 m/min cutting speed, 420 µm VB, (c) 100 m/min cutting speed, 600 µm VB.

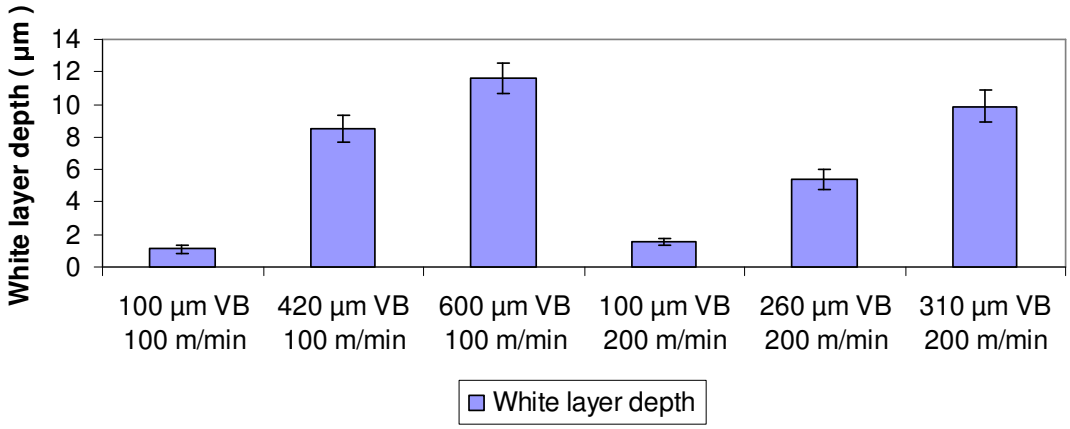

Figure 5.12. White layer depth in for cutting conditions.

5.2.3 Maximum Workpiece Surface Temperatures

The maximum workpiece surface temperature data obtained for each machining condition is shown in Table 5.4. As discussed earlier, since the temperature is not measured exactly at the trailing edge of the flank wear, the maximum temperature at the trailing edge of the flank is estimated using the analytical model described in Chapter 4 and given in Table 5.4.

Table 5.4. Measured workpiece surface temperature behind the trailing edge of the flank wear and the estimated maximum temperature at the trailing edge for machining condition.

Machining condition	Measured temperature (ºC)	Distance from flank wear trailing edge to upper edge of bead	Estimated maximum temperature (ºC)
100 VB 100 m/min	304	800 µm	433
420 VB 100 m/min	438	260 µm	497
600 VB 100 m/min	513	120 µm	744
100 VB 200 m/min	329	800 µm	532
260 VB 200 m/min	396	720 µm	675
310 VB 200 m/min	475	80 µm	668

As can be seen from Table 5.4, an increase in the estimated maximum temperature with flank wear width is observed at each machining speed. This observation is consistent with that reported elsewhere [68]. Temperature gradient between the trailing edge of the flank wear where the maximum temperature occurs and the location where the temperature is measured seems fairly high. The overall estimated maximum temperature at 200 m/min cutting speed is higher than that at 100 m/min cutting speed, which is intuitively reasonable. Note that the maximum workpiece surface temperature range is quite large as well. Most importantly, in most cases the estimated temperature is below the nominal phase transformation temperature for the steel (727 deg. C). Since white layer was observed in all machining conditions, the presence/absence of retained austenite as evidence of phase transformation during formation of white layer is checked in the following section.

5.2.3 XRD Analysis

XRD measurements of the unmachined and machined surfaces produced under different cutting conditions are shown in Figure 5.13 and Figure 5.14; α and γ represent the ferrite and the austenite phases, respectively. Note that the absolute intensity (count) of the diffracted x-rays detected by the detector is different in each x-ray diffraction pattern shown in Figure 5.14. This is due to the differences in the count time or the heights of the specimens during measurement. However, this does not make the peaks of each phase more intense because the relative intensities of each constituent phase remain constant. The higher intensity reduces the noise in the pattern as seen from Figure 5.13 and Figure 5.14. Consequently, the difference in the absolute intensity in each machined surface does not affect the presence/absence of the retained austenite nor does it affect the amount of retained austenite.

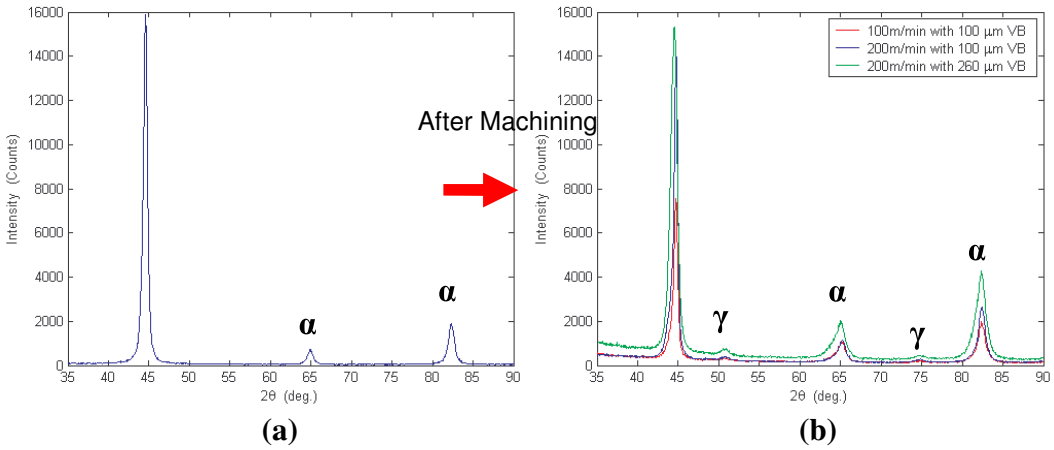

Figure 5.13. XRD profiles of (a) un-machined and (b) machined surfaces of AISI 1045 annealed steel produced at: (1) 100 m/min cutting speed, 100 µm VB, (2) 200 m/min cutting speed, 100 µm VB, (3) 200 m/min cutting speed, 260 µm VB.

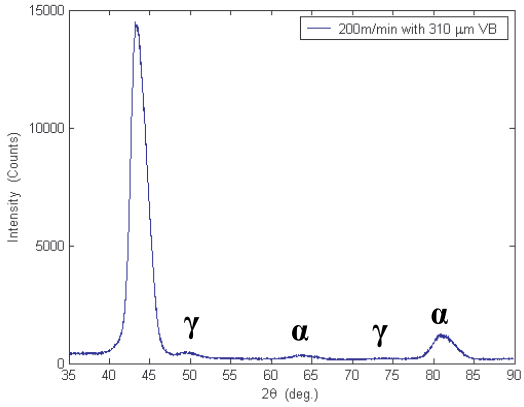

(a)

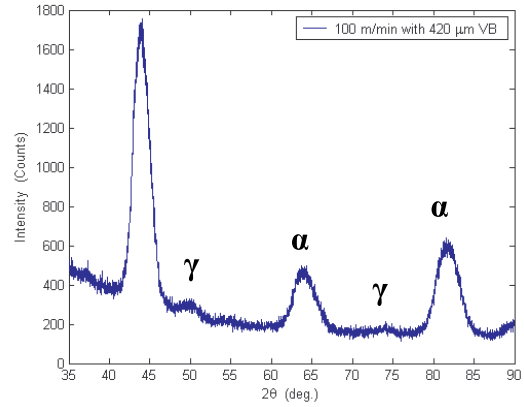

(b)

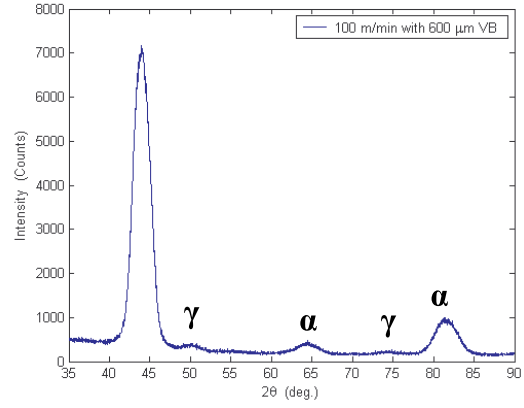

(c)

Figure 5.14. XRD profiles of AISI 1045 annealed steel machined at: (a) 200 m/min cutting speed, 310 µm VB, (b) 100 m/min cutting speed, 420 µm VB, (c) 100 m/min cutting speed, 600 µm VB.

It can be seen from Figure 5.13 (a) that no retained austenite (γ) is observed in the unmachined surface of 1045 annealed steel. On the other hand, it can be seen in Figure 5.13 (b) and Figure 5.14 that a retained austenite (γ) peak is observed in all machining conditions where a white layer is present. In these low-incidence angle measurements, the X-ray penetration depth is very small-about 200 nm for an incidence beam angle of 2-2.5°. Thus, it can be inferred that phase transformation has occurred in the sub-surface white layer during machining. Note that the relative intensity of the retained austenite γ peak is very small, less than 3%, in all cases. Long duration and slow scanning with a small incidence beam angle enables the detection of the austenite phase in a very thin layer in the machined sub-surface. Also, the volume fractions of retained austenite are estimated using the measurement procedure given in [79] and are plotted in Figure 5.15. The amount of retained austenite is seen to vary with speed and flank wear land width. This observation is generally consistent with those reported elsewhere [27, 46], albeit their measurements were made on different steels. The amount of retained austenite in the white layer produced with 100 µm VB and 200 m/min cutting speed is comparable to that obtained with Mössbauer spectrometry [80] for a similar machining condition. In hard turning, although retained austenite is present in the bulk material, a change in the amount of retained austenite after machining has been reported. The retained austenite was formed to decrease to 4% and 9 % compared to 19% in the bulk of 52100 hardened steel (62 HRC) at 91 m/min and 274 m/min cutting speeds, respectively [46]. The retained austenite increased to 33 % in the surface of 52100 hardened steel (62 HRC) machined with 210 µm flank wear at 180 m/min cutting speed, compared to 11% in the

bulk. Different thermal and mechanical effects are attributed to the observed change in the retained austenite content in hard turning.

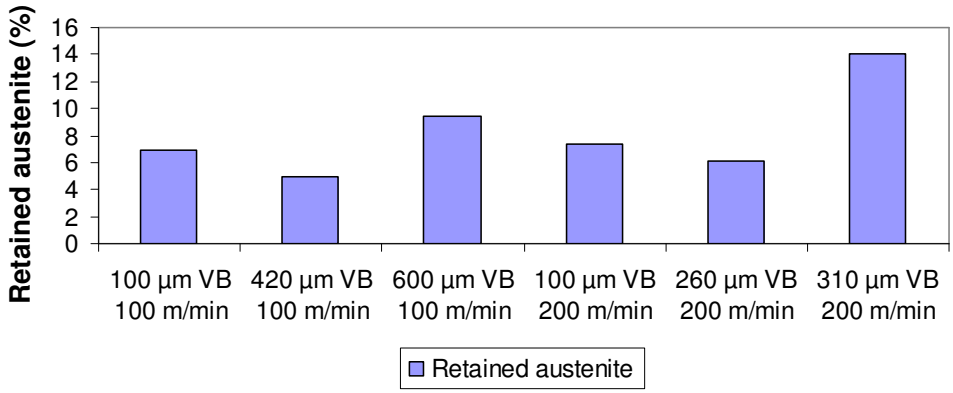

Figure 5.15. Volume fraction of retained austenite.

5.3 Analysis and Discussion

To understand the influence of thermal and mechanical effects on white layer formation, two attributes of the white layer are considered: the thickness and the amount of retained austenite present in the white layer. Note that the amount of retained austenite can influence the mechanical behavior of the steel. Specifically, it can affect the properties of white layer such as hardness and microcracking, and consequently part performance characteristics such as fatigue and wear resistance. Thus, if a similar thickness of white layer or similar amounts of retained austenite is observed at different temperatures, stresses, and strains, it can be inferred that similar thermal and mechanical effects were probably responsible for the similar white layer thickness/retained austenite contents. The following sections analyze these two features of the white layer as a

function of the estimated maximum temperature, effective stress and strain produced in the workpiece surface and calculated using the models presented in Chapter 4.

5.3.1 Effect of Temperature on White Layer Depth and Retained Austenite

In order to study the effect of temperature on white layer depth and retained austenite, the estimated maximum workpiece temperature given in Table 5.4 is superimposed on the white layer depth and retained austenite plots and shown in Figure 5.16 and Figure 5.17, respectively.

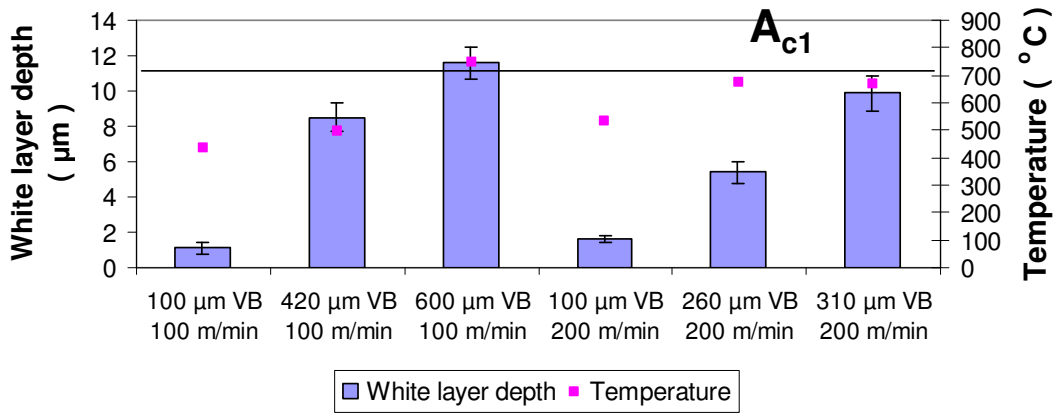

Figure 5.16. White layer depth and maximum workpiece surface temperature for each cutting condition.

As can be seen in Figure 5.16, in all cases except 600 µm VB, white layer is formed below the nominal phase transformation temperature, A_{c1}. Since in the 600 µm VB case, the maximum temperature is just above A_{c1}, one should expect only a thin white layer to form. However, it can be seen that a very thick (12 µm) white layer is formed in this case. This data clearly indicates that temperature may not be the only factor

responsible for white layer formation in machining of steels. This is also supported by the fact that a higher temperature (260µm VB at 200 m/min vs. 420 µm VB at 100 m/min in Figure 5.16) does not necessarily imply a thicker white layer. The above result clearly shows that white layer may form even when the workpiece surface is below the nominal phase transformation temperature.

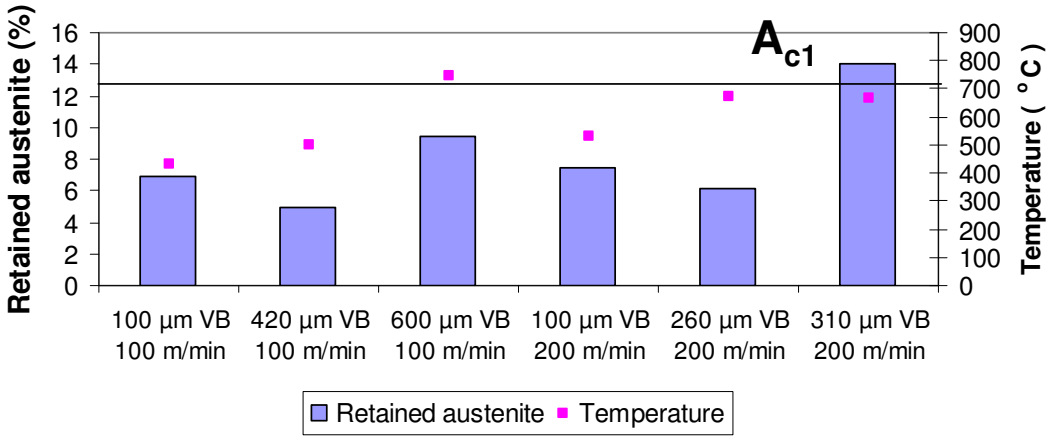

Figure 5.17. Amount of retained austenite and maximum workpiece surface temperature for each cutting condition.

It is clear from Figure 5.17 that retained austenite, as an evidence of phase transformation in the white layer, formed below A_{c1} except for the case of 600 µm flank wear at 100 m/min. Also, higher temperature (310µm VB at 200 m/min vs. 600 µm VB at 100 m/min) does not necessarily produce more amount of retained austenite. Thus, exceeding the nominal phase transformation temperature alone is not enough to account for the phase transformation in the white layer. It is therefore possible that mechanical effects associated with plastic deformation can also influence white layer formation. The following sections discuss the effects of stress and strain associated with mechanical working on white layer formation.

5.3.2 Effect of Stress on White Layer Depth and Retained Austenite

In order to examine the possible effect of stress on the white layer depth and retained austenite, the effective stress in the workpiece surface was calculated as discussed in Chapter 4 and is given in Table 5.5.

Table 5.5. The effective stress on the workpiece surface at each machining condition.

Machining condition	σ_{eff} (MPa)
100 µm VB 100 m/min	573
420 µm VB 100 m/min	355
600 µm VB 100 m/min	444
100 µm VB 200 m/min	594
260 µm VB 200 m/min	662
310 µm VB 200 m/min	657

Then, the effective stress was superimposed on the white layer depth and retained austenite plots as shown in Figure 5.18 and Figure 5.19, respectively.

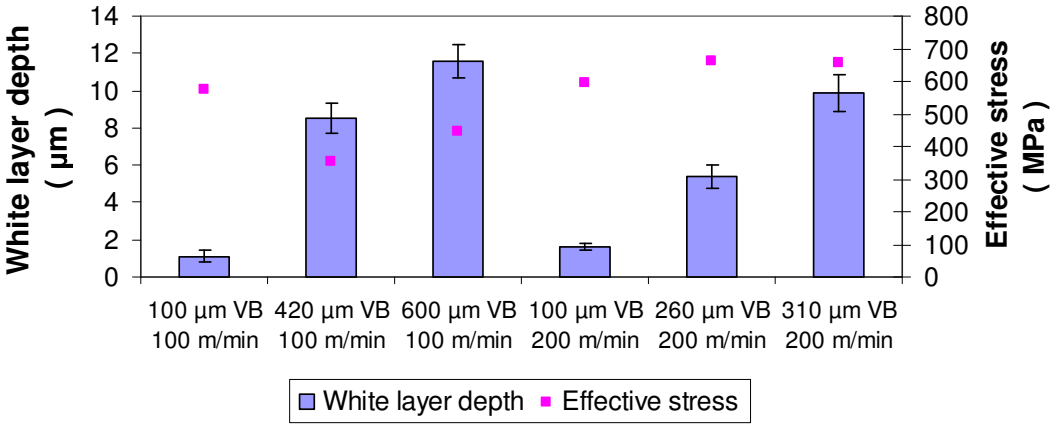

Figure 5.18. White layer depth and effective stress on the workpiece surface for each cutting condition.

Relatively high effective stress is observed in all machining conditions. In particular, relatively high effective stress is observed for the cases with flank wear land (100 µm) at both low and high cutting speeds. In addition, it can be seen that even though the maximum workpiece temperature is below A_{c1} for the 100 µm VB cases (See Figure 5.16), a thin white layer is still formed. This may be due to the high effective stress seen in Figure 5.18 for these cases. High workpiece surface temperatures combined with high effective stress (e.g. with 310 µm flank wear at 200 m/min) or moderately high effective stress (See 600 µm flank wear at 100 m/min) results in a thick white layer. This suggests the possibility that a combination of thermal and mechanical effects is responsible for the formation of white layer. Thus, the same white layer can be produced under different levels of thermal and mechanical loading as a result of the different cutting conditions.

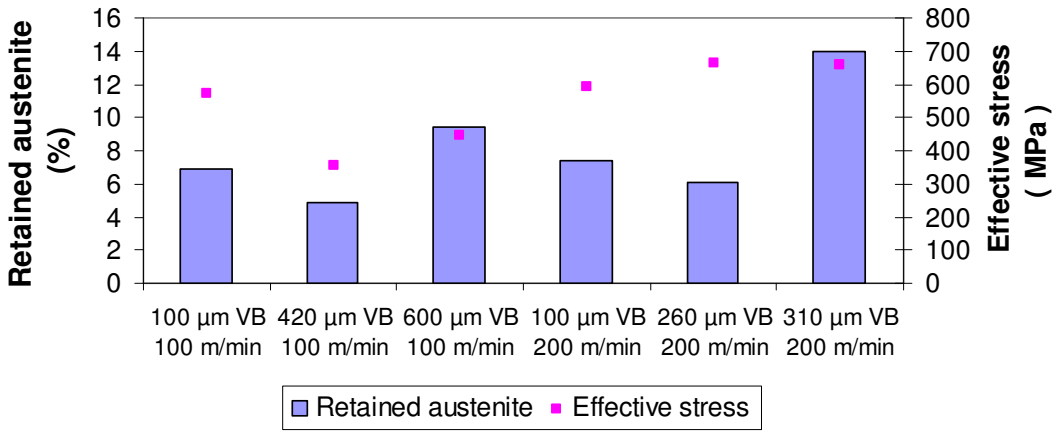

Figure 5.19. Amount of retained austenite and effective stress on the workpiece surface for each cutting condition.

As seen in Figure 5.19, the amount of retained austenite in a thin (1~2 µm thick) white layer formed with 100 µm flank wear at 100 m/min and 200 m/min cutting speeds is comparable to the thick white layer formed with 420 µm flank wear and 100 m/min cutting speed. Again, the temperature is below the nominal phase transformation

temperature except for the case of 600 µm flank wear land and 100 m/min cutting speed. Thus, it appears that high effective stress contributes to the phase transformation below the nominal austenitization temperature. The amount of stress needed to lower the phase transformation for pure iron was estimated by Griffth [26] and Darken and Gurry [81] who calculated it using the Clausius-Clapeyron equation [81]. Ramesh [47] has made similar calculations for hardened AISI 52100 steel. The calculation procedure is as follows:

Free energy change, ΔF_{tr}^{T} (cm^3-atm/gm-atom) associated with α-γ transformation in pure iron for a given atmospheric pressure, P (atm) and temperature, T (ºC) is given by [81]:

$$\Delta F_{tr}^{T} - 0.06P = 0 \qquad \textbf{(5.1)}$$

The free energy change is assumed to be the same in AISI 1045 annealed steel. For the case of VB=310 µm, 200 m/min, which has an effective stress of 662 MPa, the free energy change is estimated to be 392 cm^3-atm/gm-atom. From the ΔF_{tr}^{T} -T table of pure iron α-γ transformation given in APPENDIX A, the corresponding phase transformation temperature of pure iron is 865 ºC, which implies a 45 ºC drop in the equilibrium transformation temperature of the pure iron of 910 ºC. The 45 ºC drop in the phase transformation temperature for a given effective stress is assumed for the AISI 1045 annealed steel used in this study. An additional drop of 15 ºC due to cold working in steels is also included [47]. The total drop in A_{c1} is therefore 60 °C, leading to an A_{c1} of 727-60=667°C. The free energy change, ΔF_{tr}^{T} , the corresponding drop in the

equilibrium transformation temperature for each machining condition and the effective A_{c1} are given in Table 5.6. The drop in A_{c1} is denoted as ΔT, the effective A_{c1} is denoted as A^*_{c1} and T_{max} represents the maximum workpiece surface temperature at each machining condition. Note that T_{max} is compared with A^*_{c1} to check for phase transformation.

Table 5.6. Effective A_{c1} and the maximum workpiece surface temperature.

Machining condition	σ_{eff} (MPa)	ΔF_{tr}^{T} (cm^3-atm/gm-atom)	ΔT (ºC)	A^*_{c1} (ºC)	T_{max}	Note
100 µm VB 100 m/min	573	339	54	673	433	$A^*_{c1} > T_{max}$
420 µm VB 100 m/min	355	210	39	688	497	$A^*_{c1} > T_{max}$
600 µm VB 100 m/min	444	263	45	682	744	$A^*_{c1} < T_{max}$
100 µm VB 200 m/min	594	352	55	672	532	$A^*_{c1} > T_{max}$
260 µm VB 200 m/min	662	392	60	667	675	$A^*_{c1} < T_{max}$
310 µm VB 200 m/min	657	389	60	667	668	$A^*_{c1} < T_{max}$

As can be seen in Table 5.6, the effective A_{c1} is 667 °C due to the stress/pressure effect at 200 m/min cutting speed and 260 µm VB. This is the reason that retained austenite is observed in this case since the maximum workpiece surface temperature is 675 °C.

However, about 7% retained austenite is observed in the thin white layer in the case of 100 µm VB at 100 and 200 m/min cutting speeds, even though the surface temperatures are less than 600 ^oC. The effective A_{c1} for these cases is larger than 667 ^oC

since the effective stresses are less. Hence, there could be other factors that affect white layer formation in addition to the effect of stresses. It is noted that the Clausius-Clapeyron equation is not associated with any deformation of the material. Consequently, plastic deformation or plastic strain can be the additional factor that can explain this.

5.3.3 Effect of Plastic Strain on White Layer Depth and Retained Austenite

In order to check the effect of plastic strain on the white layer depth and retained austenite, the effective plastic strain on the workpiece surface was calculated as described in Chapter 4 and is given in Table 5.7. The effective strain is denoted as $\bar{\varepsilon}$ in Table 5.7.

Table 5.7. Workpiece surface effective plastic strain.

Machining condition	$\bar{\varepsilon}$
100 µm VB 100 m/min	2.7
100 µm VB 200 m/min	2.7
260 µm VB 200 m/min	1.8
310 µm VB 200 m/min	1.6
420 µm VB 100 m/min	1.3
600 µm VB 100 m/min	0.9

The effective strain given in Table 5.7 is superimposed on the white layer depth and retained austenite plots as shown in Figure 5.20 and Figure 5.21, respectively.

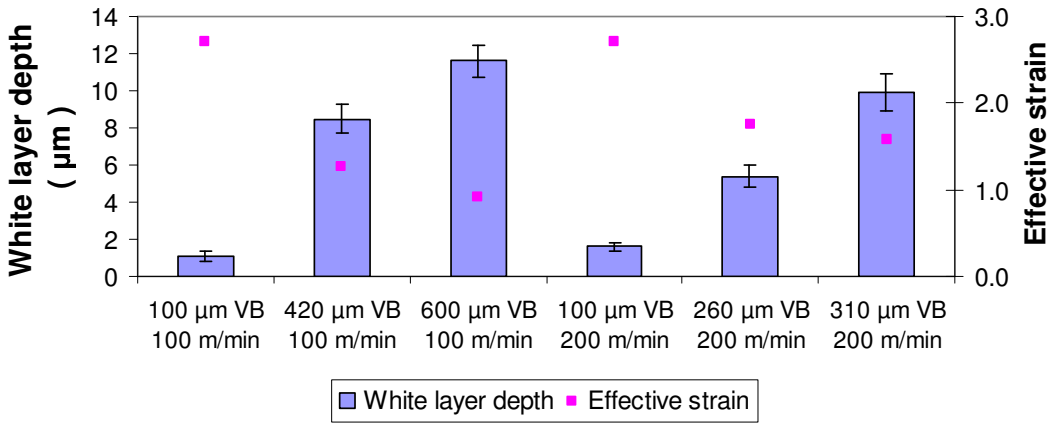

Figure 5.20. White layer depth and effective plastic strain on the workpiece surface for each cutting condition.

The sub-surface deformation due to rubbing between the flank wear land and workpiece surface is very high in these plots. Strains of 0.9-2.7 obtained from the model are high and are usually observed in mechanical working of steel [82]. Thus, it appears that the effects of plastic deformation as suggested by Griffith [26] can contribute to the formation of the white layer in the machining of AISI 1045 annealed steel. As shown in Figure 5.20, a thin white layer is observed in the surface machined with 100 µm flank wear width at 100 and 200 m/min cutting speeds even though a higher level of strain is induced. A lower temperature, less than 600 ºC, is attributed to the thin white layer formation.

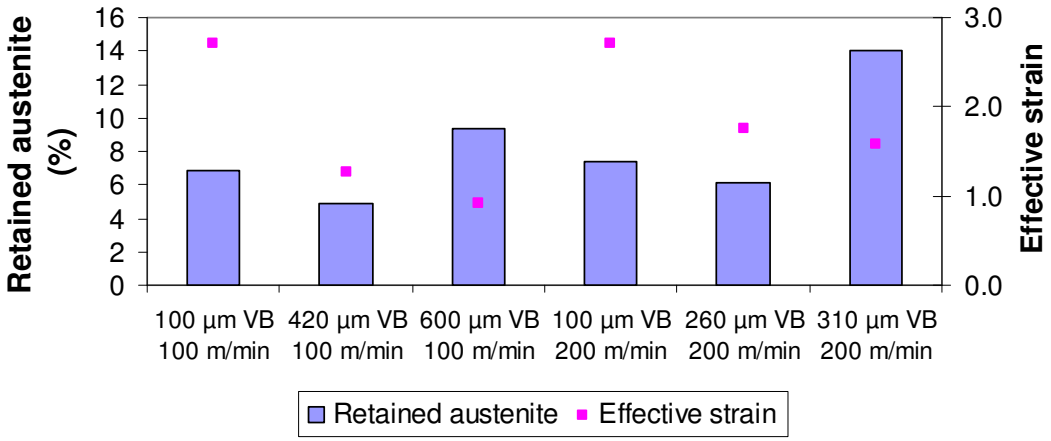

Figure 5.21. Depth of white layer and effective strain on the workpiece surface for each cutting condition

As discussed earlier, phase transformation occurred when machining with 100 µm flank wear land at 100 and 200 m/min cutting speeds even though the workpiece surface temperatures are below the stress-lowered phase transformation temperature. This can perhaps be explained in terms of strain induced phase transformation [83] usually observed in deformation processing of steel. In addition, the role of deformation in phase transformation based microstructure alteration in machining of steel can be explained by the "coffee analogy" [4]. This analogy goes as follows. With stirring of sugar in hot coffee, the sweetness can be achieved in shorter time than without stirring. This analogy suggests that plastic deformation enhances the carbon diffusion into the austenite phase, thus promotes martensitic phase transformation.

In summary, deformation in the workpiece surface during machining process also plays a role in the phase transformation leading to white layer formation. In machining of AISI 1045 annealed steel, phase transformation appears to be the major factor responsible for the formation of white layer. The reason plastic deformation plays a secondary role is as follows. Plastic flow without white layer formation has been

observed by Kim and Kwon [32] when machining AISI 1045 annealed steel. No retained austenite was observed in their study. Thus, they showed no phase transformation occurred in the machined surface. After machining at higher speeds, white layer and retained austenite were observed thus confirming phase transformation. Therefore, it can be stated that phase transformation is the major cause of white layer formation in the machining of 1045 annealed steel.

5.4 Summary

The following conclusions can be drawn from this chapter:

- The phase transformation in machining of AISI 1045 steel can occur below the nominal phase transformation, A_{c1} in Fe-C phase diagram. Mechanical working in the machining process, quantified here by the effective stress and strain, is also thought to play a role in causing phase transformation below the nominal phase transformation temperature.
- Retained austenite as an evidence of phase transformation is observed in the white layers in all machining conditions used in the tests on AISI 1045 annealed steel; the amount of retained austenite varies with the thermal and mechanical loading resulting from different cutting conditions.
- Different depths of white layers in AISI 1045 annealed steel were observed as a result of different levels of temperature, stress and strain induced by machining in a wide range of cutting speed and flank wear land.

CHAPTER 6

SEMI-EMPIRICAL PROCEDURE FOR PREDICTION OF WHITE LAYER FORMATION

After understanding the effects of thermal and mechanical loading on white layer formation in machining of steels in previous chapters, efforts have been made to develop a semi-empirical model-based procedure to predict white layer formation in AISI 1045 annealed steel using the maximum workpiece surface temperature, stress and/or strain, or forces as possible parameters. Consequently, machining tests over a wide range of cutting speeds and flank wear were conducted. Microstructure and cutting force data were obtained and analyzed. The maximum workpiece surface temperature was calculated using the model described in Chapter 4. Analysis of the data indicates a possible correlation between white layer depth, and the maximum workpiece surface temperature and the unit thrust force increase. In particular, it is found that the onset of white layer formation in the 1045 annealed steel is governed by a critical level of the combination of the maximum workpiece surface temperature and unit thrust force increase. The semi-empirical model-based procedure based on this critical combination of parameters is experimentally verified. The following sections describe the developed procedure in detail.

6.1 Semi-Empirical Procedure for Prediction of White Layer Formation

In order to develop a semi-empirical model for white layer formation in machining that accounts for both thermal and mechanical loading effects, orthogonal machining of AISI annealed 1045 steel was conducted over a wide range of cutting speeds and flank wear land widths, at which different levels of thermal and mechanical loadings are expected to occur. Machining conditions used are given in Table 6.1.

Table 6.1. Machining conditions for semi-empirical modeling of white layer formation.

Workpiece Material	AISI annealed 1045 steel
Tool Materials	Carbide (KC 730)
Cutting speed, V (m/min)	50,100,150,200 m/min
Feed, f (mm/rev)	0.1 mm/rev
Flank wear, VB (μm)	0-600 μm
Coolant	Dry machining

The force data and micrographs of the resulting workpiece microstructure were collected for each test. Since it was shown in Chapter 5 that the maximum workpiece surface temperature and the effective stress affected the white layer formation, these two quantities were calculated for each machining condition using the temperature and stress models described in Chapter 4. Also, because it was shown earlier that phase transformation occurs during the formation of white layer in machining of AISI 1045 annealed steel, the maximum workpiece temperature corresponding to the onset of white layer formation is denoted as the A_s temperature. The A_s and σ_{eff} combination needed to

generate a thin (about 1 μm thick) white layer was considered as the critical combination of parameters that separate the conditions responsible for white layer and no white layer. An attempt was first made to establish the correlation between the A_s and effective stress using the empirically determined combinations of A_s and σ_{eff}. Figure 6.1 depicts a hypothetical form of this expected correlation.

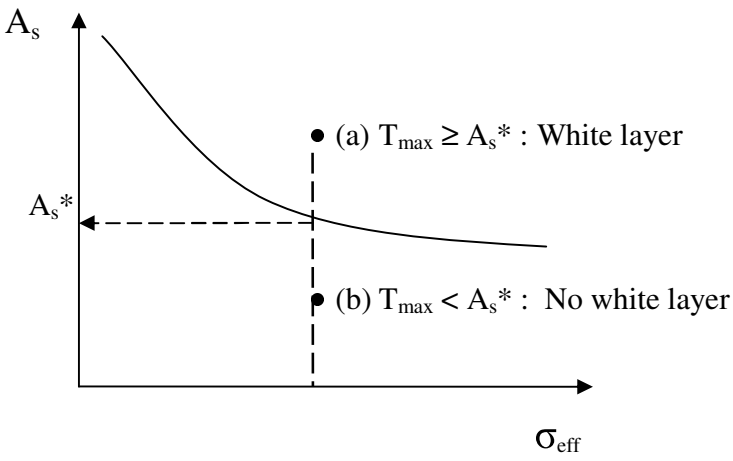

Figure 6.1. Procedure for predicting the presence/absence of white layer using the empirically derived correlation between A_s and effective stress.

Once this correlation is determined, it can be used together with the temperature model and cutting forces presented in Chapter 4 to predict the presence or absence of white layer for other cutting conditions. The procedure to predict white layer formation is depicted in Figure 6.1. For a given effective stress, if the predicted maximum workpiece surface temperature is equal to or greater than A_s^*, noted as state (a) in Figure 6.1, white layer is likely to form. Otherwise, noted as state (b) in Figure 6.1, white layer is not likely to form.

As can be seen from the above hypothetical illustration, the presence/absence of white layer and its depth are determined using a semi-empirical modeling approach. The semi-empirical approach for white layer presence/absence is experimentally verified by comparing it with actual cutting tests conducted at conditions different from those used to derive the correlation depicted in Figure 6.1. A flow chart summarizing this chapter is shown in Figure 6.2.

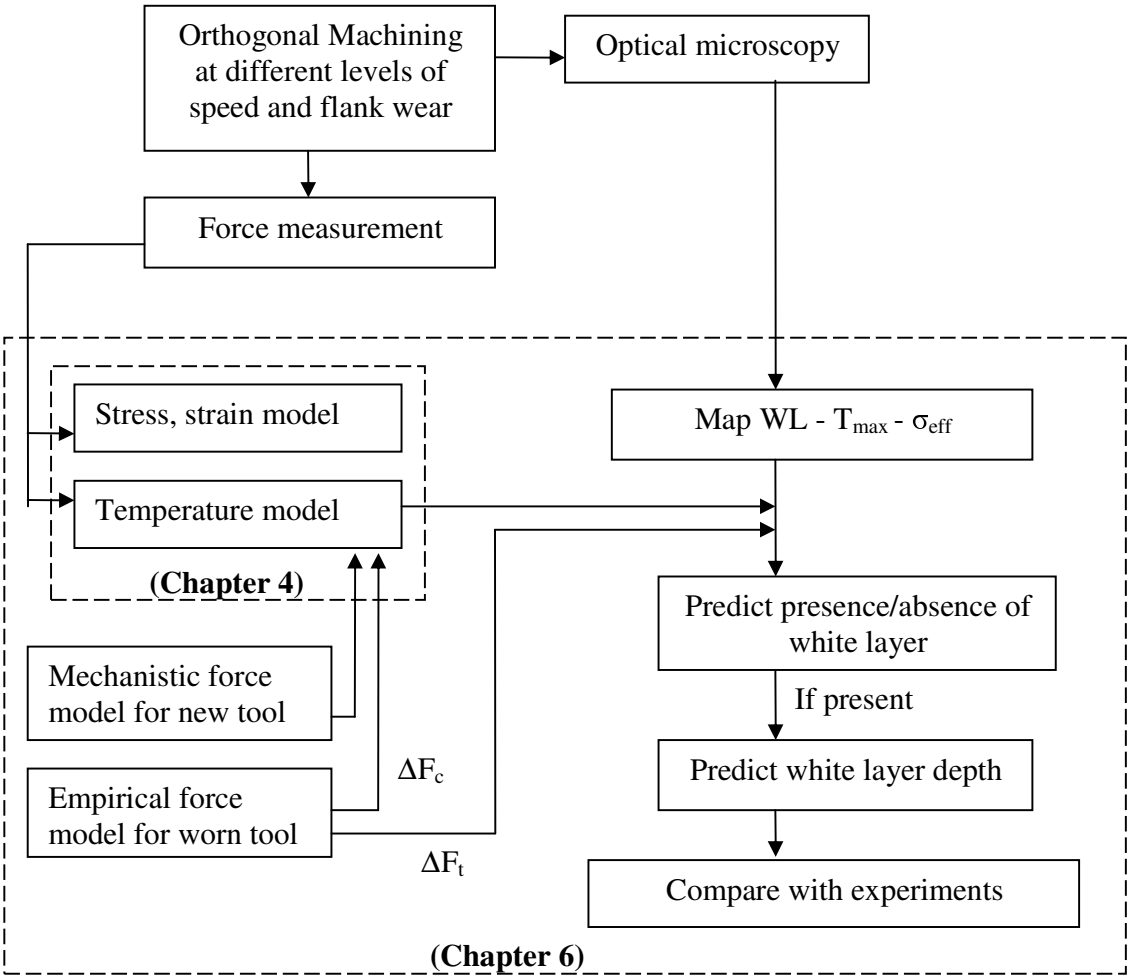

Figure 6.2. Flow chart summarizing this chapter.

6.2 Force Model Development

The knowledge of cutting forces is needed to calculate the workpiece surface temperature and stresses acting at the flank-workpiece interface when used in the prediction of white layer formation. The following sections describe the force model development in detail.

6.2.1 New Tool Force Model

The mechanistic force model outlined in past work by Haung [67] and Smithey et al. [96] is used to predict forces with a new tool. The forces at a certain cutting condition in orthogonal cutting are given as:

$$\begin{aligned} F_c &= K_n A_c \cos(\alpha) + K_f A_c \sin(\alpha) \\ F_t &= K_f A_c \cos(\alpha) - K_n A_c \sin(\alpha) \\ A_c &= t_u w \end{aligned} \tag{6.1}$$

where K_n and K_f are the specific energies in the normal and tangential directions to the rake face, α is the rake angle of the tool and t_u is the depth of cut. The specific energies are established empirically as a function of the cutting conditions and have the following general form:

$$\begin{aligned} \ln(K_n) &= a_0 + a_1 \ln(t_u) + a_2 \ln(V) + a_3 \ln(t_u)\ln(V) \\ \ln(K_f) &= b_0 + b_1 \ln(t_u) + b_2 \ln(V) + b_3 \ln(t_u)\ln(V) \end{aligned} \tag{6.2}$$

The four unknown coefficients in Eq. (6.2) are determined by conducting the following four machining tests given in Table 6.2 using a new tool and AISI 1045 annealed steel. The tool used was Kennametal NG3125L carbide (KC 730 grade) inserts

and had a rake angle of 0º. All cutting was performed dry on a Hardinge T42-SP CNC lathe.

Table 6.2. Test matrix

Test no.	Speed (m/min)	Depth of cut (mm/rev)
1	100	0.1
2	100	0.2
3	300	0.1
4	300	0.2

The cutting and thrust forces were measured in each test and input into the Eq. 6.1 to calculate the corresponding specific cutting energies, K_n and K_f. The K_n and K_f, t_u and V values for each test were input into Eq. 6.2 and solved for the four coefficients. The coefficients of the mechanistic force model determined as just described are given in Table 6.3.

Table 6.3. Coefficients of the mechanistic force model.

K_n		K_f	
a_0	7.5370	b_0	9.0264
a_1	-0.2849	b_1	0.4060
a_2	-0.0527	b_2	-0.5939
a_3	0.0156	b_3	-0.1841

The predicted new tool force is used to calculate the temperature rise in the workpiece due to the primary shear zone heat. This temperature rise is subsequently used as a measure of the thermal effect on white layer formation.

6.2.2 Worn Tool Force Model

An empirical worn tool force model was developed by conducting the machining tests given in Table 6.1. The force data at each cutting speed with different flank wear land widths were collected and are shown in Figure 6.3 as force per unit width.

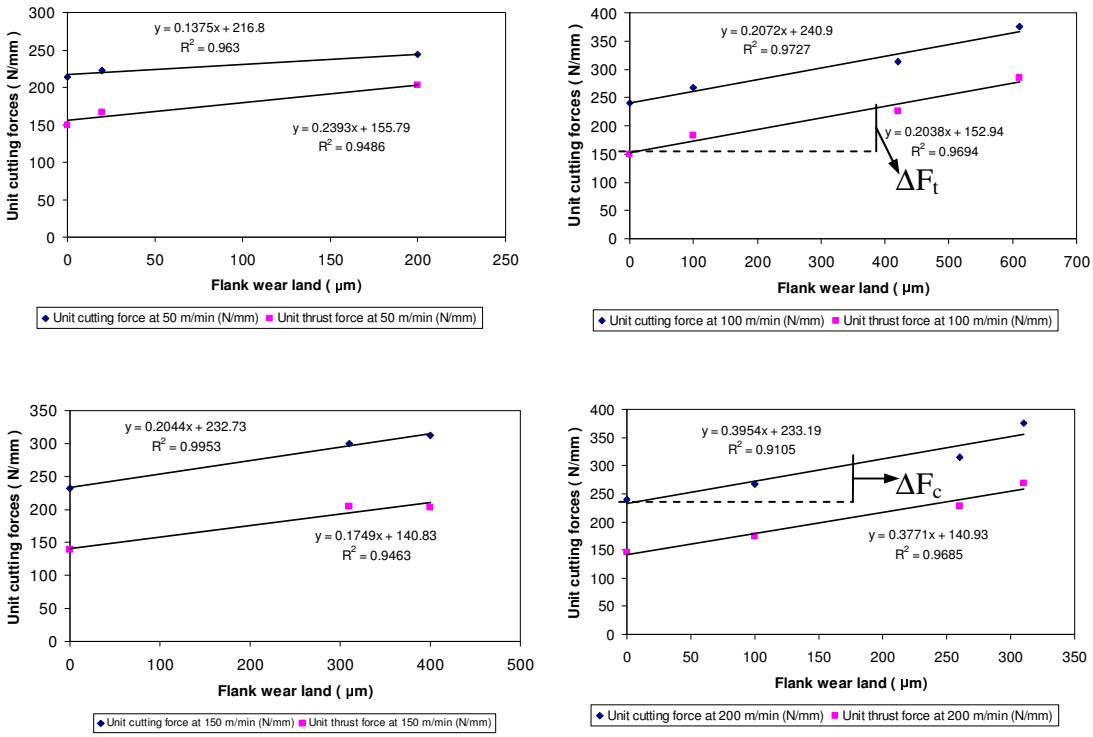

Figure 6.3. Cutting and thrust forces in machining with different flank wear lands at (a) 50 m/min, (b) 100 m/min, (c) 150 m/min and (d) 200 m/min.

As can be seen in Figure 6.3, the force data shows a linear force increase with flank wear increase as reported in literature [68,69,70]. Linear regression is employed to

develop empirical models of the worn tool force for each cutting speed. These models are used to determine the cutting (ΔF_c) and thrust force increase (ΔF_t in Figure 6.3) for a given cutting condition. The cutting force increase is used to calculate the temperature rise due to the rubbing heat source acting at the tool flank wear-workpiece interface, which is used as a measure of the thermal load acting on the machined surface. The predicted thrust force increase is also used as a measure of the mechanical effect on white layer formation.

6.3 Construction of Semi-Empirical Model of White Layer

In order to develop a semi-empirical model of white layer, machining tests were conducted at the cutting conditions given in Table 6.1. For each machining test, white layer depth was measured and correlated with the maximum workpiece temperature (calculated from the temperature model) and other parameters representing mechanical effects such as the effective stress (calculated from the stress model) and the thrust force increase (calculated from the worn tool force model). The procedure used is discussed in the following sections.

6.2.1 Workpiece Microstructure

Micrographs of the workpiece microstructures after machining were obtained for the machining conditions given in Table 6.1. The average white layer depth was obtained from 10 different points of the micrographs at each machining condition. Micrographs that reveal a thin white layer (about 1 μm thick) are shown in Figure 6.4. As can be seen in Figure 6.4, the onset of white layer (about 1 μm thick) was observed in the surfaces machined at speeds of 100~150 m/min with flank wear land widths of 100~160 μm.

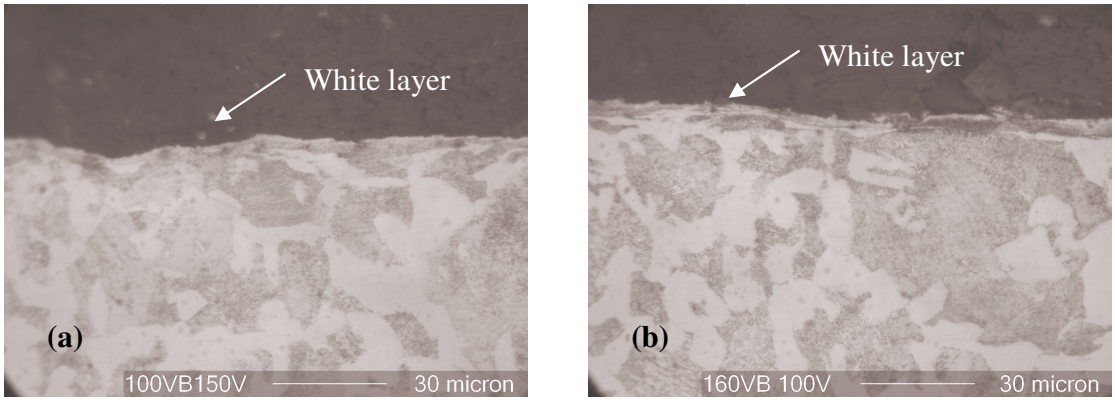

Figure 6.4. Microstructure of surface of AISI 1045 annealed steel machined at: (a) 150m/min cutting speed with 100 µm VB, (b) 100 m/min cutting speed with 160 µmVB.

Micrographs that show no white layer are given in Figure 6.5. It can be seen in Figure 6.5 that no white layer is present in the surfaces machined with small flank wear land (less than 70µm). The average white layer depths for all machining conditions are plotted in Figure 6.6.

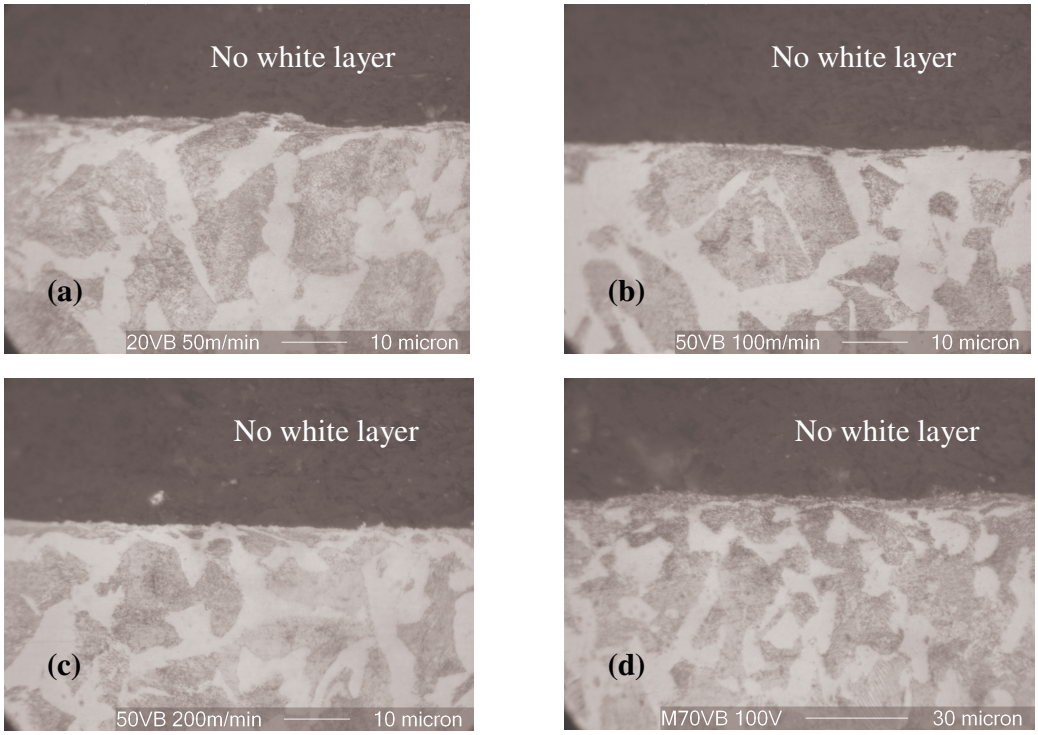

Figure 6.5. Microstructure of AISI 1045 annealed steel machined at: (a) 50m/min cutting speed with 20 µm VB, (b) 100 m/min cutting speed with 50 µmVB, (c) 200 m/min cutting speed with 50 µm VB (c) 100 m/min cutting speed with 70 µm VB.

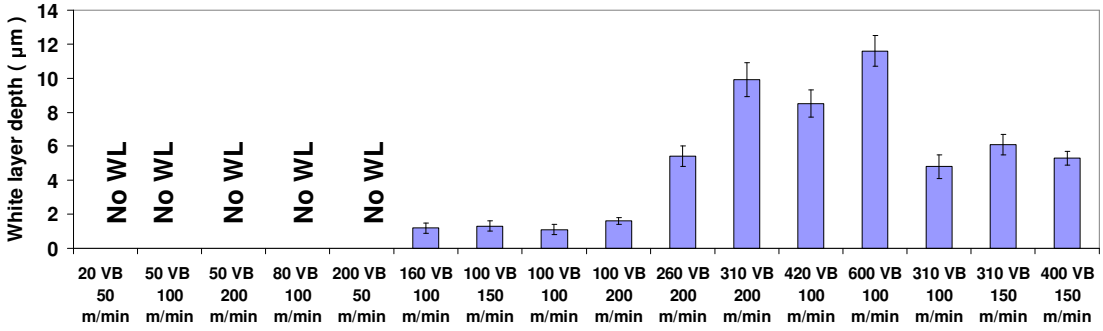

Figure 6.6. Average white layer depth.

6.2.2 Establishment of Semi-Empirical Model of White Layer Formation

The maximum temperature at the flank-workpiece interface and the effective stress, σ_{eff}, for each machining condition were calculated using the temperature and stress models described in Chapter 4 and are listed in Table 6.4.

Table 6.4. Maximum workpiece surface temperature and effective stress.

Machining condition	T_{max} (ºC)	σ_{eff} (MPa)	White layer depth (µm)
20 VB 50 m/min	309	954	0
50 VB 100 m/min	305	80	0
50 VB 200 m/min	319	450	0
80 VB 100 m/min	360	438	0
200 VB 50 m/min	320	313	0
160 VB 100 m/min	423	644	1.2
100 VB 150 m/min	448	564	1.3
100 VB 100 m/min	434	573	1.1
100 VB 200 m/min	513	594	1.6
260 VB 200 m/min	675	662	5.4
310 VB 200 m/min	662	657	9.9
420 VB 100 m/min	498	355	8.5
600 VB 100 m/min	744	444	11.6
310 VB 100 m/min	495	406	4.8
310 VB 150 m/min	612	432	6.1
400 VB 150 m/min	642	382	5.3

The maximum temperature and effective stress data in Table 6.4 is plotted as shown in Figure 6.7. Recall that the maximum temperature and the effective stress combination needed to generate a thin (about 1 µm thick) white layer is considered here as the critical combination of thermal and mechanical effect based parameters for white layer formation.

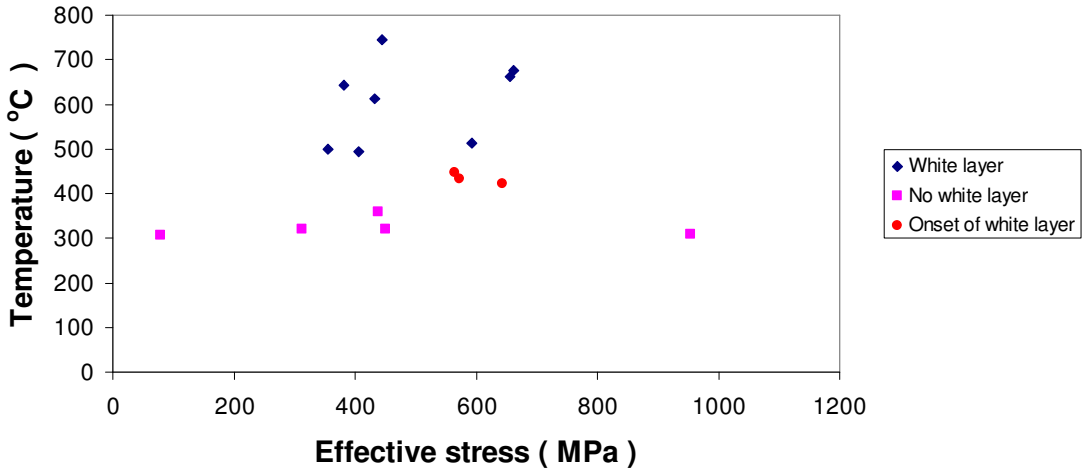

Figure 6.7. Maximum workpiece surface temperature vs. Effective stress.

As can be seen from Figure 6.7, the critical temperature level to produce about 1µm thick white layer is 420-450 ºC. However, a clean-cut trend between presence/absence of white layer and the combination of the maximum workpiece surface temperature and effective stress is not evident. Therefore, an attempt to correlate the presence/absence of white layer with other parameters that represent a measure of the mechanical effect was made. Specifically, the correlation between white layer formation and the maximum temperature and unit thrust force increase showed a good trend as seen in Figure 6.8. Since the unit thrust force increase acts on the workpiece surface, it can be considered as the parameter controlling the mechanical effect on the workpiece surface.

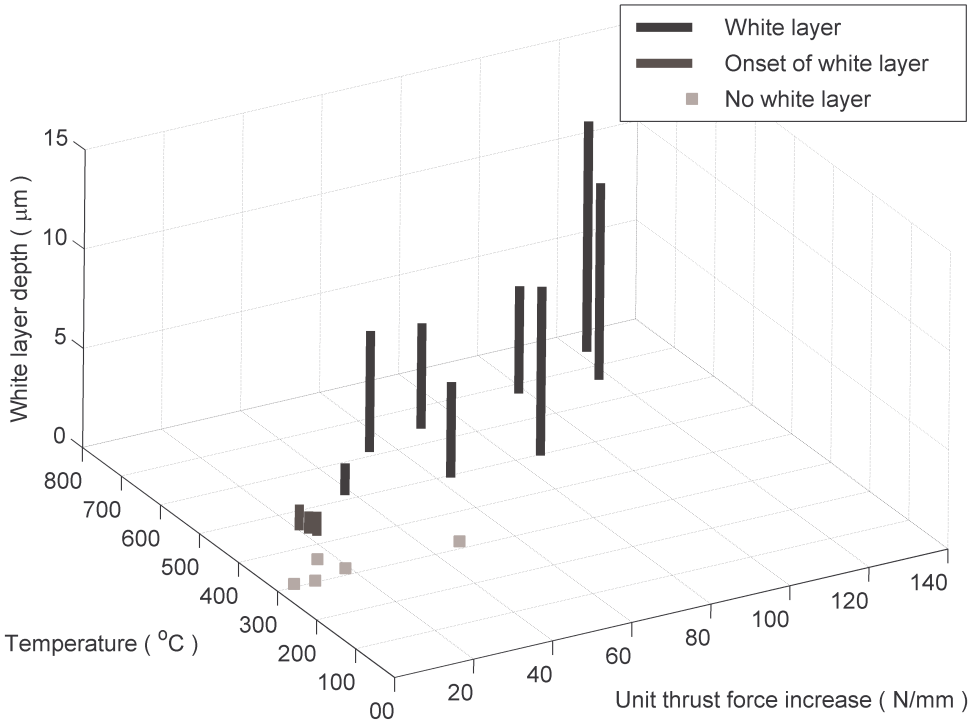

(a)

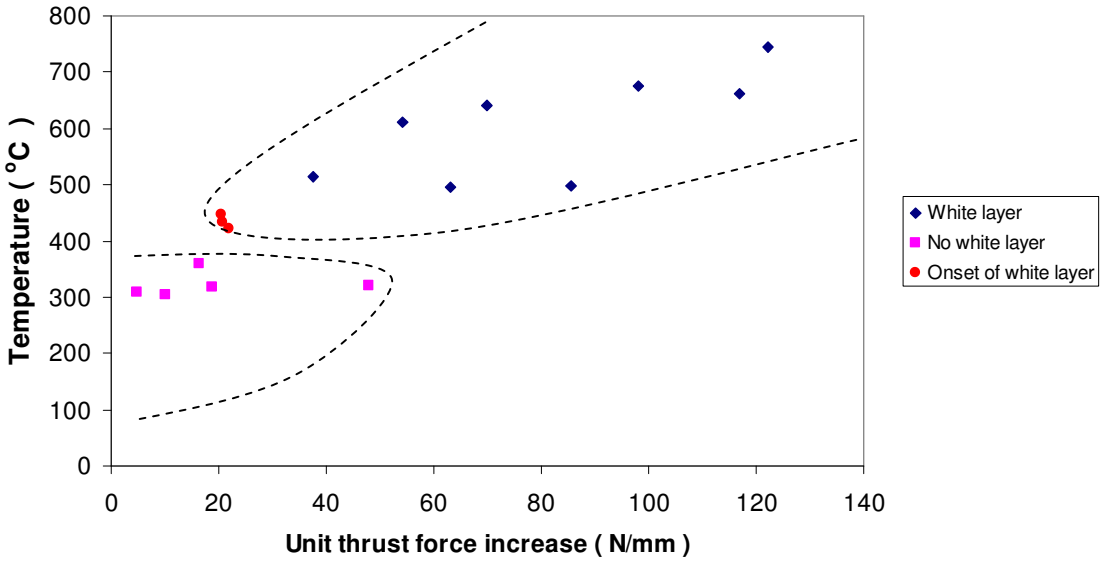

(b)

Figure 6.8. (a) White layer depth as a function of maximum workpiece surface temperature and unit thrust force increase, (b) Map of the white layer formation in the temperature-unit force domain.

The plot in Figure 6.8 can be divided into two distinct regions that delineate the no white layer region from the white layer region. Clearly, both temperature and unit thrust force increase should be higher than the critical level (420-450 ºC temperature and 20 N/mm unit thrust force increase) in order to form white layer.

In the range of 500-600 ºC temperature, a unit thrust force increase greater than 55 N/mm resulted in a thick (5-9 µm thick) white layer. In the range of 600-700 ºC, a unit thrust force increase greater than 100 N/mm led to a very thick (> 10 µm) white layer. The above white layer formation map for 1045 annealed steel can be used to determine white layer formation by predicting the maximum workpiece surface temperature and unit thrust force for a given cutting condition. The following section describes the procedure for prediction of white layer using the above white layer formation map in detail.

6.4 Validation of Semi-Empirical Procedure for Prediction of White Layer

Two machining conditions, which were not used in constructing the semi-empirical map shown in Figure 6.8 are chosen to validate the white layer formation map: (1) 225 m/min cutting speed, 0.15 mm/rev feed, 100 µm flank wear, (2) 50 m/min cutting speed, 0.125 mm/rev feed, 50 µm flank wear. For each of these conditions, the cutting and thrust forces with the new tool, and the force increase due to flank wear are predicted using the force models described in the previous section. The cutting and thrust forces with the new tool, and the cutting force increase due to tool flank wear are used as input

to the models for the maximum workpiece surface temperature. The maximum workpiece surface temperature and the thrust force increase are superimposed on the white layer formation map as shown in Figure 6.9.

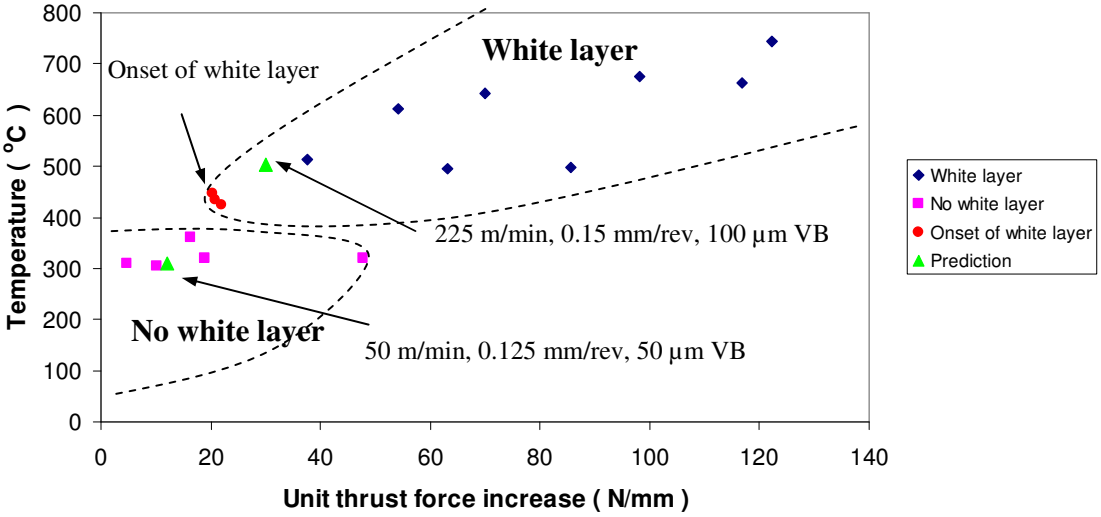

Figure 6.9. Prediction of white layer formation using the maximum workpiece temperature and thrust force increase.

As can be seen in Figure 6.9, the maximum workpiece temperature and thrust force increase at 50 m/min cutting speed, with 0.125 mm/rev feed and 50 µm flank wear are located in the region denoted as "no white layer". This implies that the thermal and mechanical loading effects are below the critical level needed to generate white layer. Consequently, no white layer is expected at this machining condition. On the other hand, the maximum workpiece temperature and thrust force increase at 225 m/min cutting speed, 0.15 mm/rev feed and 100 µm flank wear are located in the region denoted as "white layer". This indicates that the thermal and mechanical effects are sufficient to produce a white layer. In addition, since the maximum workpiece temperature, 502 ºC,

and the unit thrust force increase, 30 N/mm, predicted at this machining condition are in the range of 500-600 ºC and less than 55 N/mm, a thin (1-3 µm thick) white layer is expected at this machining condition.

Actual machining tests were conducted at these validation conditions and the micrographs of the resulting microstructures obtained are shown in Figure 6.10.

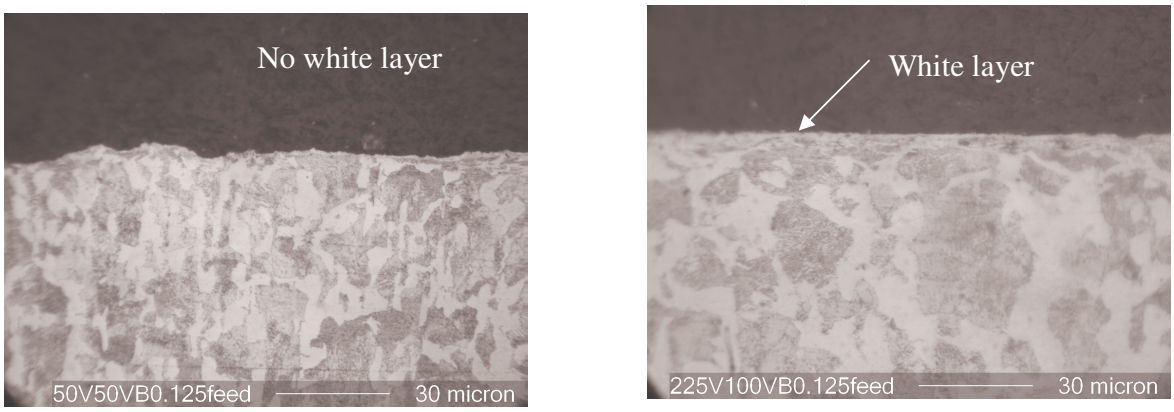

Figure 6.10. Microstructure of surface of AISI 1045 annealed steel machined at: (a) 50m/min cutting speed, 50 µm VB, 0.125 mm/rev feed, (b) 225 m/min cutting speed, 100 µmVB, 0.15 mm/rev feed.

As predicted, no white layer is observed in the machined surface at 50 m/min cutting speed, 0.125 mm/rev feed and 50 µm flank wear. Also, as predicted, 3.5 µm thick white layer is observed in the machined surface at 225 m/min cutting speed, 0.15 mm/rev feed and 100 µm flank wear.

The prediction of the presence/absence of white layer and the approximate white layer depth shows good agreement with the actual machining tests. Therefore, the developed semi-empirical procedure appears to work.

6.5 Application of Semi-Empirical Model of White Layer Formation

The semi-empirical model developed in this chapter provides knowledge about the underlying mechanism in the formation of white layer for a given machining condition. This semi-empirical model can be applied are a wide range of machining conditions, where different levels of thermal and mechanical effects occur. Previous white layer formation models which consider thermal effects only often limited to the aggressive machining conditions needed to produce temperatures above the nominal A_s temperature.

A pure empirical model to represent white layer depth as a function of machining parameters is not enough to find the optimized machining condition required to achieve the best surface integrity. The same white layer depth can be formed under different machining conditions, where different levels of thermal and mechanical effects are present. Consequently, other surface integrity metrics such as hardness and residual stress are different although white layer depth may be the same.

This model can serve as a basis for white layer prediction using fuzzy set modeling [72]. Fuzzy set modeling is based on the rule that white layer occurs when the workpiece surface temperature exceeds the nominal phase transformation temperature. Thus, if the rule that accounts for both thermal and mechanical effects on white layer formation is employed in the fuzzy modeling, the range of machining parameters that cause white layer will be changed.

6.6 Summary

The contributions of thermal and mechanical effects on white layer formation are quantified and used to develop a semi-empirical procedure for prediction of white layer formation. Machining tests on 1045 annealed steel have been conducted over a wide range of machining speeds and flank wear lands, where different levels of thermal and mechanical effects occur. For each machining condition, the maximum workpiece surface temperature was calculated using the validated temperature model and used as a thermal effect parameter in the semi-empirical procedure. The thrust force increase was calculated using the empirically derived regression relation and used as a mechanical parameter in the semi-empirical procedure. A correlation between white layer presence/absence, and the maximum workpiece temperature and thrust force increase was identified. The presence/absence of white layer was predicted using the semi-empirical procedure. Model validation was done by comparing the actual machining test results and the prediction of white layer for new cutting conditions.

CHAPTER 7

CONCLUSIONS AND RECOMMENDATIONS

7.1 Conclusions

The following conclusions can be drawn from this study:

Effect of Alloying, Heat Treatment, and Carbon Content on White Layer Formation

- No noticeable effect of alloying (1045 vs. 4340 annealed steel) on white layer formation and hardness is seen. This is possibly because the temperature was not high enough to cause α-γ transformation.

- Effect of heat treatment (4340 annealed vs. 4340 hardened steel) is to produce white layer at both cutting speeds. The retained austenite present in the bulk hardened steel enhances martensitic phase transformation, and thus promotes formation of white layer. Heat treatment leads to a substantial increase in white layer hardness (up to 2 GPa more than bulk hardness) at both cutting speeds.

- Increased carbon content of the steel (4340 vs. 52100 hardened steels) tends to increase white layer depth at the higher cutting speed while no difference is observed at the lower cutting speed. The former is attributed to the enhancement

of martensitic phase transformation with more carbon diffusing into the austenite phase. Increased carbon content tends to increase white layer hardness at both cutting speeds.

- No correlation is evident between the workpiece surface temperatures, effective stresses and strains and white layer formation or hardness when considering the effect of alloying.

- The increase in white layer depth and hardness with heat treatment appears to be associated with an increase in workpiece surface temperature and effective stress.

- When considering the effect of carbon content, higher workpiece surface temperatures and higher effective plastic strains appear to increase the white layer depth at higher cutting speeds.

Calculation of Thermal and Mechanical Effects on the Workpiece Surface

- The calculated workpiece surface temperature shows good agreement with the measured temperature data with an average error of 16%. Thus, the calculated maximum workpiece temperature is considered to be reasonable and useful for analyzing the effect of temperature on white layer formation.

- Effective stress and plastic strain on the workpiece are quantified and used to analyze the effect of mechanical deformation on white layer depth and the amount of retained austenite.

White Layer Formation Due to Phase Transformation in AISI 1045 Annealed Steel

- The phase transformation in machining of AISI 1045 steel can occur below the nominal phase transformation, A_{c1} in Fe-C phase diagram. Mechanical working in the machining process, quantified here by the effective stress and strain, also appears to play a role in causing phase transformation below the nominal phase transformation temperature.

- Retained austenite as evidence of phase transformation is observed in the white layers in all machining conditions used in the tests on AISI 1045 annealed steel. The amount of retained austenite varies with the thermal and mechanical loading resulting from the different cutting conditions.

- Different depths of white layers in AISI 1045 annealed steel were observed as a result of different levels of temperature, stress and strain induced by machining in a wide range of cutting speed and flank wear land.

Semi-Empirical Procedure of White Layer Formation

- A semi-empirical procedure for predicting the onset of white layer formation in orthogonal machining of 1045 annealed steel as a function of the maximum workpiece temperature and the unit thrust force increase was developed. This procedure accounts for both thermal and mechanical effects in the formation of white layer.

- The semi-empirical procedure has the capability of predicting presence/absence of white layer in AISI 1045 annealed steel and its approximate depth for a given range of machining conditions.

7.2 Recommendation for Future Work

White Layer Formation Mechanisms in Orthogonal Machining of Steels

- Detection of martensite phase in white layer as an evidence of phase transformation using TEM analysis. There is a hurdle in detecting martensite phase using XRD measurement because the phase is located at the same 2 theta angle as the ferrite phase.
- Identifying the sub surface workpiece temperature using a high spatial resolution infrared camera during machining under abusive conditions, which is expected to

produce a very thick white layer (>10 μm). Then, one can correlate the sub surface workpiece temperature with white layer properties such as nano hardness of white layer. This work can be applicable to grinding process as well.

- Measurement of the plastic strain by XRD characterization of the machined surface.

Effect of Alloying, Heat Treatment, and Carbon Content on White Layer Formation in Machining of Steels

- Comparison of white layer formation in machining of non-ferrous metals such as copper and titanium with that in machining of steels. Since these materials are not based on the Fe-C diagram, this study will shed light on the effects of material characteristics other than those for steels on the formation of white layer.

Calculation of Thermal and Mechanical Effects on the Workpiece Surface

- Capture the workpiece surface deformation by measuring plastic strain using XRD and correlate the microstructure alteration.

Semi-Empirical Modeling of White Layer Formation

- Correlate white layer formation with plastic work and thermal energy input to the sub surface of the workpiece. Energy consumption is a function of deformation and stress for a given volume. Thus, this study will show mechanical working in the sub surface in greater detail.

APPENDIX A

Nano indentation on

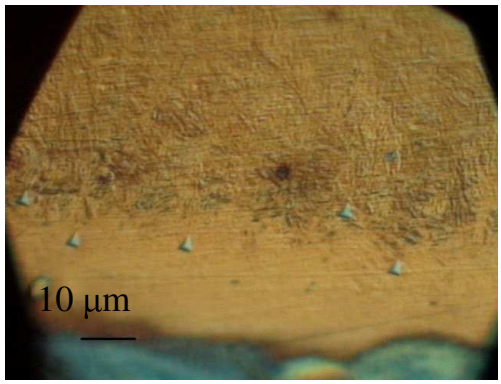

(a)

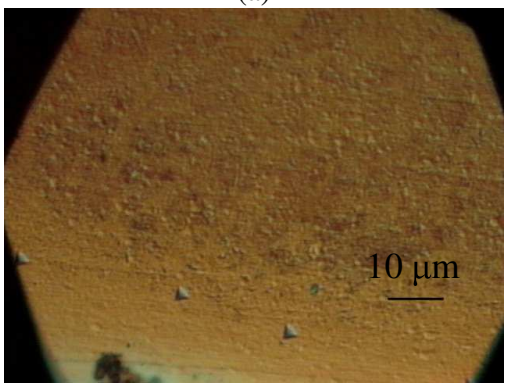

(b)

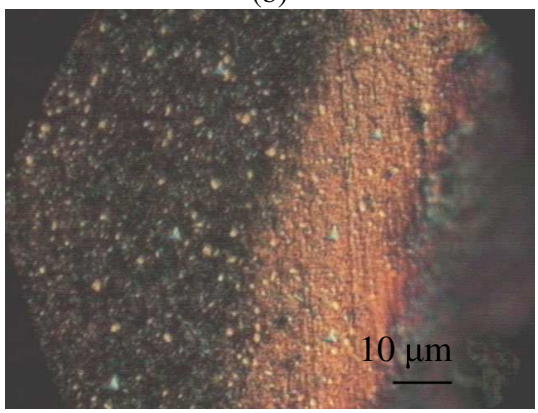

(c)

Figure A.1. Micrographs showing nano indents in the white layer and transition layer in: (a) 4340 hardened steel machined at 300 m/min with 110 μm flank wear, (b) 52100 hardened steel machined at 100 m/min with 110 μm flank wear, (c) 52100 hardened steel machined at 300 m/min with 110 μm flank wear.

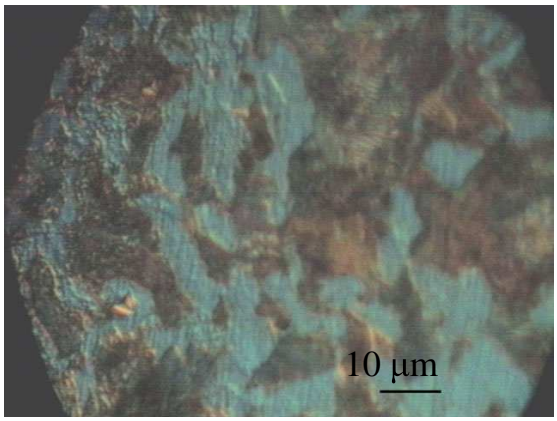

(a)

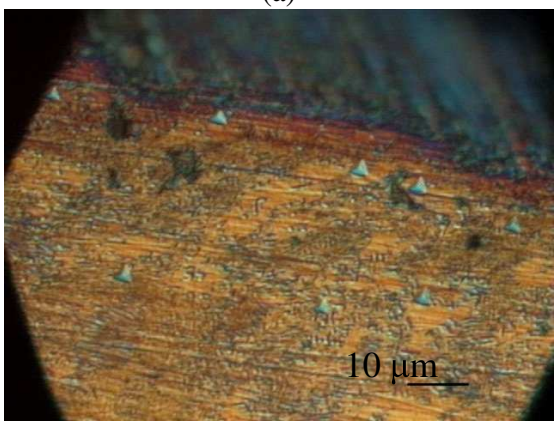

(b)

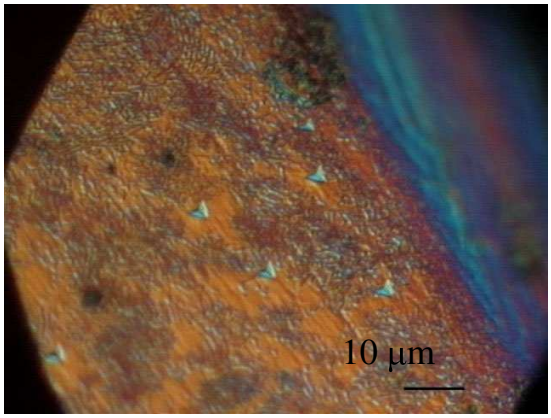

(c)

Figure A.2. Micrographs showing nano indents in the edge and bulk region in: (a) 1045 annealed steel machined at 100 m/min with 110 μm flank wear, (b) 4340 annealed steel machined at 100 m/min with 110 μm flank wear, (c) 4340 annealed steel machined at 300 m/min with 110 μm flank wear.

Table A.1. Nano-hardness test results.

Material and cutting condition	Region	Hardness (GPa)	Standard deviation (GPa)
1045 annealed steel at 100 m/min	Edge	3.758029	0.772327
	Transition	3.277488	0.968824
	Bulk	3.255945	0.5523
1045 annealed steel at 300 m/min	Edge	4.113246	0.715306
	Transition	3.557556	0.527455
	Bulk	3.184887	0.42988
4340 annealed steel at 100 m/min	Edge	4.084202	0.426985
	Transition	3.613591	0.547306
	Bulk	3.209451	0.272187
4340 annealed steel at 300m/min	Edge	3.443246	0.454676
	Transition	3.358018	0.664914
	Bulk	3.118126	0.345659
52100 hardened steel at 100m/min	White layer	9.264901	0.956142
	Transition layer	5.510622	0.963588
	Bulk	6.718223	0.544035
52100 hardened steel at 300m/min	White layer	9.428789	0.960009
	Transition layer	5.382152	0.337465
	Bulk	6.552219	0.493119
4340 hardened steel at 100 m/min	White layer	8.479373	0.64298
	Transition layer	5.543628	0.911899
	Bulk	6.752294	0.350059
4340 hardened steel at 300 m/min	White layer	8.652784	0.742691
	Transition layer	5.721758	0.728103
	Bulk	6.569142	0.35649

Table A.2 Chip thickness data for machining of AISI 1045 annealed steel at different machining speeds with different flank wear lands and 0.1 mm/rev feed.

Machining condition	100 m/min 100 µm VB	150 m/min 310 µm VB	200 m/min 100 µm VB	100 m/min 0 µm VB	150 m/min 0 µm VB	200 m/min 0 µm VB
1	0.24 mm	0.20 mm	0.18 mm	0.25 mm	0.20 mm	0.17 mm
2	0.24 mm	0.20 mm	0.17 mm	0.25 mm	0.18 mm	0.15 mm
3	0.25 mm	0.20 mm	0.17 mm	0.25 mm	0.20 mm	0.17 mm
4	0.24 mm	0.20 mm	0.17 mm	0.25 mm	0.20 mm	0.15 mm
5	0.25 mm	0.20 mm	0.17 mm	0.25 mm	0.20 mm	0.16 mm
average	0.25 mm	0.20 mm	0.17 mm	0.25 mm	0.20 mm	0.16 mm

Temperature and Force Signals

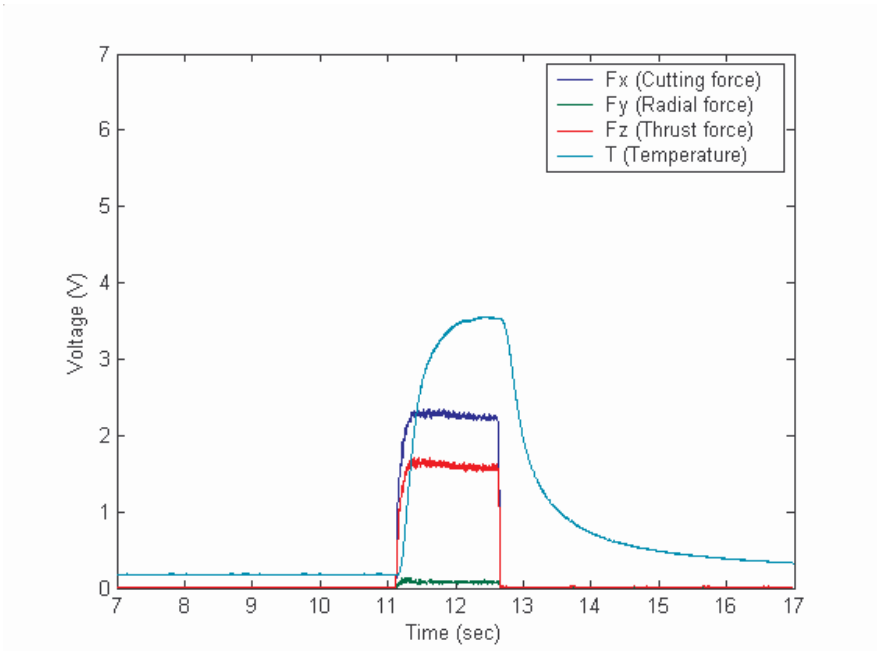

Figure A.3. Cutting forces and temperature when machining with 310 µm flank wear at 100 m/min.

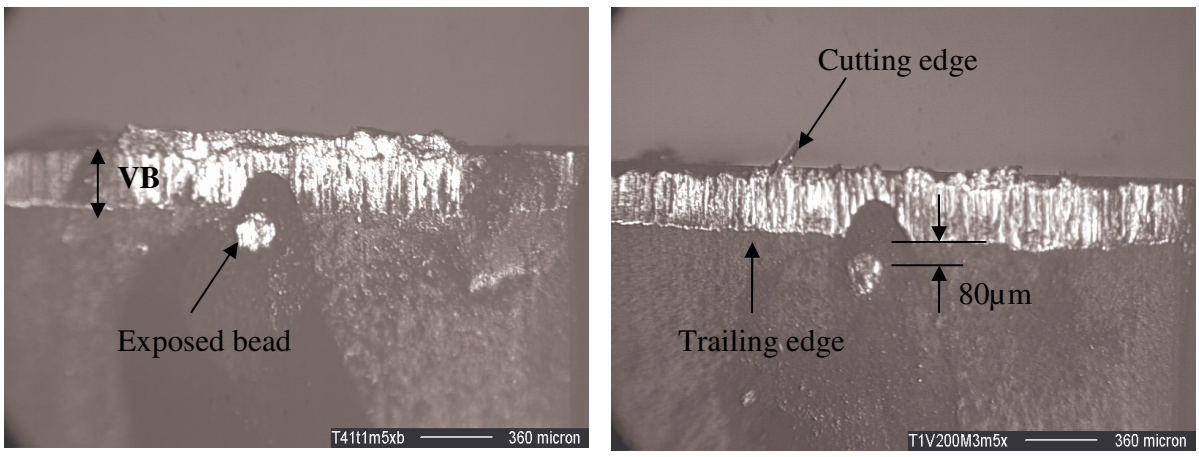

Figure A.4. Location of bead: (a) after cleaning cut, (b) after machining with 310 µm flank wear at 100 m/min.

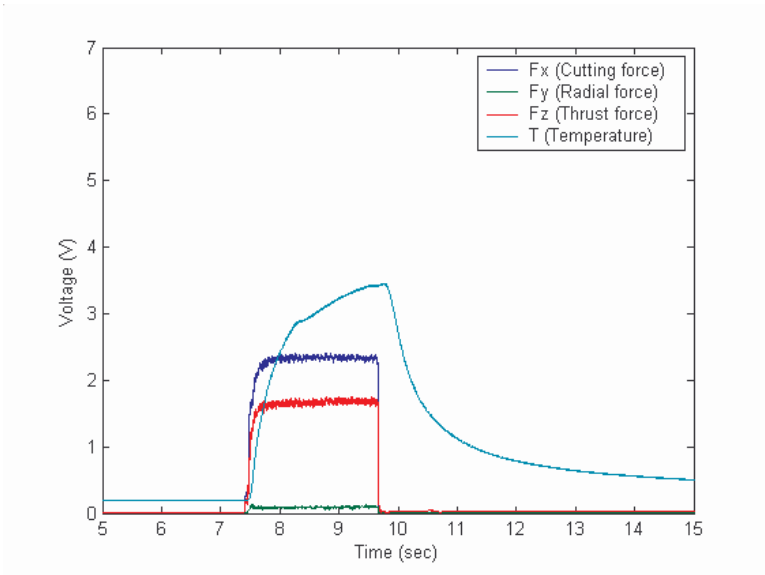

Figure A.5. Cutting forces and temperature when machining with 420 µm flank wear at 100 m/min. (replication 1)

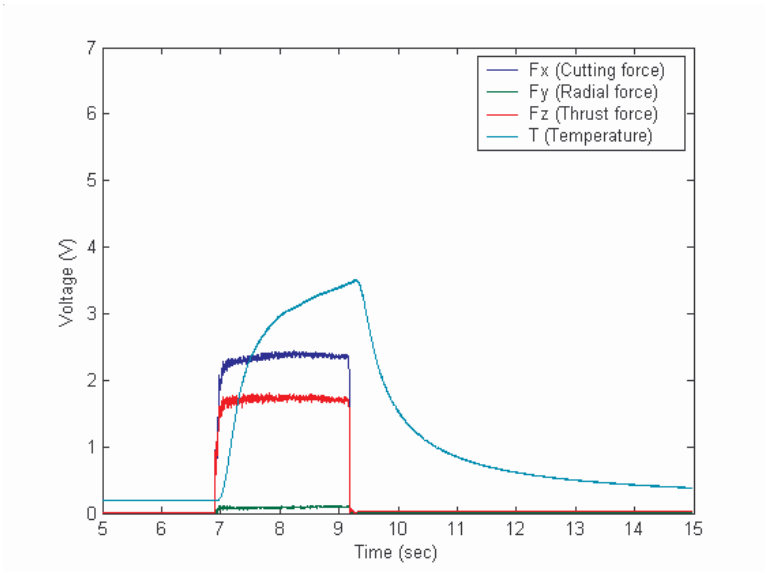

Figure A.6. Cutting forces and temperature when machining with 420 µm flank wear at 100 m/min. (replication 2)

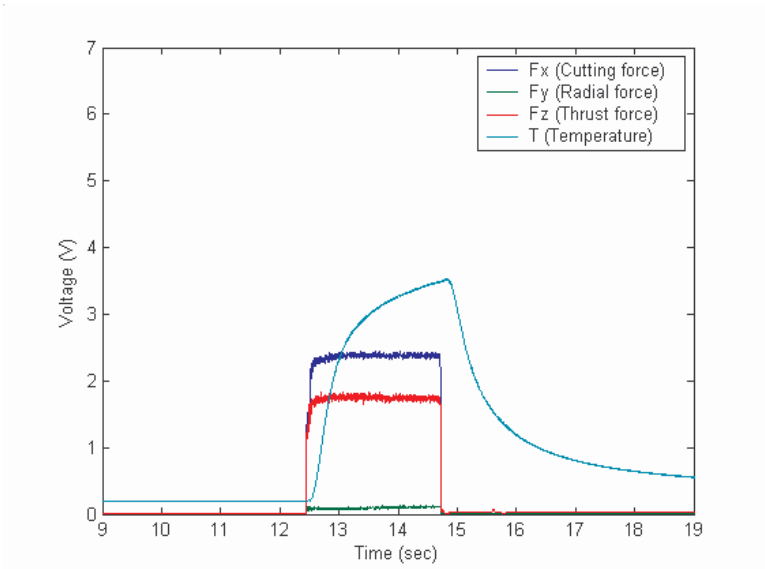

Figure A.7. Cutting forces and temperature when machining with 420 µm flank wear at 100 m/min. (replication 3)

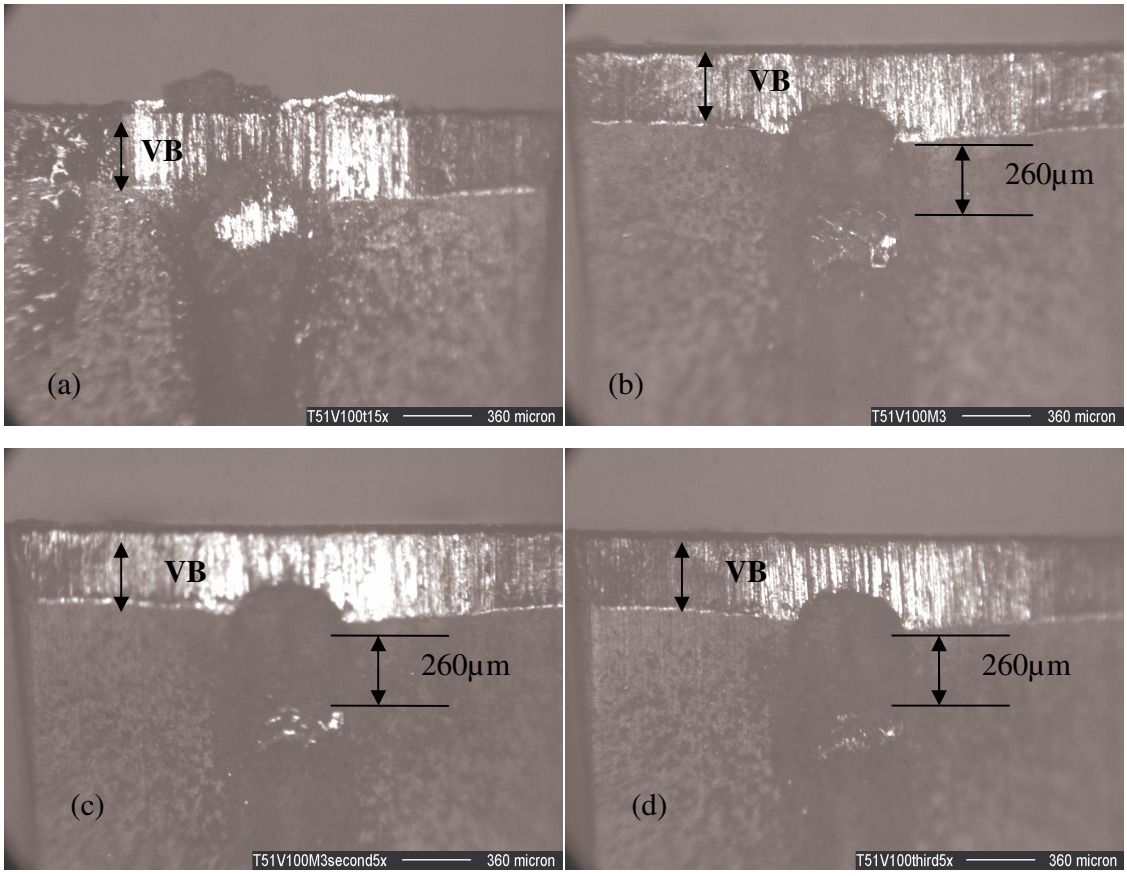

Figure A.8. Location of bead: (a) After cleaning cut, (b) After the first replication, (c) After the second replication, (d) After the third replication.

Table A.3. Free energies of the α-γ transformation in pure iron (Darken and Gurry,[81])

T, °C	ΔF_{tr}^{T} atm-cm^3/gm-atom
25	53080.12
126.84	44791.41
226.84	36555.14
326.84	28500.62
426.84	20817.84
526.84	13482.03
626.84	7769.52
726.84	3139.20
746.84	2527.88
766.84	2019.00
786.84	1532.42
806.84	1159.85
826.84	863.28
846.84	555.14
866.84	376.70
886.84	191.66
906.84	0.00
910	0.00

REFERENCES

1. Jochmann, S. and Wirtz, H., 1999, "Achieving Precision Grinding Quality by Hard Turning," Manuf. Sci. and Eng., J.W. Sutherland (Ed.), ASME MED Vol. 10, pp. 817-823.

2. Zurecki, Z., Ghosh, R. and Frey, J., 2003, "Investigation of White Layers Formed in Conventional and Cryogenic Hard Turning of Steels", Proceedings of IMECE2003-42313.

3. Eda, H., Kishi, K. and Hashimoto, S., 1981, "The Formation Mechanism of Ground White Layers", Bulletin of the JSME, Vol. 24, No. 190, pp. 743-747.

4. Shaw, M. and Vyas, A., 1993, "Heat-Affected Zones in Grinding Steel", Ann. CIRP, Vol. 43/1, pp. 279-282.

5. Guo, Y. and Sahni, J., 2004, "A Comparative Study of Hard Turned and Cylindrically Ground White Layers", International Journal of Machine Tools & Manufacture, Vol. 44, pp. 135-145.

6. Eyre, T. S. and Baxter, A., 1972, "The Formation of White Layers at Rubbing Surfaces", Tribology, pp. 256-261.

7. Turley, D. M., 1975, "The Nature of the White-Etching Layers Produced during Reaming Ultra-High Strength Steel," Mat. Sci. and Eng., Vol. 19, pp. 79-86.

8. Okusa, K., Takahashi H. and Nishizawa, M., 1978, "Behavior of White Layer during Cutting of Iron and Steels", Bull. Japan Soc. Of Prec. Engg., Vol. 12 No. 4, pp. 171-176.

9. Kruth, P., Stevens, L., Froyen, L., Lauwers, B., 1995, "Study of the White Lyaer of a Surface Machined by Die-sinking Electro-Discharge Machining", Ann. CIRP Vol. 44, pp 169-172.

10. Lee, H., Hsu F. and Tai, T., 2004, "Study of Surface Integrity Using the Small Area EDM Process with a Copper-Tungsten Electrode" Material Sciences and Engineering A364, pp 346-356.

11. Xu, Y., Fang, L., Cen, Q., Zhu, J., 2004, "Nano Structure and Transformation Mechanism of White Layer for AISI 1045 Steel during Impact Wear", Wear, Vol 258, pp.537-544.

12. Prangnell, P.B., Bowen, J. R. and Gholinia, A., 2001, "The Formation of Submicron and Nanocrystalline Grain Structures by Severe Deformation", Proceedings of the 22nd Risø International Symposium on Materials Science, pp. 105-126.

13. Karamis, M. B. and Gercekcioglu, E., 2000, "Wear Behaviour of Plasma Nitrided Steels at Ambient and Elevated Temperatures", Wear, Vol. 243, pp 76-84.

14. Baumann, G., Fecht, H.J., Liebelt, S.,1996, "Formation of White-Etching Layers on Rail Treads," Wear, Vol.191, pp. 133-140.

15. Lojkowski, W., Djahanbakhsh, M., Bürkle, G., Gierlotka, S., Zielinski, W., Fecht, H.J., 2001, "Nanostructure Formation on the Surface of Railway Tracks," Mat. Sci. and Eng., A303, pp. 197-208.

16. Lojkowski, W., Djahanbakhsh, M., Bürkle, G., Gierlotka, S., Zielinski, W., Fecht, H.J., 2001, "The Mechanical Properties of the Nanocrystalline Layer on the Surface of Railway Tracks" , Mat. Sci. and Eng., A303, 209-215.

17. Becker, P.C., 1981, "Microstructural Changes around Non-Metallic Inclusions Caused by Rolling-Contact Fatigue of Ball Bearing Steels", Metals Technology, June, pp. 234-243.

18. Akcan, S., Shah, S., Moylan, S.P., Chhabra, P.N., Chandraseksar, S., and Yang, H.T.Y., 2002, "Formation of White Layers in Steels by Machining and Their Characteristics," Met. Mat. Trans. A, Vol. 33A, pp.1245-1254.

19. Griffiths, B.J and Furze, D. C., 1987, "Tribological Advantages of White Layers Produced by Machining," J. of Tribology, Vol. 109, pp 338-342.

20. Yang, Y. Y., Fang H. S. and Huang, W. G., 1996, "A Study on Wear Resistance of the White Layer" Tribology International, Vol. 29, No. 5, pp. 425-428.

21. Manion, S. A., Stock, T.A.C., 1970, "Adiabatic Shear Bands in Steel" Int. Journ. of Fracture Mech. 6, pp. 106-107.

22. Abrao, A. M. and Aspinwall, D. K., 1996, "The Surface Integrity of Turned and Ground Hardened Bearing Steel," Wear, Vol. 196, pp. 279-284.

23. Smith, S., 2001, "An Investigation into the Effects of Hard Turning Surface Integrity on Component Service Life" Ph. D. Thesis, Georgia Institute of Technology.

24. Che-Haron, C. H., Jawaid, A., 2005, "The Effect of Machining on Surface Integrity of Titanium Alloy Ti-6% Al-4% V", Journal of Materials Processing Technology, 166,pp. 188-192.

25. Turley, D. M., 1968, “Deformed Layers Produced by Machining 70/30 brass”, The Institute of Metals, 96, pp. 82-86.

26. Griffiths, B. J., 1987, “Mechanisms of White Layer Generation with Reference to Machining and Deformation Processes,” J. of Tribology, Vol. 109, pp. 525-530.

27. Y.K. Chou, C. J. Evans, 1999, “White Layer and Thermal Modeling of Hard Turned Surfaces”, International Journal of Machine Tools and Manufacture, Vol 39, pp. 1863-1881.

28. Brinksmeir, E. and Brockhoff, T., 1999, “White Layers in Machining Steels,” Proc. 2nd Int. German and French Conf. on High Speed Machining, Darmstadt, Germany.

29. Barbacki, A. and Kawalec, M., 1997, “Structural Alterations in the Surface Layer During Hard Machining,” J. of Mat. Proc. Tech., Vol. 64, pp. 33-39.

30. Barry, J. and Byrne, G., 2002, “TEM Study on White Layer in Two Turned Hardened Steels” Mat. Sci. and Eng., A325, pp. 356-364.

31. Österle, W., Rooch, H., Pyzalla, A., Wang, L., 2001, “Investigation of White Etching Layers on Rails by Optical Microscopy, Electron Microscopy, X-Ray and Synchrotron X-Ray Diffraction,” Mat. Sci. and Eng., A303, pp. 150-157.

32. Kim, W. and Kwon, P., 2002, “Phase Transformation and Its Effect on Flank Wear in Machining Steels”, Journal of Manufacturing Science and Engineering, Vol. 124, pp. 659-666.

33. Sauvage, X., Breton, J., Guillet, A., Meyer A. and Teillet, J., 2003, “Phase Transformations in Surface Layers of Machined Steels Investigated by X-ray Diffraction and Mössbauer Spectometry”, Materials Science and Engineering, Vol. 362, pp. 181-186.

34. Akcan, S., Shah, S., Moylan, S.P., Chhabra, P.N., Chandrasekar, S.and Farris, T.N., 1999, “Chariacteristics of White Layers Formed in Steels by Machining”, Manufacturing Science and Engineering, Vol. 10, pp. 789-795.

35. Akcan, N. S., 1998, “Microstructure Analysis and Temperature Modeling in Finish Machining of Hardened Steels,” M. S. Thesis, School of Industrial Engineering, Purdue University.

36. Ramesh, A., Thiele, J., Melkote, S., 1999, “Residual Stress and Sub-surface Flow in Finish Hard Turned AISI 4340 and 52100 Steels: A Comparative Study”, Manufacturing Science and Engineering, pp. 831-837.

37. Barrow, G., 1973, “A Review of Experimental and Theoretical Techniques for Assessing Cutting Temperatures”, Annals of CIRP Vol. 22/2, pp. 203-211.

38. Komanduri, R., Hou, Z. B., 2001, “A Review of the Experimental Techniques for the Measurement of Heat and Temperatures Generated in Some Manufacturing Processes and Tribology”, Tribology International, Vol. 34, pp. 653-682.

39. M’Saoubi, R., Calvez, C. Le., Changeux, B., Lebrum, J. L., 2002, “Thermal and Microstructural Analysis of Orthogonal Cutting of a Low Alloyed Carbon Steel Using an Infrared-Charge-Coupled Device Camera Technique”, Proc Instn Mech Engrs Part B: J Engineering Manufacture, Vol. 216, pp. 153-165.

40. Boothroyd, G., Eagle, M., Chisholm, A.W.J., “Effect of Tool Flank Wear on the Temperatures Generated during Metal Cutting”,Proceedings of 8th International Machine Tool Design and Research Conf., 1967, pp. 667-680.

41. Hirao, M., 1989, “Determining Temperature Distribution on Flank Face of Cutting Tool”, J. Materials Shaping Technology, Vol. 6, pp. 143-148.

42. Müller, B., Renz, U., 2003, “Time Resolved Temperature Measurements in Manufacturing”, Measurement, Vol. 34, pp. 363-370.

43. Müller, B., Renz, U., Hoppe, S., Klocke, F., 2004, “Radiation Thermometry at a High-Speed Turning Process”, Journal of Manufacturing Science and Engineering, Vol. 126, pp. 488-495.

44. Usui, E., Shirakashi, T., Kitagawa, T., 1984, “Analytical Prediction of Cutting Tool Wear”, Wear, Vol. 100, pp. 129-151.

45. Bosheh, S.S., Mativenga, P.T., 2005, “White Layer Formation in Hard Turning of H13 Tool Steel at High Cutting Speeds Using CBN Tooling”, International Journal of Machine Tools and Manufacture (in press), pp. 1-9.

46. Ramesh, A., Melkote, S.N., Allard, L.F., Riester, L., Watkins, T.R., 2005, “Analysis of White Layers Formed in Hard Turning of AISI 52100 steel”, Material Science and Engineering A, Vol. 390, pp. 88-97.

47. Ramesh, A., 2002, “Prediction of Process-Induced Microsturctural Changes and Residual Stresses in Orthogonal Hard Machining,” Ph. D. Thesis, Mechanical Engineering, Georgia Institute of Technology.

48. Chou, Y.K., 2002, “Surface Hardening of AISI 4340 Steel by Machining: a Preliminary Investigation”, Journal of Materials Processing Technology, Vol. 124, pp. 171-177.

49. Mahajan, V. and Chou, Y.K., 2004, "Machining-Induced Surface Hardening due to Large Wear Land", Proc. Instn Mech. Engrs, Vol. 218 Part B: J. Engineering Manufacture, pp. 1647-1655.

50. Guo, Y. and Sahni, J., 2004, "A Comparative Study of Hard Turned and Cylindrically Ground White Layers", International Journal of Machine Tools & Manufacture, Vol. 44, pp. 135-145.

51. Guo, Y. and Warren, A., 2005, "Microscale Mechanical Behavior of the Subsurface by Finishing Processes", Journal of Manufacturing Science and Engineering, Vol. 127, pp. 333-338.

52. Thelning, K-E.,1984, *Steel and its Heat Treatment*, Second Edition, Butterworths.

53. Parrish, G., 1999, *Carburizing: Microstructures and Properties*, First Edition, ASM International®.

54. Krauss, G., 1989, *Heat treatment and processing principles*, ASM International.

55. Trigger, K.J., Chao, B.T., 1951, "An Analytical Evaluation of Metal Cutting Temperatures", Transactions of ASME, Vol. 73, pp. 57-68.

56. Loewen, E.G. and Shaw, M.C., 1954, "On the Analysis of Cutting-Tool Temperatures", Transactions of ASME, Vol. 76, pp. 217-231.

57. Loene, W.C., 1954, "Distribution of Shear-Zone Heat in Metal Cutting", Transaction of ASME, Vol. 76, pp. 121-125.

58. Boothroyd, G, 1963, "Temperatures in Orthogonal Metal Cutting", Proc Instn Mech Engrs, Vol. 177, No. 29, pp. 789-810.

59. Merchant, M.E., 1945, "Mechanics of the Metal Cutting Process. 1. Orthogonal Cutting and a Type 2 Chip", Vol. 16, No.5, pp. 267-275.

60. Spaans, C. 1972, "A Treatise on the Streamlines and the Stress, Strain, and Strain Rate Distributions, and on Stability in the Primary Shear Zone in Metal Cutting", Transaction of the ASME, May, pp. 690-696.

61. Oxley, P.L.B., 1989, *The Mechanics of Machining: An Analytical Approach to Assessing Machinability*, Halsted Press.

62. Chao, B.T., Trigger, K.J., 1958, "Temperature Distribution at Tool-Chip and Tool-Workpiece Interface in Metal Cutting", Journal of Engineering for Industry, pp. 311-320.

63. Jeager, J.C., 1942, "Moving Sources of Heat and the Temperature at Sliding Contact", Proceedings of the Royal Society, Vol. 56, pp. 203-224.

64. Komanduri, R., Hou, Z.B., 2000, "Thermal Modeling of the Metal Cutting Process Part 1 – Temperature Rise Distribution due to Shear Plane Heat Source" International Journal of Mechanical Sciences, Vol. 42, pp. 1715-1752.

65. Komanduri, R., Hou, Z.B., 2001, "Thermal Modeling of the Metal Cutting Process Part 2 – Temperature Rise Distribution due to Frictional Heat Source" International Journal of Mechanical Sciences, Vol. 43, pp. 57-88.

66. Komanduri, R., Hou, Z.B.,2001, "Thermal Modeling of the Metal Cutting Process Part 3 – Temperature Rise Distribution due to the Combined Effects of Shear Plane Heat Source and the Tool-Chip Interface Frictional Heat Source" International Journal of Mechanical Sciences, Vol. 43, pp. 89-107.

67. Huang, Y., 2002, "Predictive Modeling of Tool Wear Rate with Application to CBN Hard Turning", Ph. D. Thesis, Mechanical Engineering, Georgia Institute of Technology.

68. Thomsen, E. G., Macdonald, A. G., Kobayashi, S., 1962, "Flank Friction Studies with Carbide Tools Reveal Sublayer Plastic Flow", Journal of Engineering for Industry, pp. 53-62.

69. Chen, N.N.S., Pun, W. K., 1988, "Stresses at the Cutting Tool Wear Land", International Journal of Machine Tools and Manufacturing, Vol. 28. No2, pp. 79-92.

70. Waldorf, D. J., 1996, "Shearing, Ploughing, and Wear in Orthogonal Machining", Ph. D. Thesis, University of Illinois at Urbana-Champaign.

71. Barbacki, A., Kawalec, M., Hamrol, A., 2003, "Turning and Grinding as a Source of Microstructural Changes in the Surface Layer of Hardened Steel," J. of Mat. Proc. Tech.,Vol. 133, pp. 21-25.

72. Ali, Y.M., Zhang, L.C., 2004, "A Fuzzy Model for Predicting Burns in Surface Grinding of Steel", International Journal of Machine Tool and Manufacture, Vol. 44, pp. 563-571.

73. Song, H., 2003, "Thermal Modeling for Finish Hard Turning", Ph. D. Thesis, Mechanical Engineering, University of Alabama.

74. Bailey, J.A., Jeelani, S., Becker, S.E., 1976, "Surface Integrity in Machining AISI 4340 Steel", Journal of Engineering for Industry, August, pp. 999-1007.

75. Kitagawa, T., Kubo, A., Maekawa, K., 1997, “Temperature and Wear of Cutting Tools in High-Speed Machining of Inconel 718 and Ti-6Al-6V-2Sn”, Wear, Vol. 202, pp. 144-148.

76. OMEGA handbook, 2000, *The Temperature*, OMEGA engineering, inc., A-12.

77. Cullity, B.D., 1979, *Elements of X-ray diffraction*, Addison Wesley.

78. Shi, T., Ramalingam, S., 1991,“Slip-Line Solution for Orthogonal Cutting with a Chip Breaker and Flank wear”, Int. J. Mech. Sci., Vol. 33, pp. 689-704.

79. American Society for Testing and Materials, 1999, “Standard practice for X-ray determination of retained austenite in steel with near random crystallographic orientation”, American Society for Testing and Materials, Designation: E 975-95, pp. 1-6.

80. Sauvage, X., Le Breton, J.M., Guillet, A., Meyer, A., Teillet, J., 2003, “Phase Transformations in Surface Layers of Machined Steels Investigated by X-ray Diffraction and Mössbauer Spectrometry”, Material Science and Engineering A, Vol. 362, pp. 181-186.

81. Darken, L.S., Gurry, R.W., 1975, *Physical Chemistry of Metals*, McGraw-Hill.

82. Belyakov, A., Kimura, Y., Tsuzaki, K., 2005, “Recovery and Recrystallization in Ferritic Stainless Steel after Large Strain Deformation”, Material Science and Engineering A, Vol. 403, pp. 249-259.

83. Hurley, P.J., Hodgson, P.D., 2001, “Formation of Ultra-Fine Ferrite in Hot Rolled Strip: Potential Mechanisms for Grain Refinement”, Material Science and Engineering A, Vol. 302, pp. 206-214.

84. Akcan, S., Shah, S., Moylan, S.P., Chhabra, P.N., Chandraseksar, S., and Yang, H.T.Y., 2002, “Formation of White Layers in Steels by Machining and Their Characteristics,” Met. Mat. Trans. A, Vol. 33A, pp.1245-1254.

85. www.matweb.com, MatWeb: Material Property Data, March 2006.

86. Kalpakjian, S. and Schmid, S.R., 1984, *Manufacturing Processes for Engineering Materials*, Fourth Edition, Pearson Education.

87. Oliver, W. and Pharr, G., 1992, “An Improved Technique for Determining hardness and Elastic Modulus Using Load and Displacement Sensing Indentation Experiments”, J. Mater. Res., Vol. 7, No. 6, pp. 1564-1583.

88. Krauss, G., 1990, *Steels: Heat treatment and Processing Principles*, ASM International, Metals Park, OH

89. Brooks, C., 1996, *Principles of the Heat Treatment of Plain Carbon and Low Alloy Steels,* ASM International, OH.

90. Marusich, T., 2001, "Effects of Friction and Cutting Speed on Cutting Force", Proceedings of 2001 ASME IMECE2001-23313, pp. 1-9.

91. Chou, Y.K., Song, H., 2005, "Thermal Modeling for White Layer Predictions in Finish Hard Turning", International Journal of Machine Tool and Manufacture, Vol. 45, pp. 481-495.

92. M'Saoubi, R., Chndrasekaran, H., 2004, "Investigation of the Effects of Tool Micro-Geometry and Coating on Tool Temperature during Orthogonal Turning of Quenched and Tempered Steel", International Journal of Machine Tools and Manufacture, Vol. 44, pp. 213-224.

93. Shaw, M., 1984, *Metal Cutting Principles*, Oxford Science Publication.

94. ASM handbook, 1992, Metals-Handbook: *Physical Properties of Carbon and Low-Alloy Steels*, Ohio.

95. Pednekar, V., Madhavan, V., Adibi-sedeh, A.H., 2004, "Investigation of the Transition from Plane Strain to Plane Stress in Orthogonal Metal Cutting", Proceedings of IMECE, ASME International Mechanical Engineering Congress and Exposition, pp. 513-528.

96. Smithey, D., Kapoor, S., Devor, R., 2001, "A New Mechanistic Model for Predicting Worn Tool Cutting Forces", Machining Science and Technology, Vol. 5(1), pp. 23-42.

97. Doebelin, E. O., 2003, *Measurement Systems; Application and Design*, McGraw Hill, Singapore, pp. 691-713.